C.P. No. 1170

MINISTRY OF DEFENCE

AERONAUTICAL RESEARCH COUNCIL

CURRENT PAPERS

Results of a Series of Wind Tunnel Model Breakdown Tests on the Trident 1 Aircraft and a Comparison with Drag Estimates and Full Scale Flight Data

By

J. I. Simper and P. G. Hutton
Aircraft Research Association Limited

LONDON: HER MAJESTY'S STATIONERY OFFICE

1971

PRICE £1 10 net

CP No. 1170*
March, 1970

RESULTS OF A SERIES OF WIND TUNNEL MODEL BREAKDOWN TESTS ON THE TRIDENT 1 AIRCRAFT AND A COMPARISON WITH DRAG ESTIMATES AND FULL SCALE FLIGHT DATA

by

J. I. Simper

P. G. Hutton

SUMMARY

Wind tunnel measurements made on a 1:18.86 scale model of the Trident 1 have been compared with estimates and flight data. Comparisons between measured and estimated drags for various model components are in general quite good, the exception being the measured side nacelle drag increment which is at least 1.5 times an estimate ignoring interference. Apart from scatter, the general level of agreement between flight and wind tunnel results, adjusted (on an arguable basis) for differences in Reynolds number and items omitted from the model, is within ±3% except at low Mach number where the difference is as much as 6%, probably due to the thrust, and hence drag, in flight being overestimated because the propelling nozzles were unchoked. If the wind tunnel data is corrected to flight Reynolds numbers using the Prandtl-Schlichting relationship the general level of the wind tunnel results is between 0 and 5% below the measured flight data. These levels of agreement, however, are extremely sensitive to the assumptions made in the excrescence drag estimate.

Appendices have also been included which present in detail the corrections applied to the wind tunnel data together with a complete set of tables showing the method of drag estimation.

CONTENTS/

---

* Replaces A.R.C.32 252 (ARA Report No. 14)

CONTENTS

FIGURES/

FIGURES

1: Model Support Systems

2(a): Side View of Model Wing Root Trailing Edge Fillets

2(b): Aft View of Model Wing Root Trailing Edge Fillets

3(a-c): $C_L \sim \alpha$ for M = 0.50 to M = 0.92. Complete Model and Tailplane off

4(a-c): $C_L \sim \alpha$ for M = 0.50 to M = 0.92. Tailplane off, Nacelles off and Fin off

5(a-f): $C_m \sim C_L$ for M = 0 50 to M = 0.92. Complete Model and Tailplane off

6(a-c): $C_m \sim C_L$ for M = 0.50 to M = 0.92. Tailplane off, Nacelles off and Fin off

7(a,b): Tailplane angle to trim $\sim C_{L\ TRIMMED}$

8(a,b): Tailplane lift to trim $\sim C_{L\ TRIMMED}$

9(a-h): $C_D \sim$ M Drag Breakdown for C_L = 0 to C_L = 0.45

10: $C_D - \left[\frac{C_L^2}{\pi A}\right]_{TRIMMED} \sim$ M for C_L = 0 to C_L = 0.45 and c.g. positions $16\%\bar{c}$ and $25\%\bar{c}$

11: $C_D \sim$ M for Wing + Body. C_L = 0 to C_L = 0.45

12: $C_D \sim R_c$. Complete Model ($\eta_T = -2°$), M = 0.80; C_L = 0.30 compared with theoretical variation

13(a): ΔC_D (Flight-Tunnel) $\sim$ R/ft. for $16\%\bar{c}$ c.g. (variation with C_L)

13(b): ΔC_D (Flight-Tunnel) $\sim$ R/ft. for $16\%\bar{c}$ c.g. (variation with M)

14(a): ΔC_D (Flight-Tunnel) $\sim$ R/ft. for $25\%\bar{c}$ c.g. (variation with C_L)

14(b): ΔC_D (Flight-Tunnel) $\sim$ R/ft. for $25\%\bar{c}$ c.g. (variation with M)

15(a): Drag Comparison between Tunnel (Corrected) and Flight ("Flight Reynolds Number effects as for Smooth Surface")

15(b): Drag Comparison between Tunnel (Corrected) and Flight ("Flight Reynolds Number effects as for recommended mean line in Fig.13").

15(c): Drag Comparison between Tunnel (Corrected) and Flight ("No Reynolds Number effects in Flight").

16: ΔC_D (Flight - Tunnel) $\sim$ M. C_L = 0.15 to C_L = 0.35.

NOTATION/

NOTATION

A	Aspect Ratio
C_D	Drag Coefficient
$C_{D_{pr}}$	Profile Drag Coefficient
C_f	Skin Friction Coefficient
C_L	Overall Lift Coefficient
C_{L_T}	Tailplane Lift Coefficient, based on wing reference area
C_m	Pitching Moment Coefficient
c	Local chord (ft.)
$\bar{\bar{c}}$	Wing Mean Aerodynamic Chord (ft.)
K	Induced Drag Factor $\left[K = \frac{\Delta C_D \cdot \pi \cdot A}{\Delta C_L^2} \right]$
M	Freestream Mach Number
M.R.P.	Moment Reference Point
R	Reynolds number
R_c	Reynolds number based on Chord
$R_{\bar{\bar{c}}}$	Reynolds number based on $\bar{\bar{c}}$
S	Wing Reference Area (ft.^{2})
α	Fuselage incidence (degrees)
η	Elevator Angle (degrees)
η_T	Tailplane setting Angle relative to Fuselage Datum (degrees)
Λ	Sweepback Angle
λ	Form Factor
ΔC_D	Increment in C_D
ΔC_L	Increment in C_L

1. INTRODUCTION

An extremely important aspect of the design of any new aircraft is an accurate prediction of the drag of the full scale aircraft whilst at the design stage. Although the work reported herein was concerned with the Trident 1 aircraft, already in production and flying, the work was basically aimed at improving the presently available knowledge on the use of wind tunnel data to predict full scale aircraft drag.

Details are given of a series of tests made in the A.R.A. 9ft. x 8ft. transonic wind tunnel using a 1:18.86 scale model of the Trident 1. The main tests were made on a conventional single sting support but, in addition, a twin sting support system was used to determine the interference of the single sting on the measured longitudinal results. Various model configurations ranging from wing + body to complete model were tested at Mach numbers between M = 0.50 and m = 0.92 on the two types of support system. Measured drag increments from these tests were compared with drag estimates with a view to pinpointing causes of excess drag.

In the full scale flight test results, as is usual, there is insufficient independent variation of parameters for definite conclusions to be drawn on the effects of Mach number, C_L and Reynolds number. Certain assumptions have had to be made to permit an analysis of the flight data. The method of analysis followed was to assume one of three different laws for the variation of drag with Reynolds number and then deduce, for all three laws, the effects of Mach number and C_L.

The three analyses of the flight data have each been compared with wind tunnel drag results adjusted to full scale Reynolds numbers by a chosen method. Alternative methods of extrapolating measured wind tunnel drags from model to full scale Reynolds numbers have been examined. Detailed comments concerning model representation of the full scale aircraft are presented, together with a discussion of the excrescence drag estimate used in the extrapolation. The flight and wind tunnel comparison has attempted to compare drags at both low speed and in the cruise region as well as finally comparing the drag rise characteristics of both the extrapolated model results and the full scale aircraft.

Appendices are also presented which give detailed information concerning the method of drag estimation used in this report and also details of the corrections applied to the wind tunnel data.

2. DESCRIPTION OF MODEL

The model used for the present series of wind tunnel tests was a 1:18.86 scale Trident 1 (de Havilland model "N" of the D.H.121). Figure 1 shows the model mounted on both the single and twin sting support systems. For each support system a series of force and pressure measurements were taken over a range of M and α for several different configurations.

In detail the configurations tested were:-

(i) Wing + Fuselage + Wing Fence + Fin Stub

The model wings were manufactured with full allowance for the full scale aeroelastic distortion under steady level flight, i.e., 1g. conditions. The wing fences used on the model were geometrically similar to the full scale fences.

The/

The model has been tested with various sets of wing root trailing edge fillets. For this series of tests the model had the fillets known as Fillet A (port) and Fillet L + pipe (starboard) which were representative of the full scale aircraft fillets. Details of the position and geometry of these fillets is shown in Figs. 2a and 2b.

Due to the method of manufacture and design of the model rear fuselage a small piece of fin (termed "fin stub") was present for the fin off configurations. To give a smooth profile to this fin stub a wooden half body fairing was screwed to the top surface. The fin stub and fairing can be seen in Fig. B1b of Appendix B. For brevity, the words "fin stub" are omitted from further descriptions of this configuration.

(ii) Wing + Fuselage + Wing Fences + Centre Nacelle + Fin

With the addition of the fin and centre nacelle the half body fairing of configuration (i) was removed. A fairing similar to that of configuration (i) was screwed to the fin top for the tailplane off configurations thus giving a smooth finish to the top of the fin.

The centre nacelle was fitted with a wooden fairing ahead of the normal intake plane to prevent any duct flow. This fairing, shown in Fig. B1b of Appendix B, was designed to smoothly extend the nacelle external lines from just aft of the normal intake plane.

(iii) Wing + Fuselage + Wing Fences + Fin + Nacelles

The open side nacelles and mounting pylons had almost the same external geometry as the full scale aircraft, the only difference being a slightly smaller boat-tail angle at the inboard trailing edge of the model nacelles, thus giving a slightly larger base and pen-nib area. The nacelle internal geometry comprised a contraction from the inlet followed by a constant area duct to the nacelle exit plane. In addition the base area of the jet pipe was somewhat larger than a true model scale version - due to the difficulty of manufacturing a feather edge. Pitot and static pressure tubes were located approximately 0.5" from the exit plane of each nacelle.

(iv) Complete Aircraft (Wing + Fuselage + Wing Fences + Fin + Nacelles + Tailplane + Bullet)

The half body fairing on the top of the fin of configuration (iii) was removed for this configuration and replaced by the tailplane and bullet. The full scale aircraft has a moving tailplane with geared elevator but the model was simplified in having no separate elevator. When considering trimmed conditions later in the text it should be noted that at a model tailplane angle of $\eta_T = +2^\circ$ the model geometry corresponds to nearly the same as the full scale aircraft, since the elevator angle is small, but $\eta_T = -2^\circ$ on the model would correspond to about $\eta_T = -0.6^\circ$ and $\eta = -3^\circ$ for the full scale aircraft.

Although the wing had been provided with flaps and ailerons all tests in the present series were made with zero deflection settings of these surfaces. All the wing surface irregularities and control gaps were filled and smoothed to give as clean a surface as possible. Gaps between individual components, e.g., the bullet and fin intersections, were also filled and smoothed.

The/

The windscreen flats of the full scale aircraft canopy were represented but items such as aerials, windscreen wipers, pitot tubes etc., were not represented.

As mentioned earlier, configurations (i) to (iv) were tested on two different sting support systems as shown in Fig. 1. In detail these systems, and the model modifications necessary to test on these systems are as below:

(a) Single Sting - Distorted Rear Fuselage

In order to accommodate the conventional single sting and internal balance it was necessary to have a hole for the sting through the fuselage afterbody. The external geometries of the fuselage with hole (the Distorted rear fuselage) and without hole were the same except near the fuselage end where some of the fuselage surface area was lost. The term "Distorted rear fuselage" does not imply any distortion of the external rear lines but rather a shape produced by boring a circular hole (for the sting) into the true shape. Of necessity this hole removes the centre nozzle in the single sting tests. A comparison of the rear fuselage shapes of Fig. 1 will show the change in rear fuselage lines.

(b) Twin Sting + Dummy Sting - Distorted Rear Fuselage

For this version of the twin sting support system the rear fuselage shape of (a) was used. The model was mounted on twin stings which were secured to the lower surface of the outer wing panels. The rear fuselage aft of the split line was connected to the fuselage centre section through a strain gauge balance which measured the rear fuselage and empennage loads in the presence of the dummy sting.

The dummy sting projected into a blind hole but did not touch the model anywhere. The overall geometry and position of the dummy sting, with respect to the model, were the same as for the single sting used in (a), apart from small differences due to different sting deflections. It is thought on this occasion that such small differences were negligible since the measured base pressures, both single and twin sting/dummy sting were the same. The fuselage split had a gap of about 0.06" all round the fuselage periphery to ensure no contact between the fuselage centre and aft sections. To minimise the proportion of the fuselage cross section area over which the pressure varies, the gap was increased rapidly with distance from the fuselage surface by an internal chamfer on the centre fuselage. Pressure points were located on the forward facing face of the gap and were connected to a scanivalve.

(c) Twin Sting - Correct Rear Fuselage

With the dummy sting removed and the sting hole in the rear fuselage filled with a make-up piece incorporating the centre nozzle (thus giving the Correct rear fuselage geometry) the model was supported on the same twin stings as in (b). The rear fuselage balance was again fitted with a fuselage gap setting of 0.06" at the split.

The balance used for the single sting tests was the A.R.A. No. 3 $2\frac{1}{4}$" diameter strain gauge balance. The No. 2 $2\frac{1}{4}$" diameter balance was used for the twin sting tests. In addition to the usual six-component forces and moments each balance had a spare axial force bridge. The twin stings of (b) and (c) had strain gauges to measure the model normal force and pitching moment.

Boundary layer transition-fixing bands of 0.004" to 0.005" diameter Ballotini set in Araldite were applied to the upper and lower surfaces of the wings and tailplane from 5% to 7%c. Bands were also applied to the fuselage nose, centre nacelle fairing, side nacelles (externally only), nacelle supporting pylons, tailplane, bullet and fin.

In addition to the nacelle internal pressure tubes and fuselage gap statics mentioned earlier, a single chordwise row of pressure holes was present on the port wing upper and lower surface at about 16% gross semi-span. Pressure tubes were also present to measure the base pressure in the balance compartment in the single sting tests and in the sting hole in the twin sting tests with dummy sting. The centre nacelle exit plane static pressure for support system (c) was also measured.

3. TEST PROCEDURE

Since the range of test variables was slightly different for the single and twin sting series they are dealt with separately as below (further details of the running technique are given in para. (ii c) of Appendix A):-

(i) Single Sting Tests

Tests were made at atmospheric stagnation pressure, at nominal mach numbers of M = 0.50, 0.60, 0.70, 0.74, 0.78, 0.80, 0.82, 0.84, 0.86, 0.88, 0.90 and 0.92. This gave a Reynolds number range from $R_{\bar{c}} = 2.43 \times 10^6$ at M = 0.50 to $R_{\bar{c}} = 3.28 \times 10^6$ at M = 0.92 based on the mean aerodynamic chord $\bar{c} = 0.8020$ ft. The range of incidence was $\alpha = -1.5°$ to $\alpha = +6°$ at low M, and $\alpha = +5°$ at high M, in steps of 0.5°.

A total of three tailplane angles were tested ($\eta_T = 0°$, + 0.93° and +2.07° measured in a streamwise direction) with the complete model configuration. A complete model fences-off test was also made over a slightly reduced incidence range. The wing fences were present for all other breakdown tests.

An inverted model test at the above Mach numbers was made in order to determine the tunnel flow pitch angularity.

Acenaphthene tests at M = 0.50, $C_L = 0.20$, M = 0.90, $C_L = 0.20$ and M = 0.90, $C_L = 0.60$ were made with the complete model ($\eta_T = 0°$) to check the effectiveness of the boundary layer transition bands being used. These tests indicated that a turbulent boundary layer was established immediately behind each of the bands. An oil flow test at M = 0.80, $C_L = 0.27$ at the end of the complete series of tests also indicated a turbulent boundary layer behind the strips.

As a further check on transition fixing, a constant M and nominal α test was made with the complete model ($\eta_T = -2°$) at M = 0.80 during which the tunnel stagnation pressure was varied to give a range of Reynolds number $R_{\bar{c}} = 2.68 \times 10^6$ to $R_{\bar{c}} = 3.86 \times 10^6$. An incidence traverse, still at M = 0.80, was also made at the two ends of the $R_{\bar{c}}$ traverse

(ii)/

(ii) Twin Sting Tests

The Mach numbers tested were as for the single sting tests but the incidence range was reduced to $\alpha = -1^\circ$ (0.5°) + 5° at low M with the maximum incidence reducing to $\alpha = 3.5^\circ$ at high M. The $R_{\bar{c}}$ variation was similar to that of (i). The complete model tailplane angles tested were $\eta_T = -2^\circ$, 0° and $+0.93^\circ$ for the Correct rear fuselage but only $\eta_T = 0^\circ$ for the Distorted fuselage.

Wing pressures, fuselage gap pressures, nacelle internal pressures and model base pressures were all measured together with the strain gauge balance output.

4. REDUCTION OF RESULTS

The wind tunnel results have been reduced to a non-dimensional coefficient form using the following data:

	Model dimensions	Full scale dimensions
Wing area:	3.8206 ft^2	1358.6 ft^2
Wing mean aerodynamic chord:	0.8020 ft.	15.12 ft.
Aspect Ratio:	5.94	5.94

Pitching moments and trimmed drags are referred to a moment reference point at 25%$\bar{c}$ except where stated otherwise.

Corrections to the results have been applied for sting and balance deflection under load, tunnel wall constraint on incidence and drag, tunnel flow pitch angularity, empty-tunnel buoyancy, blockage (assumed zero - see Appendix A), blockage buoyancy, side nacelle internal drag, roughness drag and centre nacelle base pressure. Corrections due to sting interference on lift, drag and pitching moment have also been applied and the drag results have been corrected to a constant $R_{\bar{c}} = 3 \times 10^6$.

A more detailed breakdown and discussion of these corrections is given in Appendix A.

5. DISCUSSION

5.1 Wind Tunnel Results

5.1.1. $C_L \sim \alpha$; $C_m \sim C_L$ Results

Figures 3(a-c) and 4(a-c) present the measured $C_L \sim \alpha$ results for M = 0.50 to M = 0.92 for each of the four model configurations tested. The effect of $C_L \sim \alpha$ of adding the fin and faired centre nacelle (Configuration 690601) compared to the basic wing + body + wing fences + fin stub (690701) is negligible, whereas the addition of the side nacelles and supporting pylon (690500) is to give a slight reduction in the overall C_L (except at high C_L) together with a slight increase in the lift-curve slope. An examination of the rear fuselage loads and wing pressures obtained

in/

in the twin sting tests indicated that, although the nacelles do carry a small down load, the main reason for the negative lift increment due to nacelles is an increase in the wing upper surface pressures. This forward pressure influence of the nacelles on the wing is confined almost entirely to the upper surface.

Addition of the tailplane and bullet (690201, 690301 and 690402) increases the overall lift-curve slope by about 12%, independent of Mach number and tailplane angle, compared with the tailplane-off configurations. The effect of removing the wing upper surface fences (690101) is very small in the test range except at high incidence for $M \geq 0.84$ where there is a slight loss of lift.

In Figs. 5(a-f) and 6(a-c) are presented the $C_m \sim C_L$ results for the configurations tested. The effects of increasing Mach number for wing + body + fences + fin stub, from $M = 0.50$ to $M = 0.88$ at a constant $C_L = 0.20$, are to give a C_m change of $\Delta C_m = -0.007$ and to move the aerodynamic centre rearwards from about 19%$\bar{c}$ to about 29%$\bar{c}$. Adding the fin and centre nacelle produces a C_{m_o} change of about -0.004, i.e., a nose down increment.

Addition of the side nacelles and pylons gives a slight positive C_{m_o} increase and a slight increase in static stability. The tailplane-on results of Fig. 5 indicate a tailplane power of about $\frac{\partial C_m}{\partial \eta_T} = -0.035$/degree at low M increasing to about -0.050 at high Mach number. For a constant tailplane angle there is also a slight increase in C_{m_o} with increasing Mach number. The effect of the wing fences on both C_{m_o} and the $C_m \sim C_L$ variation is almost negligible in the test range.

5.1.2. Trimming

In Fig. 7 is presented the variation of tailplane angle to trim, over a range of trimmed C_L and Mach number, for two c.g. positions. The two c.g. positions chosen correspond with those studied in the flight data, namely 16%$\bar{c}$ and 25%$\bar{c}$. As Mach number is increased, at a constant trimmed C_L, the net effect of the C_m changes, both tailplane-off and for a constant tailplane angle, and the change in tailplane power mentioned earlier, is to increase the necessary tailplane angle to trim for both c.g. positions. For trimmed C_L's which required a negative η_T an extrapolation of the three available η_T (single sting) was made.

In Fig. 8, the effect of c.g. position on the tailplane lift necessary to trim at a given Mach number and C_L, can clearly be seen. The negative value of $\frac{\partial C_{L_T}}{\partial C_L}$ for the 16%$\bar{c}$ c.g. position is related to the fact that $\frac{\partial C_m}{\partial C_L}$ (tail-off) is also negative whereas $\frac{\partial C_m}{\partial C_L}$ (tail-off) is positive for the

25%$\bar{c}$/

25%$\bar{c}$ c.g. For the 16%$\bar{c}$ c.g., the majority of flight data being at this condition, C_{L_T} varies between about C_{L_T} = +0.002 and C_{L_T} = -0.016 for the trimmed C_L range C_L = 0 to C_L = 0.50.

5.1.3. Drag Breakdown and Comparison with Estimates

Figs. 9(a-h) show the $C_D \sim M$ results for each of the model configurations tested together with a summary, Fig. 11, of the effect of C_L on the $C_D \sim M$ characteristics of the wing + fuselage configuration.

Considering first the drag at zero lift, the measured value for the wing + fuselage + fences configuration at M = 0.50 is C_D = 0.0149*. Assuming that the drag increment due to fences is the same as that measured on the complete model, this gives C_D = 0.0147 for the wing + fuselage as compared with an estimate of C_D = 0.0146. This estimate, which is explained in detail in Appendix B, was produced by a method broadly similar to that of the Royal Aeronautical Society Data Sheets, using a reduced length/diameter ratio for the fuselage. No allowance was made for the canopy, although the windscreen flats were represented on the model. Strictly, no sectional test data are available for the Trident 1 wing section but Ref.(1) gives data for a Trident 1E section which would be expected to have similar drag characteristics at low C_L. We are able to make a simple comparison of experimental and estimated wing form factors because the two-dimensional section (corresponding to a 9% thick streamwise section at the leading edge kink on the 1E wing) had the same t/c (10.5%) as the streamwise section at the trailing edge kink on the Trident 1 wing. These results gave a form factor at M = 0.50, C_L = 0.10 which is about 7.5% below the value of $\lambda_{unswept}$ used in Appendix B. This is broadly consistent with the evidence in Ref.(2) which shows that estimates by the method of Appendix B tend to exceed measured sectional data by about 5%. As regards the variation of C_D with M prior to the steep drag-rise, the sectional data gave an increase at C_L =0.1, of 7% in $\lambda_{unswept}$ between low speed and conditions equivalent to M = 0.76 on the swept wing; this compares with a measured increase in drag for the present Trident model wing-fuselage of about 5% of the estimated wing drag at $R_{\bar{c}} = 3 \times 10^6$.

At first sight, the agreement between the measured and estimated drags for the wing + fuselage at zero lift is very good but it seems that this may be somewhat coincidental. As noted above, an improved estimate (ignoring interference effects) might give a somewhat lower value but to compensate for this, it can be argued that the measured value is increased by some wing-body interference. Tests, reported in Ref.(3), with a series of wing-body fillets have shown for example that a lower drag, by about ΔC_D = 0.0003, could be obtained with a different set of fillets at the wing root trailing edge.

At/

* This value can perhaps be reduced by ΔC_D = 0.0001 when comparing with estimates since the measured change in drag coefficient between C_L = 0 and C_L = 0.1, at M = 0.50, is about 0.0001 less than the estimated change in ideal vortex drag, thus implying some excess drag at C_L = 0.

At M = 0.50, the drag-due-to-lift factor, K, has a value of K = 1.15 up to C_L = 0.40 becoming slightly larger at higher C_L. At M = 0.78, for the reasons discussed below, the value of K has increased to 1.29 for the range up to C_L = 0.4, and 1.39 at higher C_L.

The effects of C_L on the variation of C_D with M for the wing + fuselage configuration are presented in Fig. 11. The main features (labelled on the figure) can be summarised as follows:

(A) The Mach number (M_D) for the start of the steep drag rise (defined as the Mach number at which $\frac{dC_D}{dM} = 0.05$) is at its highest (0.88_5) at C_L = 0.2, decreasing to 0.86 by C_L = 0 and 0.84 by C_L = 0.45,

(B) There is a significant increase in C_D with M below M = M_D varying from about 0.0017 at C_L = 0 to 0.0021 at C_L = 0.2, 0.0022 at C_L = 0.3, 0.0034 at C_L = 0.4 and 0.0038 at C_L = 0.45,

(C) Up to about C_L = 0.2, this increase in C_D with M below M = M_D occurs smoothly but at and above C_L = 0.25 there is a greater tendency for the increase to appear near M = 0.80, followed by a near-plateau. The range near M = 0.80 contributes 0.0008 to C_D at C_L = 0.3 rising to 0.0015 at C_L = 0.4. It is believed that the wing-root region is responsible for this premature drag-rise near M = 0.80. Pressure plotting measurements on an earlier version of the same model showed that there is a notable change in the shape of the upper-surface pressure distribution near the wing root under these conditions. A local supersonic region appeared to be extending rearwards prior to the start of the steep drag-rise for the wing as a whole and hence, it seems likely that the increase in C_D near M = 0.80 is associated with the losses due to a local shock in the wing-fuselage junction,

(D) At and above C_L = 0.35, the increase under (C) is preceded by another increase which reaches a maximum near M = 0.74. There is little change in C_D between M = 0.74 and 0.78 thus implying some recovery from the first hump. Again, pressure distributions on various models have shown that this type of hump in the variation of $C_D \sim M$ at relatively high C_L can be traced to excess profile/wave drag due to the suctions near the wing leading edge over part of the upper surface being too high at moderate Mach numbers but then decreasing to give a better conditioned peaky pressure distribution near M = M_D.

Both flow phenomena (C,D) were discussed in Ref.(4).

The C_D increment due to adding the fin and faired centre nacelle is about ΔC_D = 0.0015 for most of the test range, generally being a little more at low Mach number and low C_L and a little less at high Mach number and high C_L.

In/

In addition, major effects of Mach number are delayed slightly. A simple estimate (see Appendix B) of the extra drag of the fin and faired centre nacelle gives only $\Delta C_D = 0.0011_s$. Possible areas responsible for the excess drag are the gully between the nacelle and the fuselage and the falling top line of the nacelle as it blends with the fin. The shift of major Mach number effects to slightly higher Mach number must indicate that the influence of the fin and centre nacelle on the inner wing is beneficial which is a further hint that major adverse supercritical-flow effects occur first on the inner wing.

Adding side nacelles and pylons gave (after subtraction of the internal drag) a mean C_D increment of about 0.0021, with a small increase from low to high Mach number, except where simple differences are rendered somewhat erratic by a tendency for major Mach number effects to occur at slightly higher Mach number with nacelles than without. The flow through the nacelles was not representative of full scale and hence, whereas there is thought to be very little spillage drag penalty in cruise flight, it is likely that at typical tunnel conditions, with $\frac{A_o}{A_i} \simeq 0.43$, spillage drag is responsible for about $\Delta C_D = 0.0005$*. The remaining $\Delta C_D \simeq 0.0016$ is 1.5 times a simple estimate (see Appendix B) ignoring interference effects. At $C_L = 0.45$ the nacelle drag increment has increased to about $\Delta C_D = 0.0024$, up to about M = 0.78. After removal of the spillage drag penalty this leaves about 1.8 times the simple estimate.

Features which might lead to excess drag on the nacelles and pylons are (a) the divergent channels between the rear parts of the nacelles and the fuselage, (b) the slope discontinuity where the "jet pipe" projects beyond an extrapolation of the nacelle profile, (c) the bluff base on the model jet pipe and the considerable projected base area of the pen-nib fairing**, and (d) the proximity of the pylon leading edge to the intake lip***.

In defining increments due to adding the tailplane and bullet it is necessary to specify the tail setting in some way. For comparison with estimates it seems best to choose the condition at which the tailplane carries no lift. The measured drag increment for the tailplane + bullet varies, for all Mach numbers below the steep drag-rise, between about $\Delta C_D = 0.0024$ at $C_L = 0$ and $\Delta C_D = 0.0019$ at $C_L = 0.40$, compared with an estimate of $C_D = 0.0022$ (see Appendix B). As with the wing, the estimate for the tailplane drag may

be/

---

* An interpolation of data in Ref.(5) was made to produce this spillage drag figure.

** Low speed wind tunnel tests at Hatfield on these nacelles and pylons, in isolation, gave higher drag coefficients than tests on smaller scale nacelles which had a better representation of the full scale nacelle boattail and pennib. As reported in Ref.(6), this drag difference could be partly accounted for by a low energy region in the nacelle wake, shown by a pitot wake traverse, caused by the pitot pressure tube in the nacelle duct.

*** Tests in the A.R.A. tunnel on another configuration with aft mounted nacelles have shown that extending the nacelles forward sufficiently to bring the peak-suction region on the forecowl (in isolation) ahead of the leading edge of the pylon can give a significant reduction in drag, particularly at high Mach number. These results are reported in Ref.(7).

be about 5% too high (see Ref.(2)) but this would still mean that the measured drag is above estimate at low C_L and below estimate at high C_L. Two points should be mentioned here. The first, at $C_L = 0$, the tailplane setting for $C_{L_T} = 0$ is about $\eta_T = +2°$ and at this setting, the mechanical design of the bullet is such that there is a pronounced forward facing step on the top of the bullet. This step, a likely source of excess drag, is not present at the tailplane angles required to trim at high C_L. Second, it is possible that the tailplane-off datum is really somewhat "unfair": it contains a rather crude half-body fairing on the top of the fin and also, one can argue that the fin itself is "changed" from a low to a high aspect ratio surface by the addition of the tailplane with its end plate effect. It may be preferable therefore to compare the combined measured fin + tailplane drag increment with the combined estimate. When this is done, it is found that the measured increment varies from $\Delta C_D = 0.0042$ at $C_L = 0$, $M = 0.5$ to $\Delta C_D = 0.0033$ at $C_L = 0.40$, $M = 0.5$, compared with an estimate of C_D for the fin + tailplane of $C_D = 0.0033_8$.

As with the other rear fuselage components, the tailplane tends to delay the steep drag rise, again presumably by its effect on the inner wing. The drag creep on the complete model is of the same order of magnitude as on the wing + fuselage + fences configuration.

With the centre of gravity at 25%$\bar{c}$, the trim drag penalty, i.e., the difference between the trimmed and $C_{L_T} = 0$ curves, is very small and appears to be swamped by experimental scatter for most of the test range. Fig.10 shows however, that with the 16%$\bar{c}$ c.g. the trimmed drag is higher than with the 25%$\bar{c}$ c.g. by an amount that increases steadily with C_L up to $\Delta C_D = 0.0004$ to 0.0006 (depending on M) at $C_L = 0.45$.

The variation of the complete model drag with Reynolds number is compared with theory in Fig. 12. Although no individual experimental points are shown on this figure a check on the experimental curve showed that 97% of the experimental points were within $\Delta C_D = \pm 0.0001$ of the mean line.

The relative slopes of the two curves, together with the results from the flow visualization tests described earlier, indicate that the model boundary layer was fixed by the Ballotini transition fixing bands. The theoretical variation of Fig. 12 is based upon the Prandtl-Schlichting $C_f \sim R$ variation of Ref.(8). The 20% difference in slopes, between theory and measurement of Fig. 12, can be reduced to 10% by the use of the Spalding and Chi relationship of Ref.(9). A possible cause of the slope difference, between theory and measurement, could be a slight overfixing of the boundary layer at high R, with a consequent extra roughness drag penalty, the roughness band being of optimum size at low Reynolds number.

5.2 Flight Results

5.2.1 Introduction

Before embarking on a detailed discussion of the method of analysis of the flight data of Ref.(10), and the results of the flight/tunnel drag comparison, it is worth noting several important points about the data. The full scale aircraft drag was obtained from Net thrust where Net thrust = Gross thrust - Intake momentum drag. Gross thrust was obtained by jet pipe pressure measurement using nine pressure probes in each jet pipe, together with a Rolls-Royce sea level calibration curve of Effective Jet pipe area ~ Jet pipe pressure ratio. Intake momentum drag was estimated using Rolls-Royce sea level test bed mass flow measurements, with an allowance of 2% pressure loss for the centre engine intake, at the measured low pressure stage $\frac{\text{r.p.m.}}{\sqrt{T_1}}$, the T_1 being obtained from the measured outside air temperature. The measurements were made with the aircraft in a clean condition (flaps and undercarriage up) during straight and level cruises with all engines operating. Although all data were recorded during trimmed flight it should be noted that the aircraft c.g. position was not constant throughout the test series. The majority of data is for a mean forward c.g. at 16%$\bar{c}$. In most cases the propelling nozzles were choked but for some data, particularly at low M, the nozzles were unchoked, as determined from an examination of the measured exit nozzle pressures.

5.2.2 Methods of Analysis

In order to highlight any trends in the flight drag data relative to the wind tunnel data, and to examine the effects of Reynolds number in flight, drag differences between individual flight data points and trimmed tunnel drag results (corrected to $R_{\bar{c}} = 3 \times 10^6$) for the same M, C_L and c.g. position have been plotted against the Reynolds number of the flight points in Figs. 13 a, b and 14 a, b. Fig. 13 presents data for the forward c.g. with the points identified according to C_L in Fig. 13a and according to M in Fig. 13b. Figure 14 is a similar presentation of the aft c.g. data. The most important points from these curves are presented below:-

(i) In a particular M and C_L band the unchoked data points appear to have a higher drag than the choked data points by about $\Delta C_D = +0.0005$. According to Ref.(11), which gives values of A_o/A_i for each data point, at a cruise $C_L = 0.25$ for the choked data the mean $A_o/A_i = 0.560$ whilst the mean $A_o/A_i = 0.578$ for the unchoked data. From Ref.(11), these two figures would imply a difference in spillage drag of only about $\Delta C_D = 0.0000_8$, i.e., a small additional drag increment due to having unchoked propelling nozzles. It should be noted here that gross thrusts, as determined from jet pipe pressure measurements together with a Rolls-Royce sea level calibration curve of Effective jet pipe area ~ Jet pipe pressure ratio would generally be subject to larger random errors for an unchoked than a choked nozzle, and also that systematic errors due to the influence of the external flow on the nozzle flow are possible for an unchoked nozzle. In addition, altitude effects on

effective/

effective jet pipe areas are generally largest for nozzle pressure ratios below and around choking conditions. For the Spey engine however these effects are small.

(ii) The low Mach number data points ($M < 0.60$) throughout the complete Reynolds number range tend to have a higher (flight - tunnel) drag increment than data points at higher Mach numbers ($M = 0.60$ to 0.80). It should be noted that in the (flight - tunnel) drag increment mentioned above, the tunnel drag is corrected to $R_{\bar{c}} = 3 \times 10^6$. At low Mach number most data points are for an unchoked condition and accordingly, from (i), could have a small additional spillage drag increment and significant errors in thrust measurement.

(iii) In the absence of any other definite trends, either with Mach number of C_L, in ΔC_D (flight - wind tunnel) a mean line has been drawn through the 16%$\bar{c}$ c.g. data which may represent the shape of the mean flight profile drag variation with Reynolds number although the apparent experimental scatter remaining in the flight data makes it impossible to be any more definite. Up to $R = 3.03 \times 10^6$/ft. ($R_{\bar{c}} = 45.8 \times 10^6$ Full scale) this line is parallel to the simple profile drag estimate derived in Appendix B. The derived flight line is considered to be a fair mean of all the 16%$\bar{c}$ (i.e., both choked and unchoked data). For $R > 3.03 \times 10^6$/ft, one can conclude that the value of ΔC_D (flight - tunnel) remains constant at $\Delta C_D = -0.0039$. To avoid any confusion at this point, it is worth reiterating that the "tunnel" results have been corrected to a single Reynolds number ($R_{\bar{c}} = 3 \times 10^6$) and hence, a "constant value of ΔC_D" implies no change in the flight drag with Reynolds number. As mentioned earlier this mean line has been drawn considering only the 16%$\bar{c}$ data. It will be seen however, that the mean line is also a good fit to the 25%$\bar{c}$ data in Fig. 14. Comparing the overall mean variation of $\Delta C_D \sim R/ft$ with the variation of profile drag ~ Reynolds number of a rough plate, Ref.(8) would indicate an equivalent distributed roughness of approximately 0.00045 inches on the full scale aircraft.

5.3 Wind Tunnel - Flight Comparison

5.3.1 Correction of Flight Results

In Figs. 15 (a-c) are presented a comparison of the wind tunnel and measured flight drags both adjusted to comparable conditions, each figure being for a different method of analysis of the flight data.

In all these figures the 25%$\bar{c}$ flight data has been corrected to the further forward 16%$\bar{c}$ c.g. position by using the ΔC_D (due to c.g. movement) differences of Fig. 10. This correction to the flight data assumes that the flight and wind tunnel trim drag penalties, due to c.g. movement, are the same. Each flight data point has been corrected to a nominal C_L in the range $C_L = 0.15\ (0.05)\ 0.35$ according to whichever C_L it was nearest. As with the drag correction necessary to account for a change in c.g. position the above correction is derived from the wind tunnel results. In this case the assumption is that the variation of C_D with C_L in flight, for C_L changes of less than 0.025, can be taken as the same as in the wind tunnel. Only the wind tunnel curves have been corrected for spillage, but as discussed earlier the spillage drag in flight is thought to be insignificant.

Dealing/

Dealing next with Reynolds number corrections to the flight data, Figs. 15 (a-c) are distinguished by the labels "Flight Reynolds number effects as for smooth surface", "Flight Reynolds number effects as for recommended mean line in Fig. 13" and "No Reynolds number effects in flight" respectively. A value of $R = 2.4 \times 10^6$/ft full scale ($R_{\bar{c}} = 36.3 \times 10^6$) was chosen as a convenient datum and the flight data were corrected to that datum using the methods (detailed below) implied by the three labels. For Fig. 15a, the variation with Reynolds number over the whole flight range of $R = 1.92 \times 10^6$/ft to $R = 3.62 \times 10^6$/ft ($R_{\bar{c}} = 29.0 \times 10^6$ to $R_{\bar{c}} = 54.6 \times 10^6$) was assumed to be parallel to the simple drag estimates of Appendix B. For Fig. 15b, the same variation was assumed for $R < 3.03 \times 10^6$/ft ($R_{\bar{c}} = 45.8 \times 10^6$) and a constant correction of $\Delta C_D = + 0.00044$ was applied to data points taken at $R > 3.03 \times 10^6$ i.e., the variation was assumed to be parallel to the mean line drawn through the data in Fig. 13. For Fig. 15c no Reynolds number corrections were applied as Reynolds number was assumed to have no effect in the flight test range. As can be deduced from Fig. 13a, the C_L and Reynolds number distribution of the flight data is insufficient for the effects of each to be separated. The low C_L points are generally at a higher Reynolds number than the high C_L points and hence, since the Reynolds number corrections of Figs. 15a and 15b are the same up to $R = 3.03 \times 10^6$/ft, there will be a tendency for the low C_L curves of Figs. 15a and 15b to be different, and the high C_L curves to be the same.

5.3.2 Correction of Wind Tunnel Results

The wind tunnel data of Fig. 10 was originally corrected to a constant $R_{\bar{c}} = 3 \times 10^6$. The further corrections to a constant $R_{\bar{c}} = 36.3 \times 10^6$ ($R = 2.4 \times 10^6$/ft full scale) in Figs. 15 (a-c) have been made by extrapolating parallel to the estimated $C_{D_{pr}} \sim R_{\bar{c}}$ variation of Appendix B. The correction from model to full scale conditions results in a change of profile drag of $\Delta C_D = -0.0056_s$, based on the Prandtl-Schlichting relationship of Ref.(8). It is suggested later that it might be more appropriate to use a more recent relationship, e.g., Spalding and Chi (Ref.(9)) which forms the basis of the R.Ae.S.D.S.68020. An alternative method of converting the wind tunnel data to flight conditions is discussed later in section 5.3.3 (ii).

An allowance of $\Delta C_D = 0.0021$ (from Ref.(12)) has been added to account for items not present on the model, items such as silencers, thrust reversers, internal flow systems, gaps and all excrescences. It should be noted that an earlier estimate (Ref.(13)) of the drag of items not present on the model gave $\Delta C_D = 0.0026$ for the same items as in Ref.(12). As a measure of the uncertainty in the above figures it is worth noting that combining individual terms from Refs.(12) and (13) could give any drag allowance between $\Delta C_D = 0.0016$ and $\Delta C_D = 0.0031$. In addition a spillage drag correction of $\Delta C_D = -0.0005$ has been applied to the tunnel results. The net correction of $\Delta C_D = -0.0040_s$ has been applied to the 16% $\bar{c}$ wind tunnel results of Fig.10 to produce the wind tunnel carpet plots in Figs.15(a-c).

It/

It is realised that the use of the same Reynolds number correction in Fig. 15c as used in Figs. 15a, b is somewhat inconsistent with the definition of Fig. 15c. It is common practice, however, to assume no Reynolds number effect in flight but still to assume a full "smooth surface" profile drag variation when correcting the wind tunnel results to a typical flight Reynolds number. If the wind tunnel results were corrected by assuming a "smooth surface" variation only to $R = 1.9 \times 10^6$/ft., which is the highest Reynolds number to which the profile drag may be assumed to vary and still be consistent with the assumptions of the flight analysis of Fig. 15c, the extrapolated wind tunnel results would be $\Delta C_D = 0.0004$ higher.

5.3.3 Comparisons

The correlation between the adjusted wind tunnel results and the three flight data analyses will be discussed in the order of (i) the correlation between the flight and wind tunnel drag levels over most of the Mach number range, (ii) the low M comparison and (iii) the drag rise Mach number agreement.

(i) In Fig. 16 the drag differences, both absolute and as a percentage of the low speed corrected wind tunnel drag, (i.e., wind tunnel drag corrected to $R_{\bar{c}} = 36.3 \times 10^6$ and with an allowance for items not present on the model) between each flight analysis and the corrected wind tunnel results are plotted against Mach number. At $C_L = 0.15$ and 0.20 the agreement is with about +1% to +5% over the whole Mach number range, and nearly so at $C_L = 0.25$, although at $C_L = 0.35$ the agreement is within about +5% only over the range M = 0.59 to M = 0.81 (the highest flight data point). If the Spalding and Chi relationship (Ref.(9)) were used instead of Prandtl-Schlichting (Ref.(8)) the effect would be to reduce the estimated difference in profile drag, between tunnel and flight Reynolds numbers, by about $\Delta C_D = 0.0004$, which would improve this general level of agreement to about ±3%. It is not possible to suggest conclusively from Fig. 16 which of the three flight data analyses is the best, but it should be remembered that the analysis used in Fig. 15b includes an attempt to deduce the effect of Reynolds number from the flight data (see Fig. 13).

The comparison between flight and tunnel results for drag due to lift depends very much on the assumptions made about Reynolds number effects in flight. The analysis with the "Flight Reynolds number effects as for smooth surface" shows a much slower variation with C_L than the other analyses, and much poorer agreement between tunnel and flight. For example, at M = 0.70 in the range $C_L = 0.15$ to $C_L = 0.30$, the induced drag factor for the above analysis is K = 1.01 compared with values of K.= 1.31, 1.12 and 1.18 for the "No Reynolds number effects in flight", "Flight Reynolds number effects as for recommended mean line in Fig. 13" and wind tunnel results. These values provide further support - on plausibility grounds - to accepting the "Flight Reynolds number effects as for recommended mean line in Fig. 13" analysis, although it should be remembered that the high Reynolds number data cover only a small C_L range.

(ii)/

(ii) The mean lines through the flight data exhibit, with the exception of the $C_L = 0.15$ line of Fig. 15a, a reduction in C_D with M up to about M = 0.65 whereas the wind tunnel data shows either a very small decrease or a rise in C_D between M = 0.50 and M = 0.65. At $C_L = 0.15$ the wind tunnel data has a net increase in C_D of $\Delta C_D = 0.0001$ whereas the flight data falls by $\Delta C_D = 0.0004$ (Figs. 15b, 15c) and increases by $\Delta C_D = 0.0002$ (Fig. 15a). At $C_L = 0.35$ the wind tunnel data has an increase in C_D of $\Delta C_D = 0.0005$ whilst the flight data has reductions of $\Delta C_D = 0.0008$ (Fig. 15c) and $\Delta C_D = 0.0010$ (Figs. 15a, 15b).

It will be seen that, with only one exception at $C_L = 0.30$, the low speed end of the flight curves, where there is an opposite trend to the wind tunnel, have been drawn through unchoked data. The reason for the different behaviour with Mach number in flight and wind tunnel is not clear but possible interpretations of the results are (a) that high drags at low M and high C_L are measured in flight because of some feature of the aircraft not represented on the model or (b) that the thrust measurements with unchoked nozzles are in error because of external flow and/or altitude effects. The present difference between the flight data analysis using the "Flight Reynolds number effects as for recommended mean line in Fig. 13" and the corrected wind tunnel curves at M = 0.50, is within +5% at $C_L = 0.15$ rising slowly to +8% at $C_L = 0.35$. A less favoured method of extrapolating to flight Reynolds numbers is to assume that the excess drag (the difference between measured and estimated drag in the wind tunnel) to be proportional to profile drag, i.e., varies with Reynolds number. Values extrapolated to flight conditions would be between $\Delta C_D = 0.0007$ and $\Delta C_D = 0.0005$ lower, i.e., shapes of curves are very similar but overall levels are changed. Agreement between adjusted tunnel and flight results is clearly better if the first method of correcting to flight Reynolds numbers is used but strictly, in this case the excess drag is too small and the uncertainties too large to prove conclusively which would be the better method in general.

(iii) Except perhaps at $C_L = 0.15$ there are insufficient flight data points at very high Mach number to enable a sufficient distinction to be drawn between the start of the steep drag-rise and scatter in the data. At $C_L = 0.15$ the scatter band appears narrow enough to conclude that M_D (defined as the Mach number at which $\frac{dC_D}{dM} = 0.05$) is given as $M_D = 0.88$ by both the wind tunnel and flight results. At $C_L = 0.25$ the results could be interpreted as suggesting good agreement between flight and wind tunnel, but at higher C_L's no firm conclusions can be drawn.

Due to the reduction of C_D with M at low Mach number a definition of M_D using a certain drag increment (say $\Delta C_D = 0.0020$) above a low speed value, typically M = 0.50, is somewhat inappropriate for the flight results.

6. CONCLUSIONS/

6. CONCLUSIONS

From a series of wind tunnel tests on a model of the Trident 1 aircraft and a comparison of the test results with estimates the following conclusions can be drawn:-

(1) At near zero lift the measured and estimated drags for the wing + body configuration are in close agreement. At low Mach number the value of the induced drag factor is about K = 1.15. At about M = 0.74 and for $C_L > 0.30$ the rate of variation of C_D with C_L^2 has increased due to the onset of compressibility effects on the profile/wave drag of the outer wing. Between M = 0.78 and M = 0.84 compressibility effects in the wing root region tend to produce a drag increase, which increases in magnitude with C_L, before the start of the steep drag-rise.

(2) The measured fin + faired centre nacelle drag increment varies between $\Delta C_D = 0.0018$ at $C_L = 0$, M = 0.50 and $\Delta C_D = 0.0014$ at $C_L = 0.45$, M = 0.50 compared with an estimate of $\Delta C_D = 0.0011_5$. The effect of Mach number throughout the C_L range is to slightly reduce the measured increment. Possible causes of the excess drag, at $C_L = 0$, are nacelle/fuselage interference, the falling top line of the fin and faired centre nacelle intersection and the presence of a rather crude half body fairing, on top of the fin, in the tailplane-off configurations.

(3) After allowance for the nacelle internal drag the measured side nacelle + pylon drag increment varies from about $\Delta C_D = 0.0020$ at $C_L = 0$, M = 0.50 to $\Delta C_D = 0.0024$ at $C_L = 0.45$, M = 0.78 compared with an estimate, ignoring interference effects, of $\Delta C_D = 0.0010_5$. A spillage drag allowance (peculiar to the model) reduces the measured increment to between about 1.5 and 1.8 times the simple estimate. Besides interference effects in the nacelle/fuselage gully, some of the excess drag may be base drag on the pen-nib fairing and the thick walls of the nacelle jet pipe. These base drag effects may not be representative of the full scale aircraft.

(4) At zero tail lift the measured tailplane + bullet drag increment generally varies between about $\Delta C_D = 0.0024$ (e.g., at $C_L = 0$, M = 0.50) and $\Delta C_D = 0.0019$ ($C_L = 0.40$, M = 0.78) compared with an estimate of $C_D = 0.0022$. The low measured drag increment at high C_L probably has no real significance because the combined fin and tailplane measured drag increment is never below estimate. One possible reason for the high drag at low C_L is the presence of a step on the top surface of the bullet.

(5) The addition of each rear fuselage component tends to delay the start of the steep drag rise slightly. At $C_L = 0$ the onset (defined on page 12) occurs at $M_D = 0.86$ for the wing + body with $M_D = 0.88_5$ at $C_L = 0$ for the complete model; at $C_L = 0.25$ the corresponding figures are $M_D = 0.88$ and $M_D = 0.88_5$ respectively.

(6)/

(6) At low C_L the trim drag penalty (defined on page 14) is very small and within the experimental scatter for both c.g. positions considered. With increase of C_L to 0.45 the penalty increases to between ΔC_D = +0.0004 and ΔC_D = +0.0005 for the 16%$\bar{c}$ position and remains very small for the 25%$\bar{c}$ position.

From a comparison of the wind tunnel drag results corrected to a datum full scale Reynolds number, after making allowance for items not present on the model, with three analyses of the available flight data the following points have emerged:-*

(7) In general, except for the range to be discussed in conclusion 8, the level of agreement, apart from scatter, between flight and wind tunnel results adjusted (on an arguable basis) for difference in Reynolds number and items omitted from the model is within ±3%. If the wind tunnel data is corrected to flight Reynolds numbers using the Prandtl-Schlichting relationship the general level of the wind tunnel results is between 0 and 5% below the measured flight data. The absolute standard of agreement is very sensitive to the assumptions made in the estimate of excrescence drag.

(8) In contrast with the wind tunnel results which showed an increase in C_D with Mach number between M = 0.50 and M = 0.65, the flight results apparently show a marked decrease in C_D as Mach number is increased to M = 0.65. Using the basis for adjustment of tunnel results to flight conditions which gave the best agreement in conclusion 7, the wind tunnel underestimates the flight drag, at M = 0.50, by up to 3% at C_L = 0.15 and up to 7% at C_L = 0.35. Possible systematic errors in gross thrust determination, with unchoked propelling nozzles, are suggested as a possible cause of the disagreement.

(9) At C_L = 0.15 the flight and wind tunnel values of M_D (defined on page 19) are in agreement. At C_L's up to 0.25 it is possible to interpret the flight data to show good agreement with the corrected wind tunnel results. At higher C_L's the flight test range is insufficient to draw any conclusions.

(10) The variation of C_D with Reynolds number in flight appears to be parallel to that of the estimated profile drag for $R_{\bar{c}} < 45.8 \times 10^6$ with no variation for $R_{\bar{c}} > 45.8 \times 10^6$. If this is a correct interpretation of the results, and scatter and very limited ranges of independent variation of parameters does leave some doubt, it implies an equivalent sand grain roughness of about 0.00045".

The use of wind tunnel results with a correction for the change to full scale Reynolds numbers, and an allowance for items not present on the model, to predict the full scale aircraft drag therefore gives encouraging results in the cruise region, when account is taken of the uncertainties in these terms. At low Mach number and high C_L the agreement is disappointing, perhaps due to the uncertainties in thrust measurement mentioned in conclusion 8.

REFERENCES/

---

* Conclusions 7 - 9 ignore the comments concerning inaccurate representation of the full scale nacelles on the wind tunnel model mentioned in conclusion (3). The effect of this on the model might be to give a higher nacelle drag increment than that with the correct nacelles, consequently the level of the quoted wind tunnel results, used in the wind tunnel/flight comparison might be slightly higher than it should be. It should be noted again that the wind tunnel results have been corrected for estimated spillage drag.

REFERENCES

No.	Author(s)	Title, etc.
1	Hawker Siddeley Aviation Ltd	Unpublished data.
2	H. H. Pearcey and J. Osborne	On estimating two dimensional section drag. A.R.C.27 872. 28th March, 1966.
3	J. I. Simper	The comparison of the drag of two sets of wing root trailing edge fillets on a Trident 1 model. ARA Model Test Note T.1/12. November, 1968.
4	A. B. Haines	Subsonic aircraft drag An appreciation of present standards. ARA Wind Tunnel Note No. 66. A.R.C.29 662. November, 1967.
5	C. R. Palmer	Engine pod drag. Rolls-Royce (Hucknall) Brochure HK 15. March, 1964.
6	Hawker Siddeley Aviation Ltd	Unpublished data.
7	A. B. Haines and J. G. Wingfield	Results of a test programme designed to exploit the favourable and alleviate the unfavourable interference effects of an aft-fuselage nacelle installation ARA Report No. 13. To be published.
8	Clutter, D. W.	Charts for determining the skin friction coefficients on smooth and on rough flat plates at Mach numbers up to 5.0 with and without heat transfer. Douglas Report ES 29074. P.81944. April, 1959.
9	D. B. Spalding and S. W. Chi	The drag of a compressible turbulent boundary layer on a smooth flat plate with and without heat transfer. J. Fluid Mechanics. Vol. 18. Pages 117-143. May, 1963.
10	Hawker Siddeley Aviation Ltd	Unpublished data.
11	D. H. Tipper	Unpublished data.
12	Hawker Siddeley Aviation Ltd	Unpublished data.
13	Hawker Siddeley Aviation Ltd	Unpublished data.

APPENDIX A/

APPENDIX A

Corrections to Wind Tunnel Data

Corrections to the wind tunnel data contained in this report have been applied in two stages:-

(i) Corrections applied during the computing of the raw tunnel data and

(ii) Corrections applied to the final computed wind tunnel data.

The derivations of these two different sets of corrections are detailed below:-

(i) Corrections applied during computing

(a) Sting and Balance Deflections

Static loadings were conducted prior to the wind tunnel tests to determine $\frac{\partial \alpha}{\partial N}$ and $\frac{\partial \alpha}{\partial m}$, the sting and balance angular deflections due to normal force and pitching moment respectively. These values were used to find the deflections which were then used to modify the nominal incidence.

(b) Tunnel Flow Angularity

Since the tunnel flow was not perfectly aligned with the tunnel working section walls a correction, to account for the flow pitch angularity, was applied to the nominal model incidence. This pitch angularity was determined from a comparison of model erect and inverted $C_L \sim \alpha$ data at various M. The angular correction was defined as that angle necessary to give the same zero lift angle for both the erect and inverted curves.

(c) Tunnel Flow Constraint

Because of a flow constraint imposed by the tunnel working section walls on the working section flow a correction to the lift and drag data was applied. This correction was derived from a combination of theory and factors based on a test with the tunnel working section walls "open and closed" using another model of similar size.

(d) Base Pressure

At this stage the drag results were corrected to a condition of free stream static pressure in the sting hole or the centre nozzle as applicable by use of measured static pressures. Note should be taken, however, of the comments in para. (ii) (c) concerning sting interference.

(ii) Corrections to the Computed Results

(a) Reynolds Number

Since the drag breakdown tests were made at a constant stagnation pressure of 1 atmosphere the computed drags, for any Mach number traverse, are at different Reynolds numbers ranging from $R_{\bar{c}} = 2.43 \times 10^6$ at M = 0.50 to $R_{\bar{c}} = 3.28 \times 10^6$ at M = 0.92. For this reason it was necessary to refer all

drags/

drags to a datum Reynolds number which was chosen as $R_{\bar{c}} = 3 \times 10^6$. Using the estimated $C_{D_{pr.}} \sim R_{\bar{c}}$ variations of Fig. B2, and assuming that the actual model $C_D \sim R_{\bar{c}}$ variations were parallel to the appropriate theoretical curves, than a Reynolds number drag correction, ΔC_D, was found by comparing the estimated $C_{D_{pr.}}$ for any test point $R_{\bar{c}}$ with $C_{D_{pr.}}$ at the datum $R_{\bar{c}}$.

In the extrapolation to flight Reynolds numbers it was assumed that, in the R gap between tunnel and flight, the $C_D \sim R_{\bar{c}}$ variation was parallel to the estimated $C_{D_{pr.}}$ variation. Using this variation an increment, ΔC_D, was subtracted from the measured wind tunnel drags to give the estimated flight drags at $R_{\bar{c}} = 30.24 \times 10^6$. In the estimates for tunnel and flight conditions due account was taken of differences in boundary layer transition positions and in the geometry of the centre nacelle (faired in the tunnel but open in flight) (see Tables B1 to B5 of Appendix B).

(b) Balance Drift

The measurement of drag of each of the various model breakdown configurations was effectively split into two stages, the main body of the run in which an incidence traverse at each M was made, followed by a set of data points at near zero C_L, one at each Mach number, as the tunnel speed was reduced.

Balance drift, due to temperature gradients across the balance, was considered to be zero during the second part of the run, since it was made quickly, and hence any drift indicated by the final wind-off scan was assumed to have taken place in the first part of the run, i.e., the incidence traverses. Accordingly the final set of data points were adjusted for any drift present and, assuming this second set of data points to now be correct, the incidence traverses were adjusted to the level of the corrected data points (the same correction was applied to all data points in any one incidence traverse) thus giving the final set of corrected incidence-traverse results, $C_D \sim C_L$ or $C_D \sim \alpha$. Typical corrections were $\Delta C_D = 0.0003$ at low Mach number and $\Delta C_D = 0.0001$ at high Mach number.

(c) Sting Interference

Due to the presence of the support sting in the single sting tests the measured model lift, drag and pitching moment included some interference effects. From a comparison of the rear end results for the two sets of twin sting configurations (Correct rear fuselage and Distorted rear fuselage with dummy sting) values of this sting interference on lift, drag and pitching moment were derived and applied to the single sting test results.

In order to measure only the rear fuselage loads of the model it was necessary to have a split in the fuselage. Since the sting interference was the difference between the model external loads with the Correct and Distorted rear fuselages, the internal pressure loads, due to the split, were corrected to a common datum which was chosen as working section static pressure.

Although/

Although both the single and twin sting-Distorted rear fuselage drags were corrected for base pressure, typically $C_{P_B} = 0.2$, the correction could have been ignored. This is because the sting correction to drag is simply the difference between Correct and Distorted rear fuselage loads, and since the base pressures were the same, the base pressure correction cancels out.

The underlying assumption in the above method of deriving sting interference corrections is that there is no sting effect upstream of the fuselage split line. From an examination of a limited number of wing pressures it was apparent that this assumption was not completely valid and a correction of $\Delta C_D = -0.0001$, at all Mach numbers, has been applied for these forward effects.

(d) Buoyancy

Due to the static pressure gradients existing in the empty tunnel a correction for the overall buoyancy effect on drag of the model on the single sting was allowed for. This correction was obtained by integrating the product of local static pressure and rate of change of model cross sectional area along the length of the model at each test Mach number. No buoyancy correction was applied to the twin sting results because it would not have any effect on the sting incremental corrections. Corrections were $\Delta C_D = +0.0003$ at low Mach number and $\Delta C_D = -0.0006$ at high Mach number for the complete model.

(e) Blockage and Blockage Buoyancy

It has been common practice in the past to include a blockage correction to Mach number in the corrections applied to model data. From the series of tests referred to in (i) (c) above it appears, however, that within the M-range of these Trident 1 tests the blockage correction is trivial at the centre of the model and a correction of zero has therefore been applied.

The blockage buoyancy correction to drag, due to the model induced longitudinal pressure gradient, was obtained from a knowledge of the theoretical form of the model interference velocity distribution and actual model dimensions together with the results of the (i) (c) tests. The interference velocity varies along the length of the model, being trivial at the mid-point and over the forward part and positive over the rear: hence a buoyancy correction in the sense of reducing the measured drag by an amount increasing with Mach number. The corrections applied varied from $\Delta C_D = -0.0002$ at low Mach number to $\Delta C_D = -0.0006$ at high Mach number for the complete model.

(f) Internal Drag

A drag correction arising from the internal flow of the two side nacelles was estimated using the Net Standard definition of internal drag. Nozzle pressures, measured just inside the nozzle exit plane, were used together with estimates of the nacelle boundary layer thickness. The calculated drag correction was then applied to the "side nacelle on" configurations. An estimate of the drag of the nacelle pitot tube was also made and applied to the measured drags. The total estimated internal drag correction varied from $\Delta C_D = -0.00052$ at $M = 0.50$ to $\Delta C_D = -0.00036$ at $M = 0.90$.

(g)/

(g) Spillage Drag

An interpolation of spillage drag data for axisymmetric pods of various highlight/maximum diameter ratios and various lengths was made to obtain a wind tunnel spillage drag figure which varied slightly with Mach number from about $\Delta C_D = 0.0004_8$ to $\Delta C_D = 0.0006$, (compared with about $\Delta C_D = 0.0001$ for the spillage drag in flight). In view of the uncertainties in the interpolation of the data, together with the fact that the Trident 1 pods are not axisymmetric, a constant spillage drag correction of $\Delta C_D = -0.0005$ was incorporated in the drag allowance used to extrapolate from model to full scale flight conditions (as presented in Figs. 15 (a-c)). No spillage drag allowance has been applied to Figs. 9, 10, 13 and 14.

(h) Drag Penalty of Roughness Bands

From a series of tests on a different model of similar size and shape, tests in which the size of roughness band and Ballotini was varied, an estimate of the drag penalty for the Trident 1 model was made and applied to the measured drags. This penalty was estimated to vary between $\Delta C_D = 0.0001$ at $M = 0.50$ and $\Delta C_D = 0.0002$ at $M = 0.90$.

APPENDIX B

Profile Drag Estimates for the Trident 1

The principal aim of this report has been to compare the measured wind tunnel model drag and the full scale aircraft drag. An essential step in this comparison is the need to be able to accurately predict how the aircraft profile drag will vary between the model and full scale Reynolds number ranges. For the sake of completeness, estimates of the model and full scale profile drag have been presented in some detail with explanatory notes where applicable.

Before discussing the estimates themselves, it is worth noting several important points about the model representation of the full scale aircraft.

On the full scale aircraft there are about 200 excrescences comprising such items as air vents, air intakes, aerials, blisters, fairings, etc. Obviously not all of these items could be represented on a model, in fact it would be meaningless to represent some of them due to the "non-scale effect" of the boundary layer. On the Trident 1 model, no excrescences have been represented and hence any model - full scale comparison must consider the magnitude of the aircraft excrescence drag.

With the exception of excrescences the only major difference between the model and full scale aircraft is in the centre nacelle representation. During the wind tunnel tests the centre nacelle had a wooden fairing fitted ahead of the proper air intake plane. This should be noted when comparing the model and full scale estimated profile drags for the complete aircraft configuration - the estimates at model scale are for a faired centre nacelle.

With regard to the estimates the first important point of debate is in the definition of the various model components. Fig. B1a indicates the intersection lines on all components except the fin-centre nacelle unit, the actual intersection planes being normal to the paper. The side nacelle-pylon, pylon-fuselage and tailplane-bullet intersection lines are coincident with the physical intersection lines.

The intersection line of the wing-fuselage has been defined along the wing "Rib 1 datum" line. It will be seen that, on the wing upper surface, the defined and actual model intersection lines are coincident although on the wing lower surface they are not. For the sake of this analysis the area bounded by the actual wing (lower surface) - fuselage intersection line and the defined intersection line has been termed as fuselage wetted area and treated accordingly.

Fig. B1b indicates the intersection lines for the fin-centre nacelle unit. The portion classed as fin stub is treated with the fuselage and, as indicated, has a half body fairing for the "fin off" configurations. A similar fairing on top of the fin is treated as fin wetted area and is present for the "tailplane-off, fin-on" configuration. The centre nacelle is defined by the bounding lines of the fin and fin stub. Although the rear half of the centre nacelle has a fin section the boundary layer originating from the centre nacelle sweeps across it and hence, it is classed as centre nacelle and treated as such.

For brevity, the fuselage configurations considered in the estimates have been abbreviated to A, B, C and D. In detail the effect of each configuration on the fuselage wetted area is detailed below:-

Configuration A/

Configuration A (Fuselage alone)

Fuselage forebody + parallel section (circular throughout) + afterbody. The total wetted area includes the area of the fin stub and fin stub fairing.

Configuration B (Wing + fuselage)

As configuration A but with the wing root and fillet area subtracted from the total wetted area of configuration A and the wing area inboard of the Rib 1 datum line added to configuration A.

Configuration C (Wing + fuselage + fin + centre nacelle)

As configuration B except that the fin stub fairing wetted area is subtracted from configuration B.

Configuration D (Wing + fuselage + fin + centre nacelle + side nacelles + pylons and tailplane and bullet on or off)

As configuration C except that the fuselage root area of the two side nacelle pylons has been subtracted from the wetted area of configuration C.

In general the estimates are self-explanatory and follow current practice. There are several interpretations of how certain effects should be considered e.g., definition of fuselage fineness ratio to be used in determining the fuselage form factor and the effect of wing sweep angle on the wing form factor. The definitions used for the above examples and others are presented later in this Appendix.

Fig. B2 presents the C_D (estimated profile drag) $R_{\bar{c}}$ for each of the wind tunnel configurations tested, together with an extra curve for the fuselage alone configuration.

TABLE B1

PROFILE DRAG OF FUSELAGE

	MODEL SCALE			FULL SCALE		
Reference Dimensions						
Wing Area (ft^2)	3.8206			1358.6		
Gross Wing Mean Chord $\bar{\bar{c}}$ (ft)	0.8020			15.12		
Lengths (ft)[1]						
Forebody	1.140			21.5		
Parallel Section[2]	2.492			47.0		
Afterbody	1.908			36.0		
Total	5.540			104.5		
Maximum Body diameter(ft)	0.643			12.125		
Effective Fineness ratio[3]	0.148			0.148		
Wetted Areas (ft^2)[4]						
Configuration A	9.597					
B	9.421					
C	9.328					
D	9.241			3286		
R per ft. ($\times 10^{-6}$)	3	4	5	2	3	4
$R_{\bar{\bar{c}}}$ ($\times 10^{-6}$)	2.406	3.208	4.010	30.24	45.36	60.48
R (body length) ($\times 10^{-6}$)	16.62	22.16	27.70	209	314	418
% Transition position[5]	1.5	1.5	1.5	0	0	0
Form factor (λ)[6]	1.114	1.114	1.114	1.116	1.116	1.116
Flat Plate C_f[7]	0.00278	0.00265	0.00260	0.00193	0.00184	0.00175
($\lambda \times$ Flat Plate C_f)	0.00310	0.00295	0.00289	0.00215	0.00205	0.00195
D/q (ft^2)						
Configuration A	0.0298	0.0283	0.0277			
B	0.0292	0.0278	0.0272			
C	0.0289	0.0275	0.0270			
D	0.0286	0.0273	0.0267	7.065	6.736	6.408
C_D						
Configuration A	0.00780	0.00741	0.00725			
B	0.00764	0.00728	0.00712			
C	0.00756	0.00720	0.00707			
D	0.00749	0.00715	0.00699	0.00520	0.00496	0.00472

TABLE B2/

TABLE B2

PROFILE DRAG OF FUSELAGE

	MODEL SCALE			FULL SCALE		
Reference Dimensions						
Wing Area (ft^2)	3.8206			1358.6		
Gross Wing Mean Chord $\bar{\bar{c}}$ (ft)	0.8020			15.12		
Streamwise Local Chords (ft)						
Root[8]	1.282			24.18		
Trailing Edge Kink	0.857			16.16		
Tip[9]	0.348			6.56		
% Thickness-Chord Ratio[10]						
Root	10.18			10.18		
Trailing Edge Kink	10.54			10.54		
Tip	10.00			10.00		
Wetted Area (ft^2)[11]	6.05			2153		
R per ft ($\times 10^{-6}$)	3	4	5	2	3	4
$R_{\bar{\bar{c}}}$ ($\times 10^{-6}$)	2.406	3.208	4.010	30.24	45.36	60.48
% Transition Position	5	5	5	0	0	0
λ Unswept[12]						
Root	1.335	1.335	1.335	1.342	1.342	1.342
Trailing Edge Kink	1.348	1.348	1.348	1.356	1.356	1.356
Tip	1.330	1.330	1.330	1.340	1.340	1.340
50% Chord Sweep[13] (degrees)						
Inner Panel	21.35	21.35	21.35	21.35	21.35	21.35
Outer Panel	31.10	31.10	31.10	31.10	31.10	31.10
λ Swept[14]						
Root	1.291	1.291	1.291	1.297	1.297	1.297
Trailing Edge Kink (inboard sweep)[15]	1.302	1.302	1.302	1.310	1.310	1.310
Trailing Edge Kink (outboard sweep)[16]	1.256	1.256	1.256	1.262	1.262	1.262
Tip	1.242	1.242	1.242	1.249	1.249	1.249
Flat Plate C_f[7]						
Root	0.00338	0.00324	0.00308	0.00240	0.00224	0.00215
Trailing Edge Kink	0.00366	0.00348	0.00334	0.00254	0.00240	0.00229
Tip	0.00432	0.00414	0.00392	0.00292	0.00272	0.00262
Total $\frac{D}{q}$ (ft^2)[17]	0.02809	0.02700	0.02575	7.038	6.603	6.304
C_D	0.00735	0.00706	0.00674	0.00518	0.00486	0.00464

TABLE B3/

TABLE B3

PROFILE DRAG OF FIN

	MODEL SCALE			FULL SCALE		
Reference Dimensions						
Wing Area (ft^2)	3.8206			1358.6		
Gross Wing Mean Chord $\bar{\bar{c}}$ (ft)	0.8020			15.12		
Mean Chord (ft)	0.828			15.60		
Wetted Areas (ft^2)[18]						
Fin	0.370			131		
Fin & Fin Fairing	0.481					
% Thickness Chord Ratio	10			10		
R per foot ($\times 10^{-6}$)	3	4	5	2	3	4
$R_{\bar{\bar{c}}}$ ($\times 10^{-6}$)	2.406	3.208	4.010	30.24	45.36	60.48
R Fin Mean Chord ($\times 10^{-6}$)	2.484	3.312	4.140	31.20	46.80	62.40
% Transition Position[5]	5	5	5	0	0	0
λ Unswept[12]	1.330	1.330	1.330	1.340	1.340	1.340
50% Chord Sweep (degrees)	35.5	35.5	35.5	35.5	35.5	35.5
λ Swept[14]	1.218	1.218	1.218	1.225	1.225	1.225
Flat Plate C_f[7]	0.00370	0.00352	0.00337	0.00256	0.00241	0.00230
λ Swept x Flat Plate C_f	0.00451	0.00429	0.00411	0.00314	0.00295	0.00281
$\frac{D}{q}$ (ft^2)						
Fin	0.00167	0.00159	0.00152	0.411	0.400	0.368
Fin & Fairing	0.00217	0.00206	0.00198			
C_D						
Fin	0.00044	0.00042	0.00040	0.00031	0.00029	0.00027
Fin & Fin Fairing	0.00057	0.00054	0.00052			

TABLE B4/

TABLE B4

PROFILE DRAG OF NACELLES AND PYLONS

	MODEL SCALE			FULL SCALE		
Reference Dimensions						
Wing Area (ft^2)	3.8206			1358.6		
Gross Wing Mean Chord $\bar{\bar{c}}$ (ft)	0.8020			15.12		
Lengths (ft)						
Centre Nacelle[19] (C.N.)	1.740			25.0		
Side Nacelle (S.N.)	0.796			15.0		
Pylons	0.849			16.0		
Maximum Equivalent Diameter[20] (ft)						
C.N.[19]	0.266			2.83		
S.N.	0.144			2.72		
Wetted Areas (ft^2)						
C.N.[19][21]	0.804			242		
S.N. (two)[22]	0.821			292		
Pylons (two)	0.163			58		
$\left[\frac{d}{l}\right]$ C.N.[19]	0.153			0.113		
$\left[\frac{d}{l}\right]$ S.N.	0.181			0.181		
% t/c Pylons	8.4			8.4		
R per foot ($\times 10^{-6}$)	3	4	5	2	3	4
$R_{\bar{\bar{c}}}$ ($\times 10^{-6}$)	2.406	3.208	4.010	30.24	45.36	60.48
R length C.N. ($\times 10^{-6}$)	5.220	6.960	8.700	50	75	100
R length S.N. ($\times 10^{-6}$)	2.388	3.184	3.980	30	45	60
R length Pylons ($\times 10^{-6}$)	2.547	3.396	4.245	32	48	64
% Transition Position[5]						
C.N.	2.5	2.5	2.5	0	0	0
S.N.	1	1	1	0	0	0
Pylons	1	1	1	0	0	0
Form Factor (λ)						
C.N.[6]	1.106	1.106	1.106	1.074	1.074	1.074
S.N.[6]	1.152	1.152	1.152	1.158	1.158	1.158
Pylons[12]	1.282	1.282	1.282	1.284	1.284	1.284
Flat Plate C_f[7]						
C.N.	0.00330	0.00312	0.00304	0.00237	0.00222	0.00214
S.N.	0.00378	0.00360	0.00350	0.00257	0.00242	0.00231
Pylons	0.00375	0.00356	0.00344	0.00256	0.00240	0.00229

TABLE B4 (Continued)

R per ft. ($\times 10^{-6}$)	3	4	5	2	3	4
$\lambda \times$ Flat Plate C_f						
C.N.	0.00365	0.00345	0.00336	0.00254	0.00238	0.00230
S.N.	0.00434	0.00414	0.00403	0.00298	0.00281	0.00268
Pylons	0.00480	0.00456	0.00440	0.00329	0.00309	0.00294
$\frac{D}{q}$ (ft^2)						
C.N.	0.00293	0.00277	0.00270	0.615	0.576	0.556
S.N.	0.00356	0.00340	0.00331	0.870	0.821	0.783
Pylons	0.00078	0.00074	0.00072	0.191	0.179	0.171
C_D						
Centre Nacelle	0.00077	0.00073	0.00071	0.00045	0.00042	0.00041
Side Nacelles	0.00093	0.00089	0.00087	0.00064	0.00061	0.00058
Pylons	0.00020	0.00019	0.00019	0.00014	0.00013	0.00013

TABLE B5/

TABLE B5

PROFILE DRAG OF TAILPLANE AND BULLET

	MODEL SCALE			FULL SCALE		
Reference Dimensions						
Wing Area (ft^2)	3.8206			1358.6		
Gross Wing Mean Chord $\bar{\bar{c}}$ (ft)	0.8020			15.12		
Lengths (ft)						
Tailplane (Mean Chord)	0.478			9.0		
Bullet	1.183			22.3		
Bullet Maximum Effective Diameter(ft)	0.146			2.76		
$\left[\frac{d}{l}\right]$ Bullet	0.123			0.123		
% t/c Tailplane	9			9		
Wetted Areas (ft^2)						
Tailplane	1.589			565		
Bullet[23]	0.337			120		
R per foot ($\times 10^{-6}$)	3	4	5	2	3	4
$R_{\bar{\bar{c}}}$ ($\times 10^{-6}$)	2.406	3.208	4.010	30.24	45.36	60.48
$R_{\bar{c}}$ Tailplane ($\times 10^{-6}$)	1.434	1.912	2.390	18.0	27.0	36.0
R length Bullet($\times 10^{-6}$)	3.549	4.732	5.915	44.6	66.9	89.2
% Transition Position - Tailplane[5]	5	5	5	0	0	0
% Transition Position - Bullet[5]	3.5	3.5	3.5	0	0	0
λ Unswept - Tailplane[12]	1.295	1.295	1.295	1.304	1.304	1.304
50% Chord Sweep - Tailplane (degrees)	27.5	27.5	27.5	27.5	27.5	27.5
λ Swept - Tailplane[15]	1.233	1.233	1.233	1.239	1.239	1.239
λ Bullet	1.080	1.080	1.080	1.087	1.087	1.087
Flat Plate C_f[7]						
Tailplane	0.00406	0.00386	0.00370	0.00276	0.00260	0.00249
Bullet	0.00345	0.00328	0.00317	0.00241	0.00226	0.00216
λ x Flat Plate C_f						
Tailplane	0.00500	0.00476	0.00456	0.00342	0.00322	0.00309
Bullet	0.00373	0.00354	0.00342	0.00262	0.00246	0.00235
D/q (ft^2)						
Tailplane	0.00794	0.00755	0.00724	1.931	1.820	1.748
Bullet	0.00126	0.00119	0.00105	0.315	0.295	0.282
C_D Tailplane	0.00208	0.00198	0.00190	0.00142	0.00134	0.00128
C_D Bullet	0.00033	0.00031	0.00028	0.00023	0.00022	0.00021

TABLE B6/

TABLE B6

SUMMARY OF TRIDENT I PROFILE DRAG ESTIMATES

	MODEL SCALE			FULL SCALE		
R per foot ($\times 10^{-6}$)	3	4	5	2	3	4
$R_{\bar{c}}$ ($\times 10^{-6}$)	2.406	3.208	4.010	30.24	45.36	60.48
C_D Fuselage Alone	0.00780	0.00741	0.00725			
C_D Wing + Fuselage	0.01499	0.01434	0.01386			
C_D Wing + Fuselage + Fin + Centre Nacelle	0.01625	0.01553	0.01504			
C_D Wing + Fuselage + Fin + Centre Nacelle + Side Nacelles	0.01731	0.01656	0.01602			
C_D Complete Aircraft	0.01960	0.01873	0.01808	0.01357	0.01283	0.01224

NOTES ON TABLES B1 - B5/

NOTES ON TABLES B1 - B5

The following brief notes are intended to provide additional information on the method, or source of data, used in Tables B1 to B5

The numbered comments and references etc. refer to the numbers in the Tables.

(1) The "lengths" in Table 1 are projected lengths along the horizontal fuselage datum as opposed to lengths measured along the surface of the body.

(2) Although the length of the parallel section is not used in the estimates it should be noted that it is greater than (2 × Maximum Body Diameter).

(3) This is defined as:-

Effective fineness ratio =

$$\frac{\text{Maximum body diameter}}{\text{length(forebody+afterbody)} + (2 \times \text{Maximum Body Diameter})}$$

(4) From the definition of the four configurations A, B, C and D, it is apparent that the fuselage wetted area is different for each configuration. Considering in detail how the wetted area of C (for example) is derived, we have the following breakdown for the model:-

Forebody wetted area	=	1.692 ft²
Parallel section wetted area	=	5.035 ft² (For A)
Afterbody wetted area	=	2.870 ft² (For A)
Area of two wing roots	=	0.520 ft² (Subtracted)
Area of fin stub fairing	=	0.093 ft² (Subtracted)
Wing area inboard of Rib I datum	=	0.344 ft² (Added)

Considering all these components we have the total fuselage wetted area of Configuration C

$$= (5.035 + 2.870 + 1.692) + (0.344 - 0.520) - 0.093$$

$$= 9.328 \text{ ft}^2.$$

The wetted areas themselves were obtained by graphically integrating the component periphery over its axial length.

(5) Each component of the full scale aircraft has been assumed, for the purpose of the estimates, to have leading edge transition. For the model, transition has been assumed to take place at the start of the roughness band on each component surface.

(6) Obtained from an interpolation of R.Ae.S.Data Sheets Bodies 02.04.01 and 02.04.02 (2nd. Issue, January 1947).

(7) Obtained from an interpolation of M = 0, $C_f \sim R_\ell$ curves of Douglas Report No. ES 29074 (April, 1959).

(8)/

(8) Wing root chord defined as being in the Rib 1 datum plane, i.e., 70.43" full scale from the fuselage centre line.

(9) The tip chord has been defined as the streamwise chord length, at the tip station, of the lines projected along the wing leading and trailing edges.

(10) Although only three streamwise thickness-chord ratios are presented the wing integration of (17) used data for 8 stations.

(11) The wing wetted area is defined as (4 x plan area bounded by the Rib 1 datum line, the wing leading and trailing edges and the rounded tip).

(12) Obtained from R.Ae.S.Data Sheets Wings 02.04.03(a) (April, 1953).

(13) The inner panel is defined as being from the Rib 1 datum to the streamwise chord through the t.e. kink, the outer panel being from the streamwise chord through the t.e. kink to the tip station.

(14) The definition of the swept Form Factor (λ swept) used throughout these estimates is:-

$$\lambda_{swept} = (\lambda_{unswept} - 1) \cos^2 (\Lambda_{0.5c}) + 1$$

where $\Lambda_{0.5c}$ is the angle of sweepback at 0.5c.
The effect of using either $\Lambda_{0.25c}$ or $\Lambda_{t_{max}}$ for this wing, is to reduce the value of λ_{swept}. Using $\Lambda_{0.25c}$ would give a reduction of 2.3% in λ_{swept} compared with the present estimate. Using the $\Lambda_{t_{max}}$ would give a reduction of 1.3%.

(15)(16) Although there is no discontinuity in the variation of streamwise t/c across the trailing edge - leading edge kink line there is a discontinuity in the $\Lambda_{0.5c}$, hence the reason for presenting two values of λ_{swept} at the kink. (15) uses Λ of the inboard panel and (16) uses Λ of the outboard panel.

(17) Total $\left[\frac{D}{q}\right]$ is obtained from an integration of the product of the local chord, local skin friction coefficient and the local swept form factor i.e.,

$$\text{Total}\left[\frac{D}{q}\right] = 4 \int_{\text{Rib 1 datum}}^{\text{tip}} (C_f \times c \times \lambda_{swept})_{local} \, d(\text{span})$$

(18) Figure B1b indicates the definitions used for the fin and fin + fairing wetted areas. When the tailplane and bullet are added the fin fairing is removed.

(19)/

(19) It will be noted that the full scale and model size figures are not in a direct scale ratio to each other. This is because the the full scale aircraft has an open centre nacelle whereas the model has a faired centre nacelle as in Fig. B1b.

(20) Maximum equivalent diameter of the open nacelles is given by

$$\text{M.E.D.} = \sqrt{(\text{Max. C.S.A.} - \text{exit nozzle area})\ \frac{4}{\pi}}$$

For the faired centre nacelle:-

$$\text{M.E.D.} = \sqrt{(\text{Max. C.S.A.})\ \frac{4}{\pi}}$$

(21) The wetted area of the centre nacelle does not include any area covered by the fin on top of the nacelle or area covered by the fin stub, on which the centre nacelle is located, at the bottom.

(22) The wetted area of the side nacelles does not include any area covered by the supporting pylons and is only the external area between the nacelle highlight plane and the end of the propelling nozzle plane i.e., no nacelle internal area is included.

(23) Bullet wetted area does not include any area covered by the fin or the tailplane.

BW

FIG. B1a)

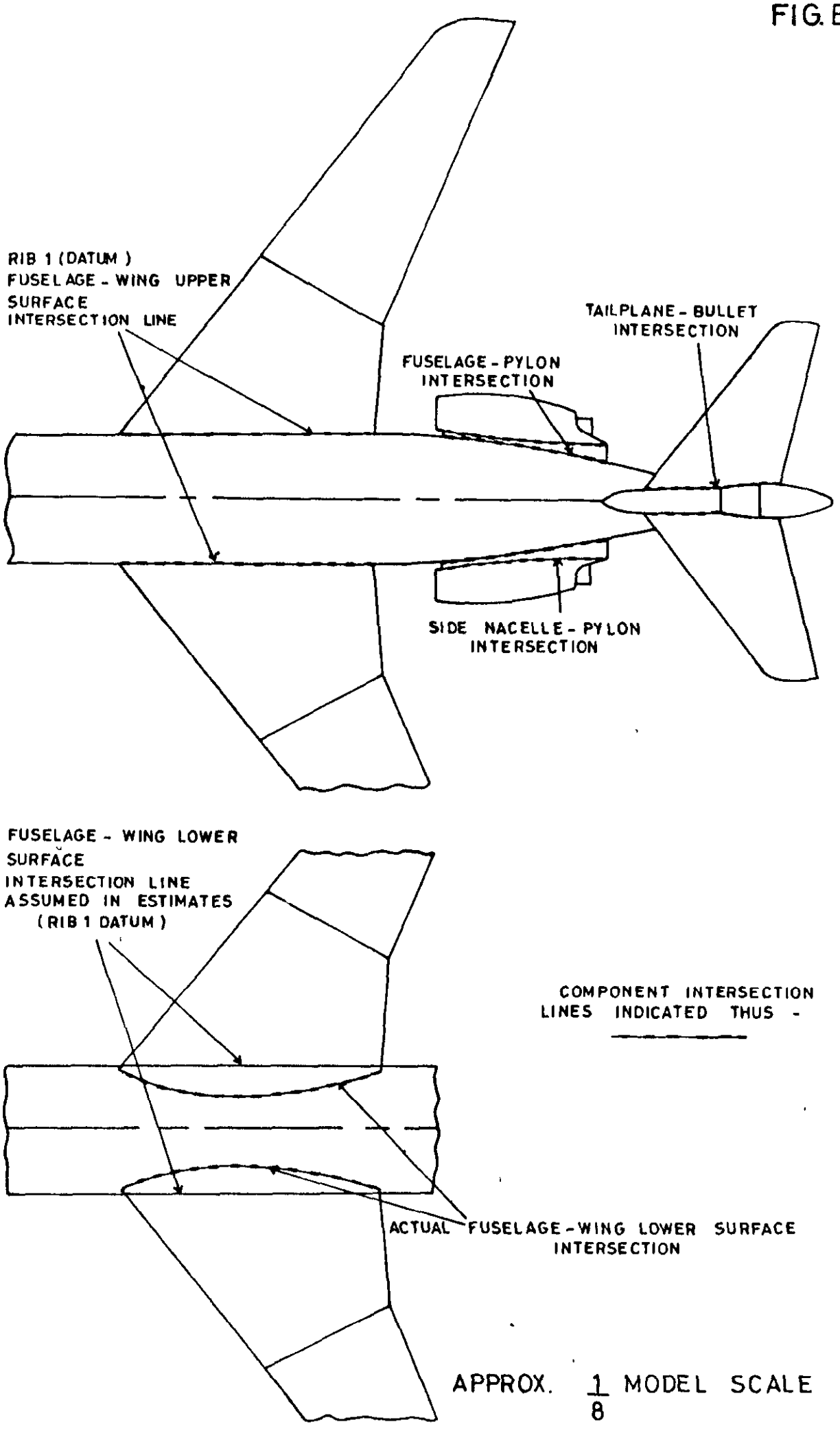

FIG B1a) INTERSECTION LINES FOR TRIDENT 1 MODEL.

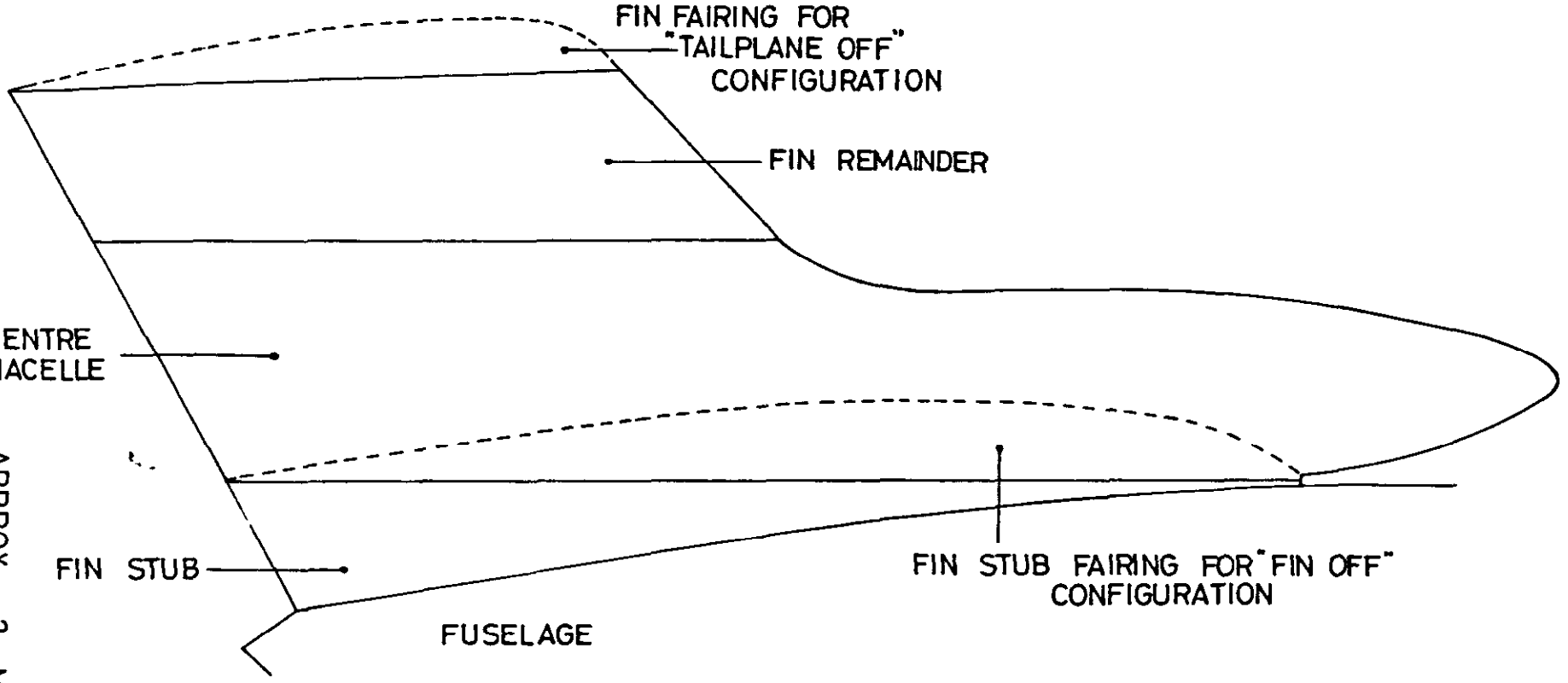

FIG. B1b) INTERSECTION LINES FOR FUSELAGE - FAIRED CENTRE NACELLE - FIN UNIT

FIG.B2

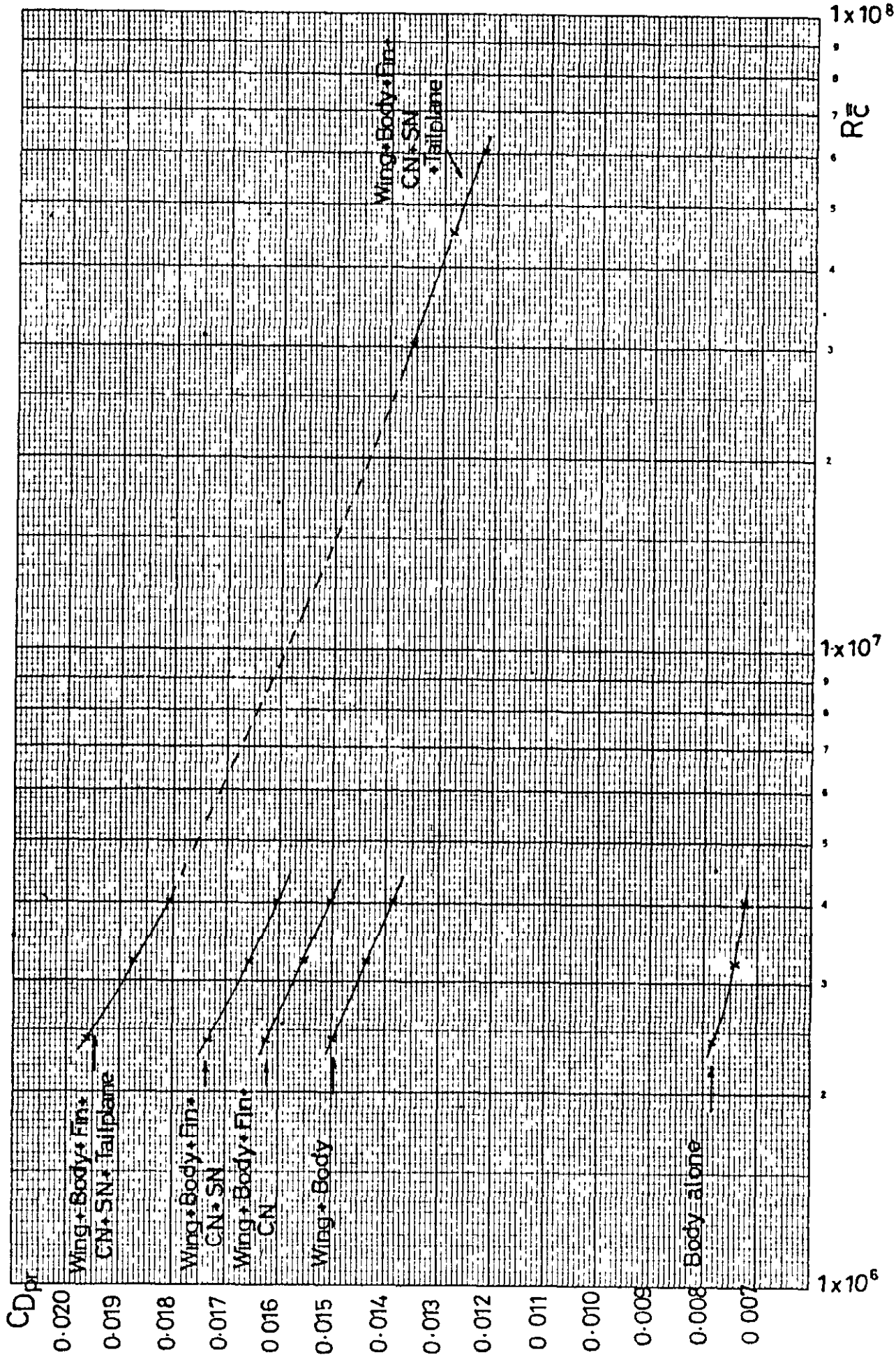

FIG. B2 ESTIMATED PROFILE DRAG VARIATION WITH REYNOLDS NUMBER.

FIG 1

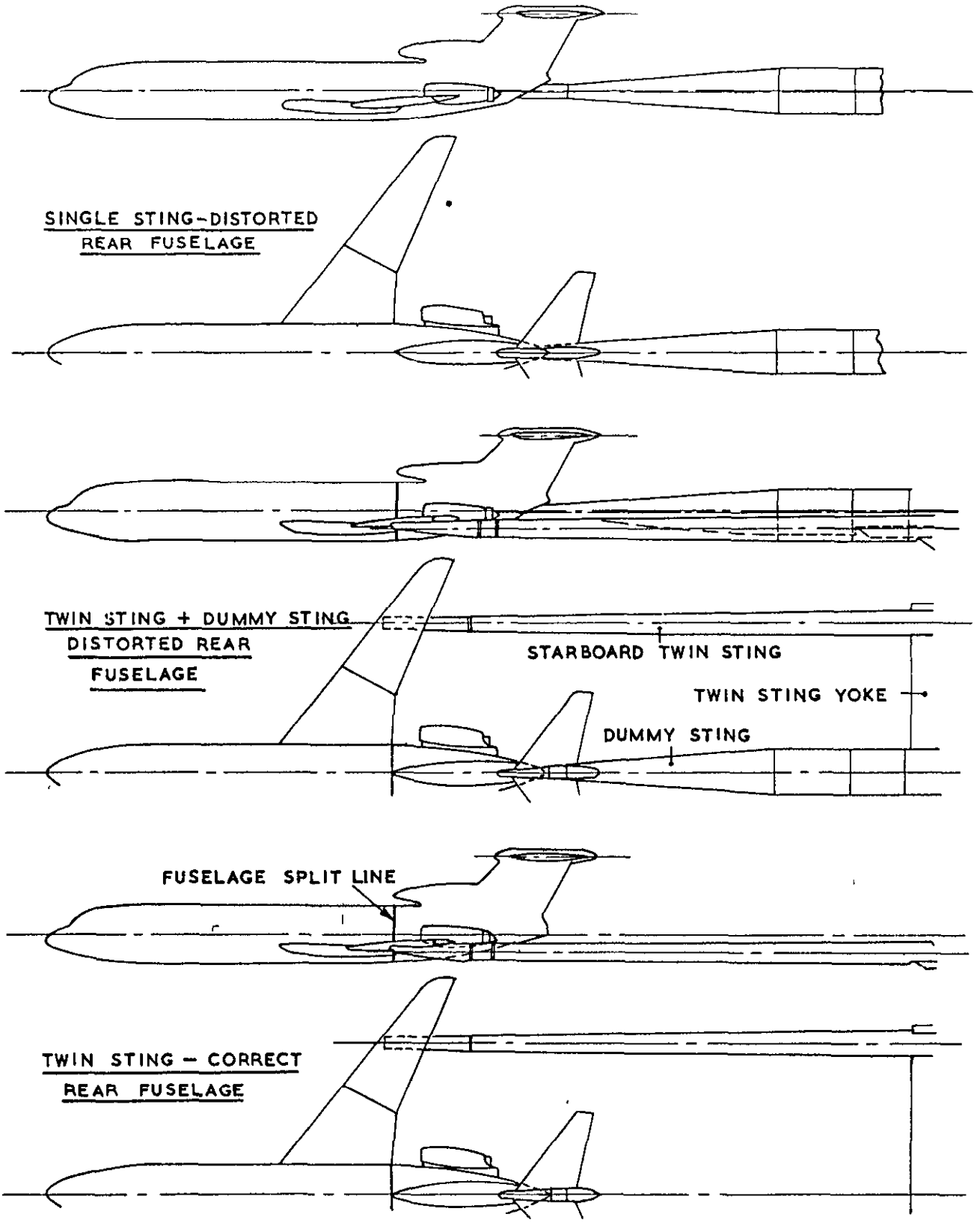

FIG. 1 MODEL SUPPORT SYSTEMS.

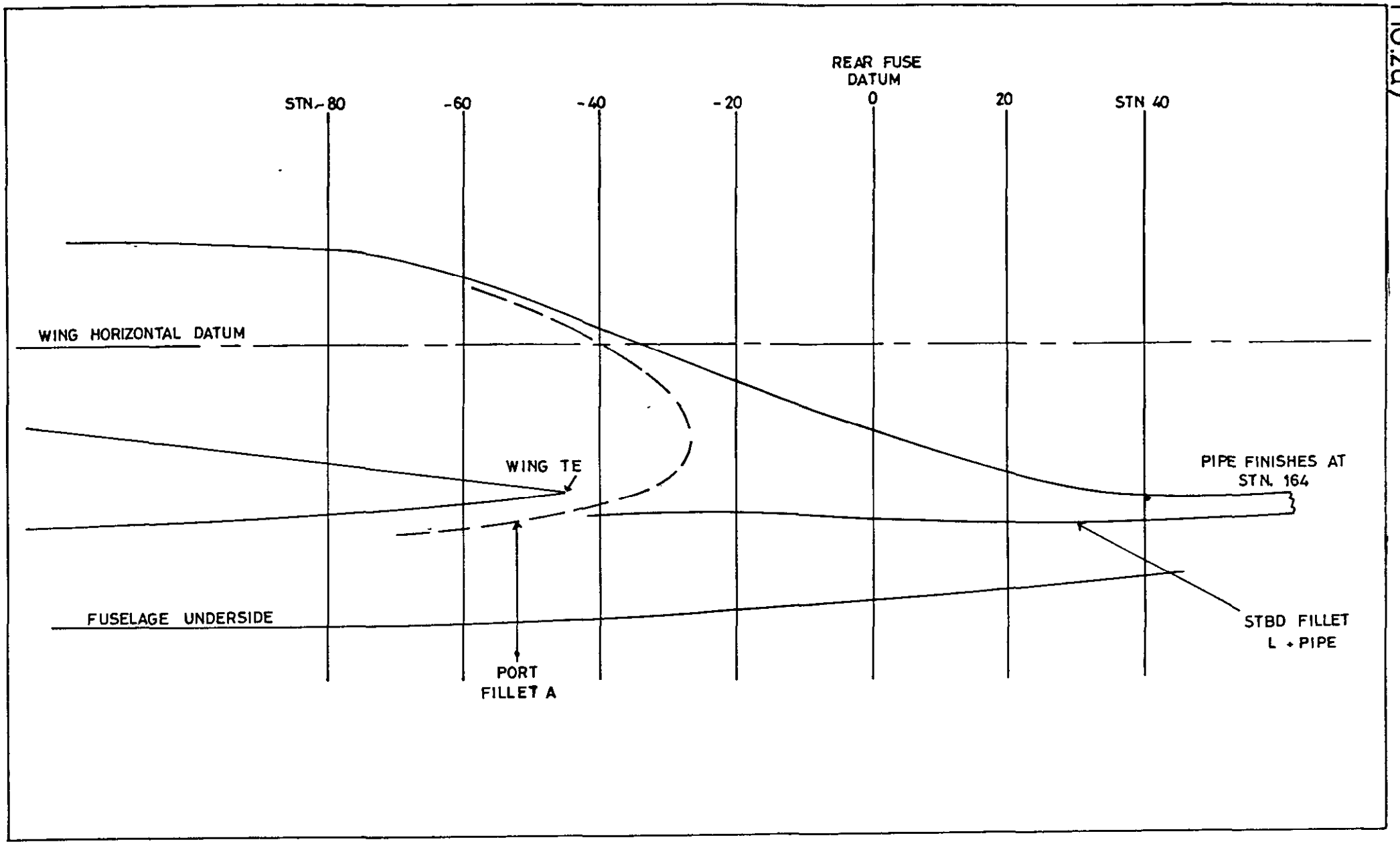

FIG.2a)

FIG. 2a) SIDE VIEW OF MODEL WING ROOT TRAILING EDGE FILLETS.

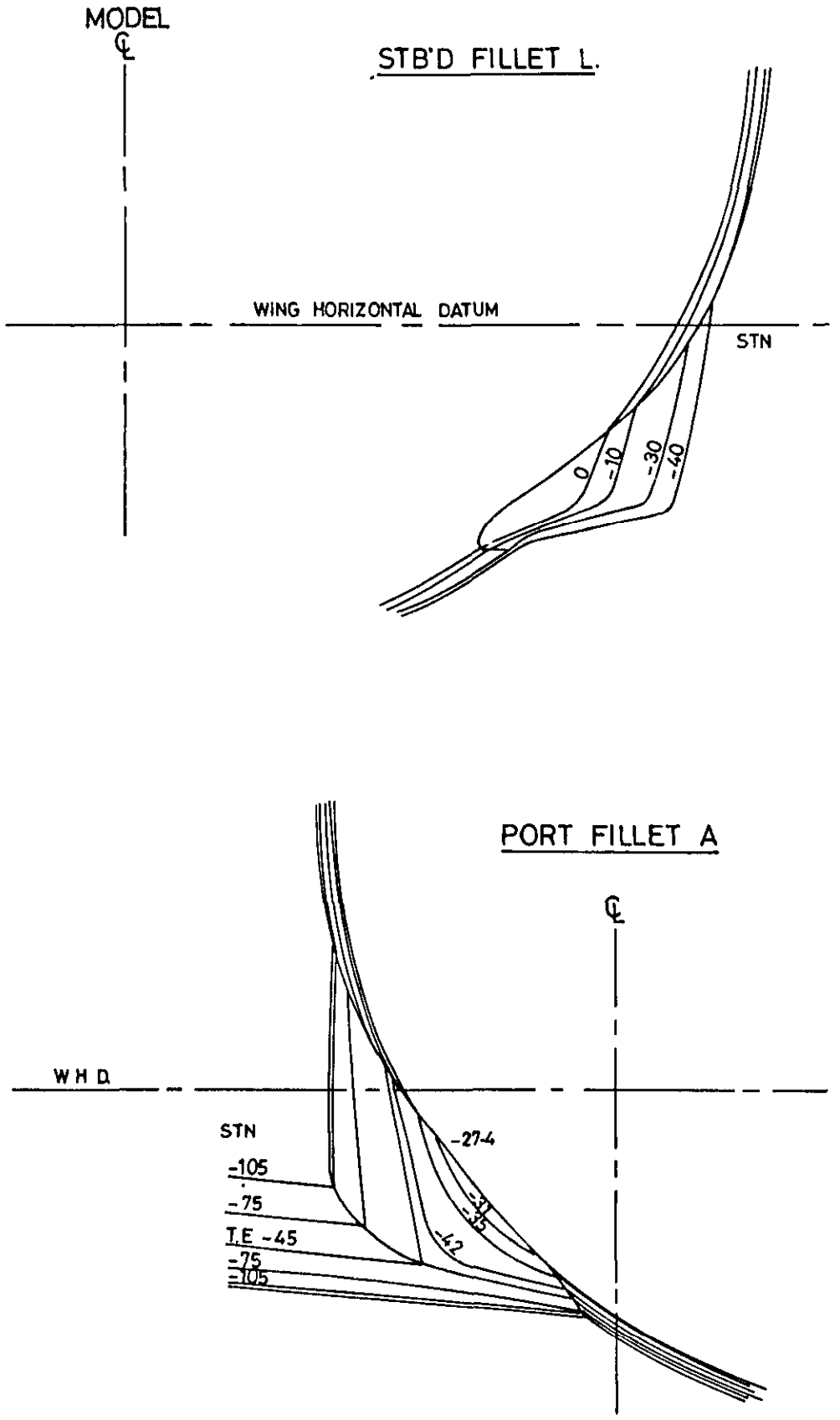

FIG. 2b) AFT VIEW OF MODEL WING ROOT TRAILING EDGE FILLETS

FIG. 3a)

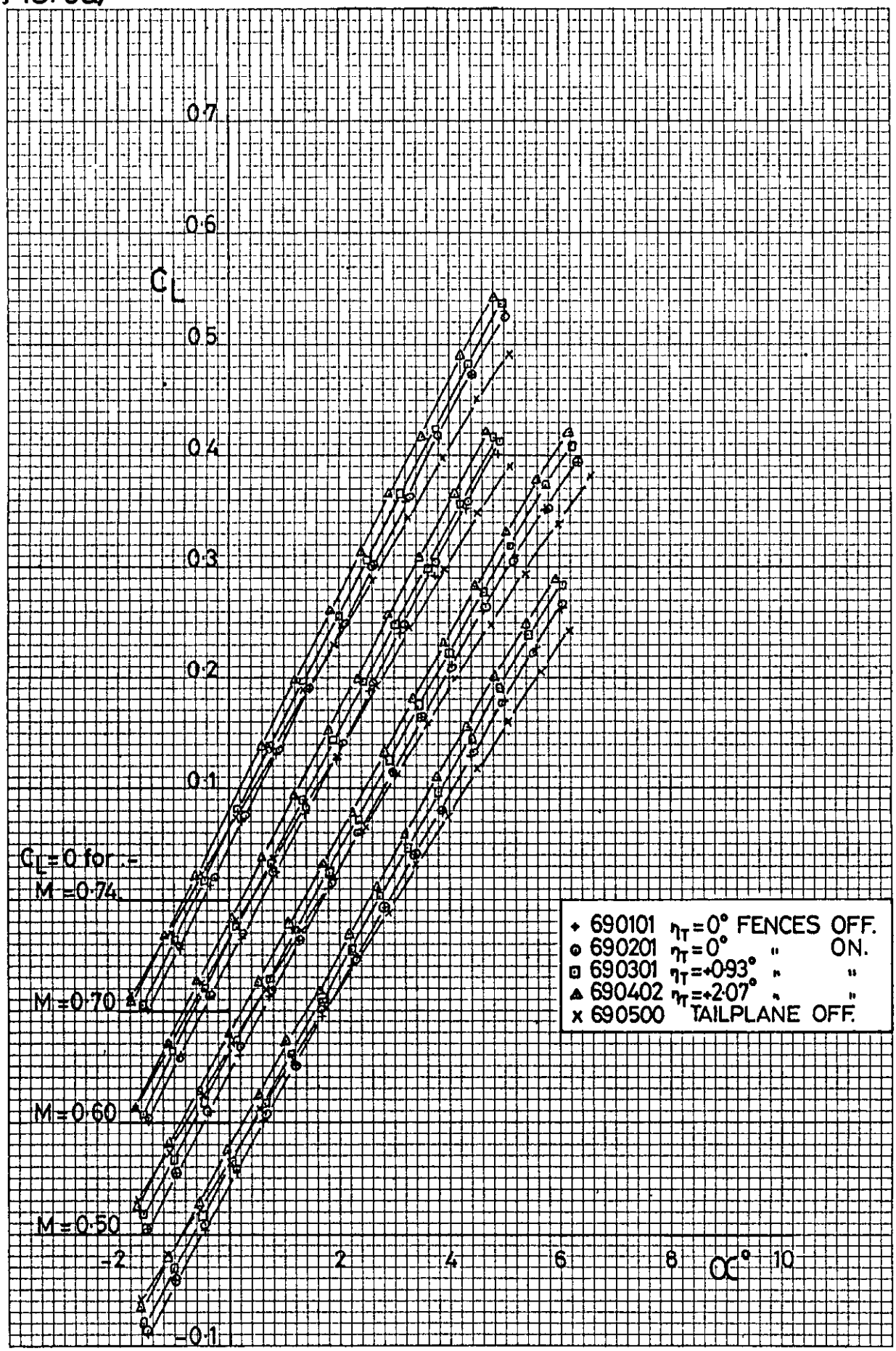

FIG. 3a) $C_L \sim \alpha$.

FIG. 3b)

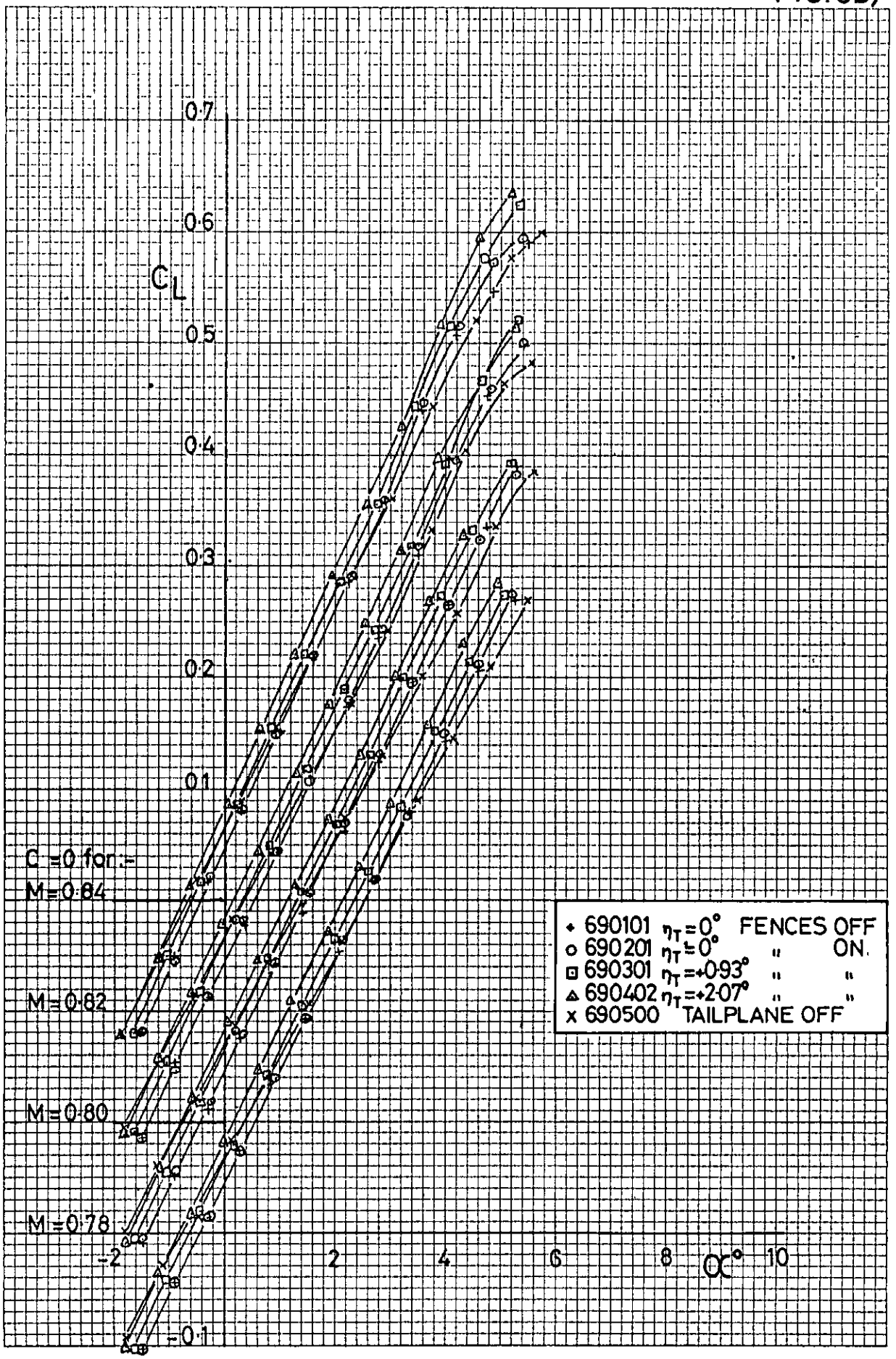

FIG. 3b) $C_L \sim \alpha$.

FIG. 3c)

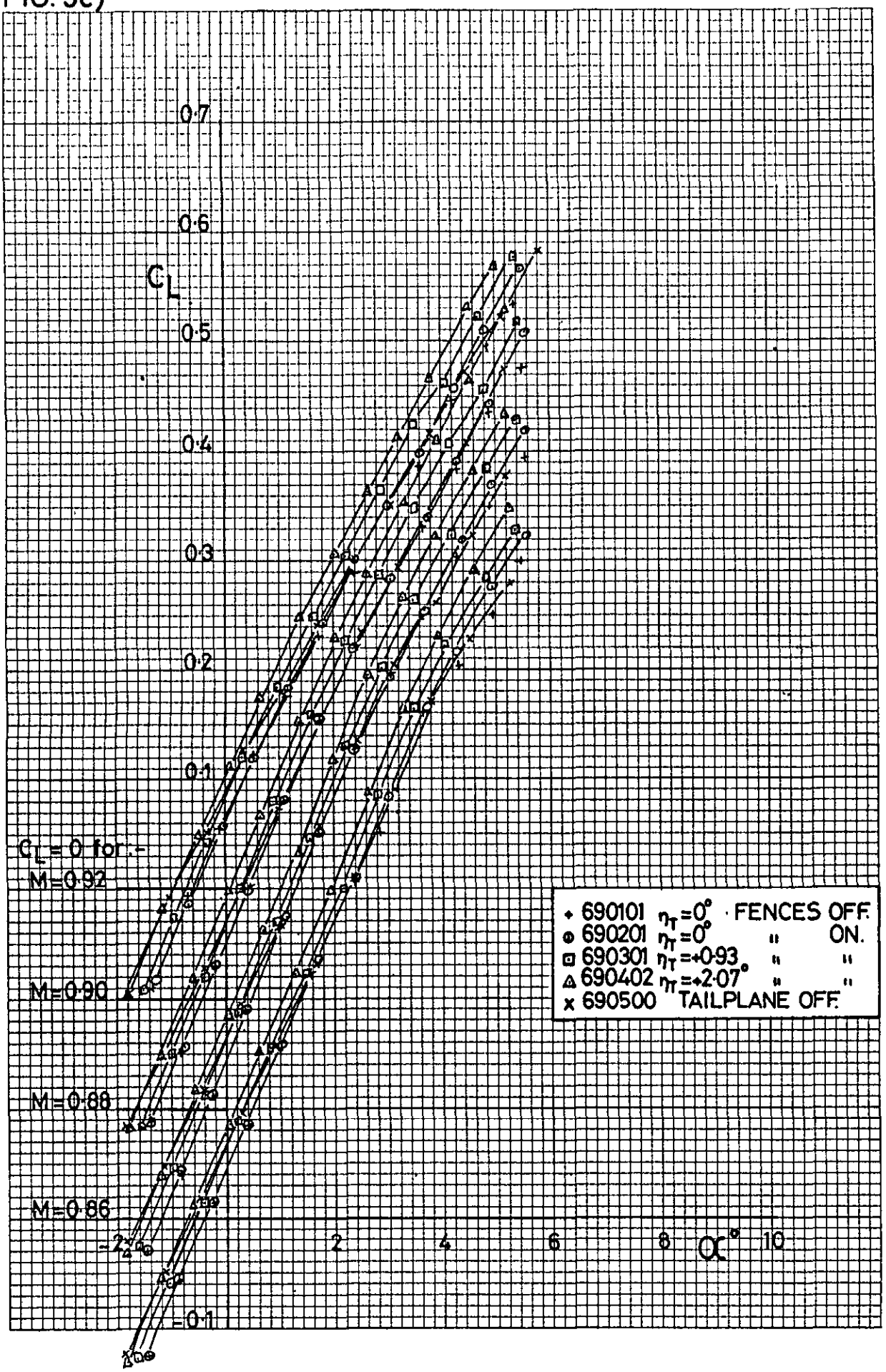

FIG. 3c) $C_L \sim \alpha$.

FIG. 4a)

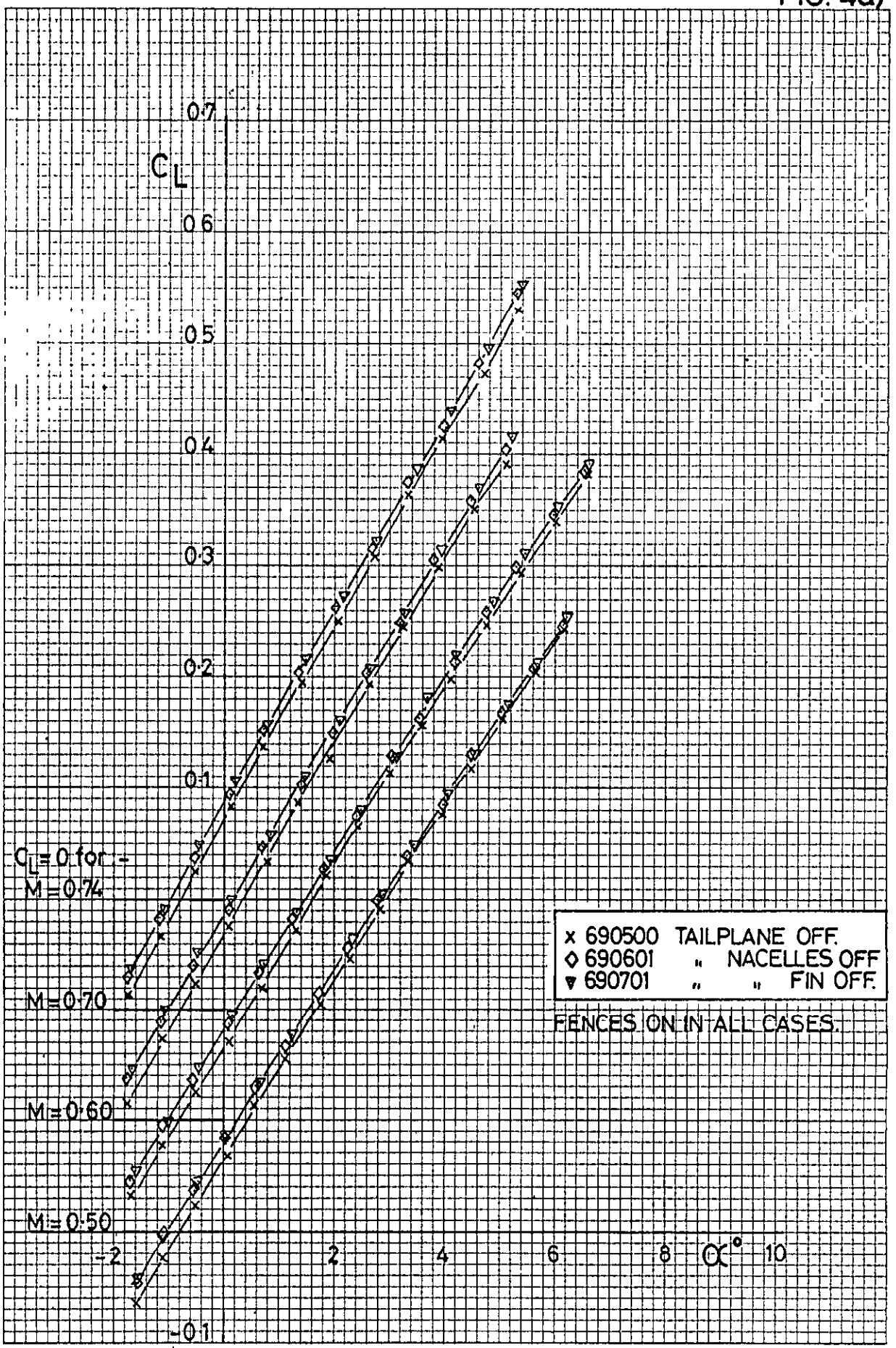

FIG. 4a) $C_L \sim \alpha$.

FIG. 4b)

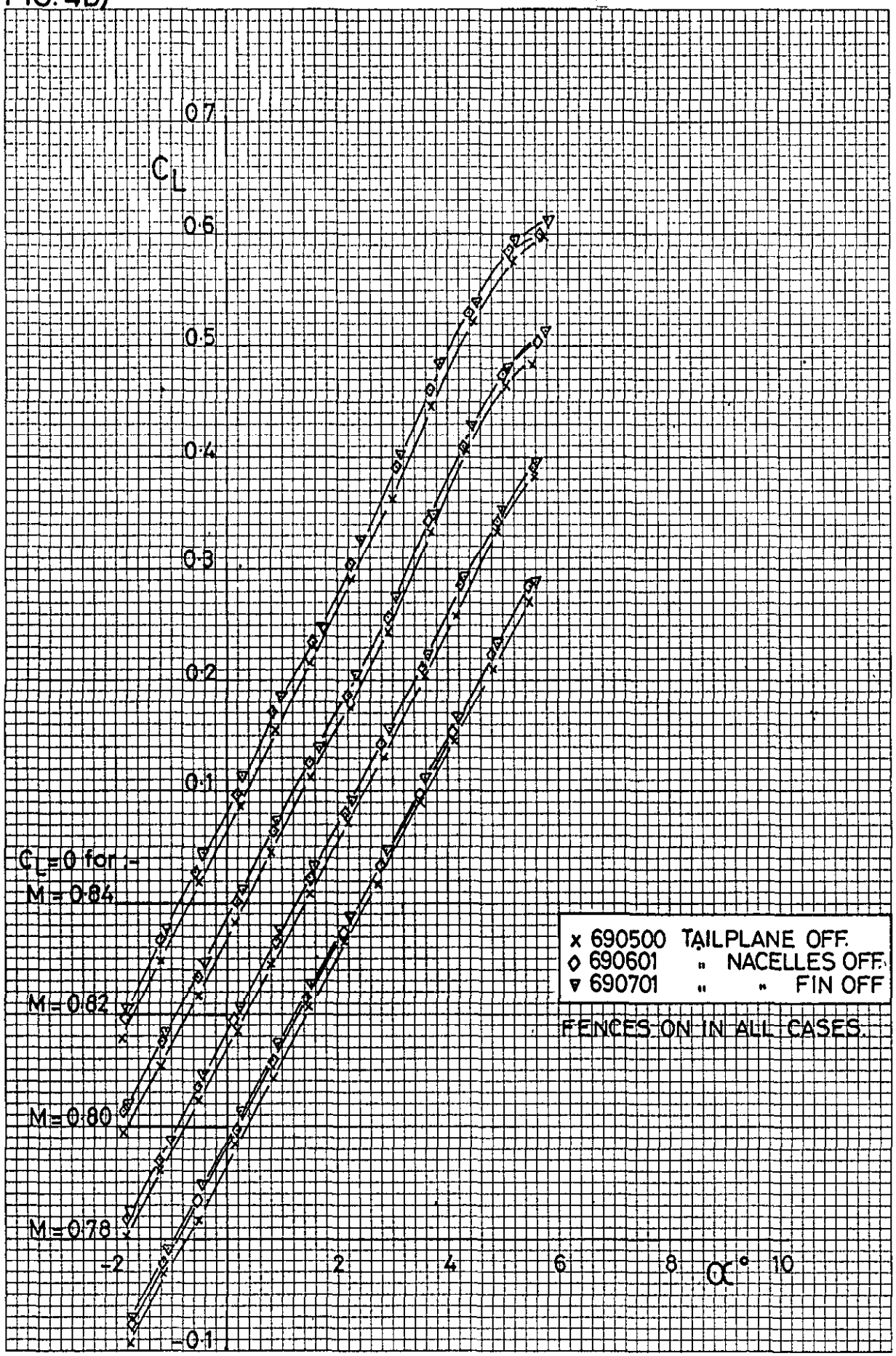

FIG. 4b) $C_L \sim \alpha$.

FIG. 4c)

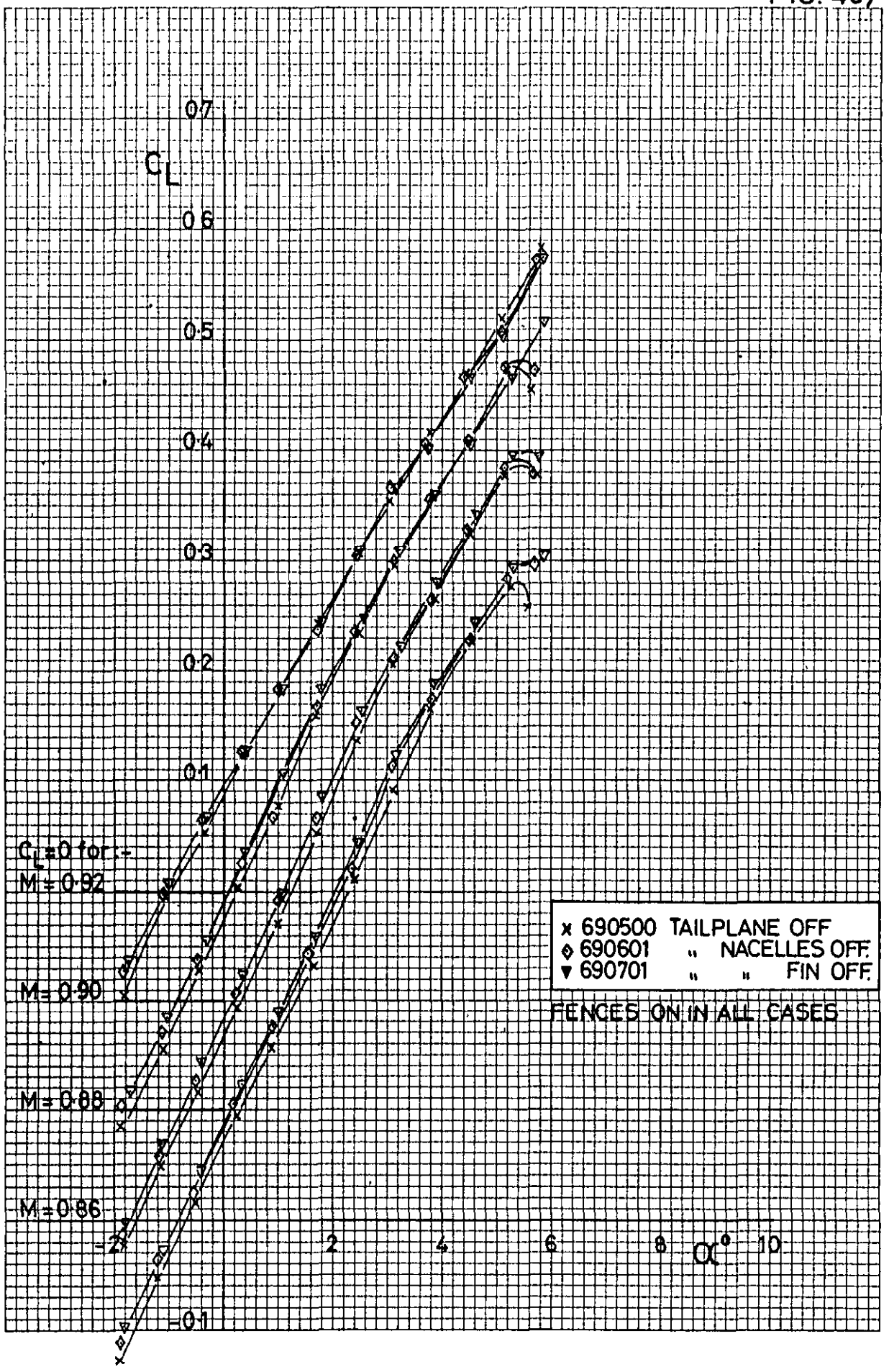

FIG. 4c) $C_L \sim \alpha$.

FIG. 5a)

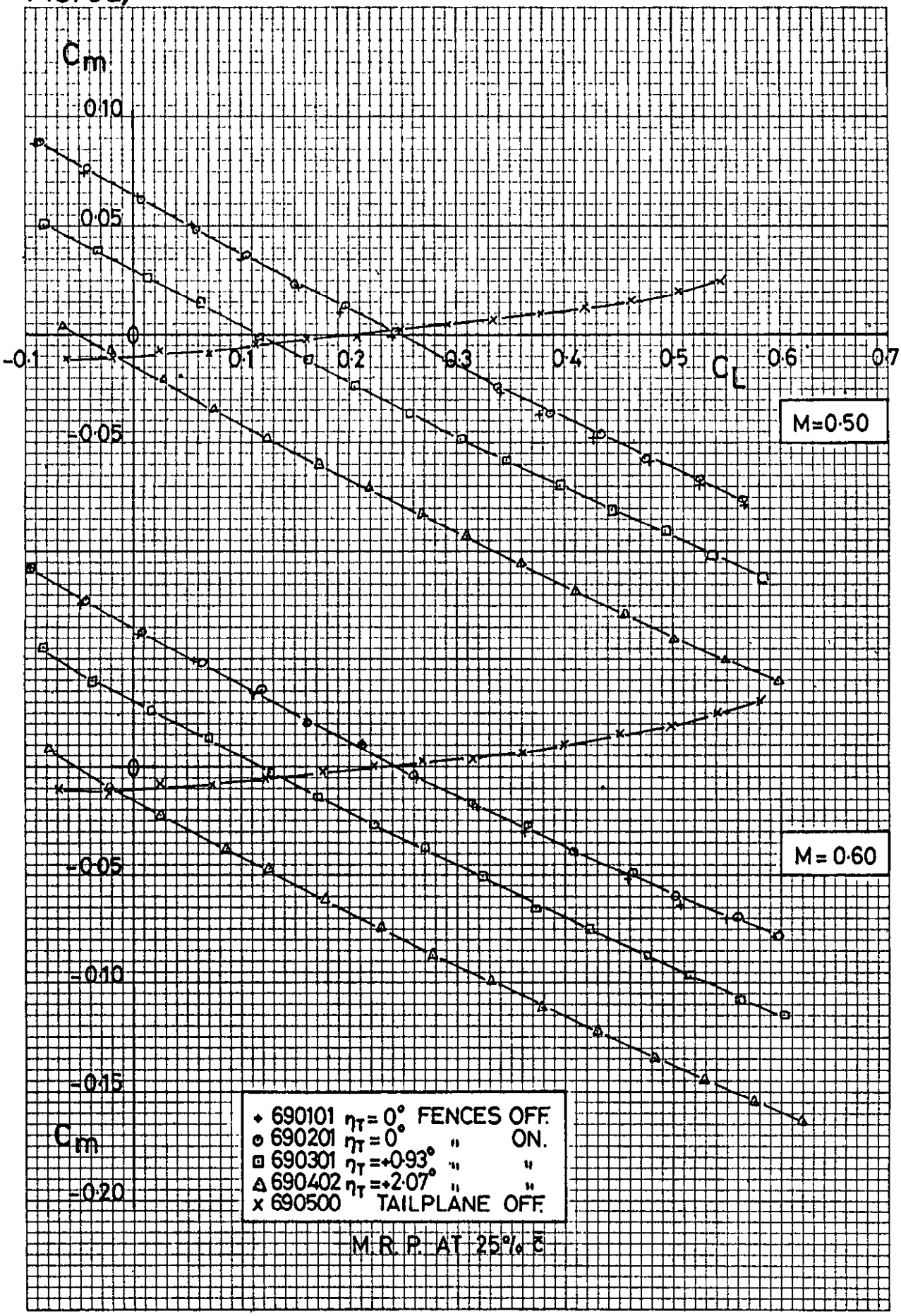

FIG. 5a) $C_m \sim C_L$

FIG. 5b)

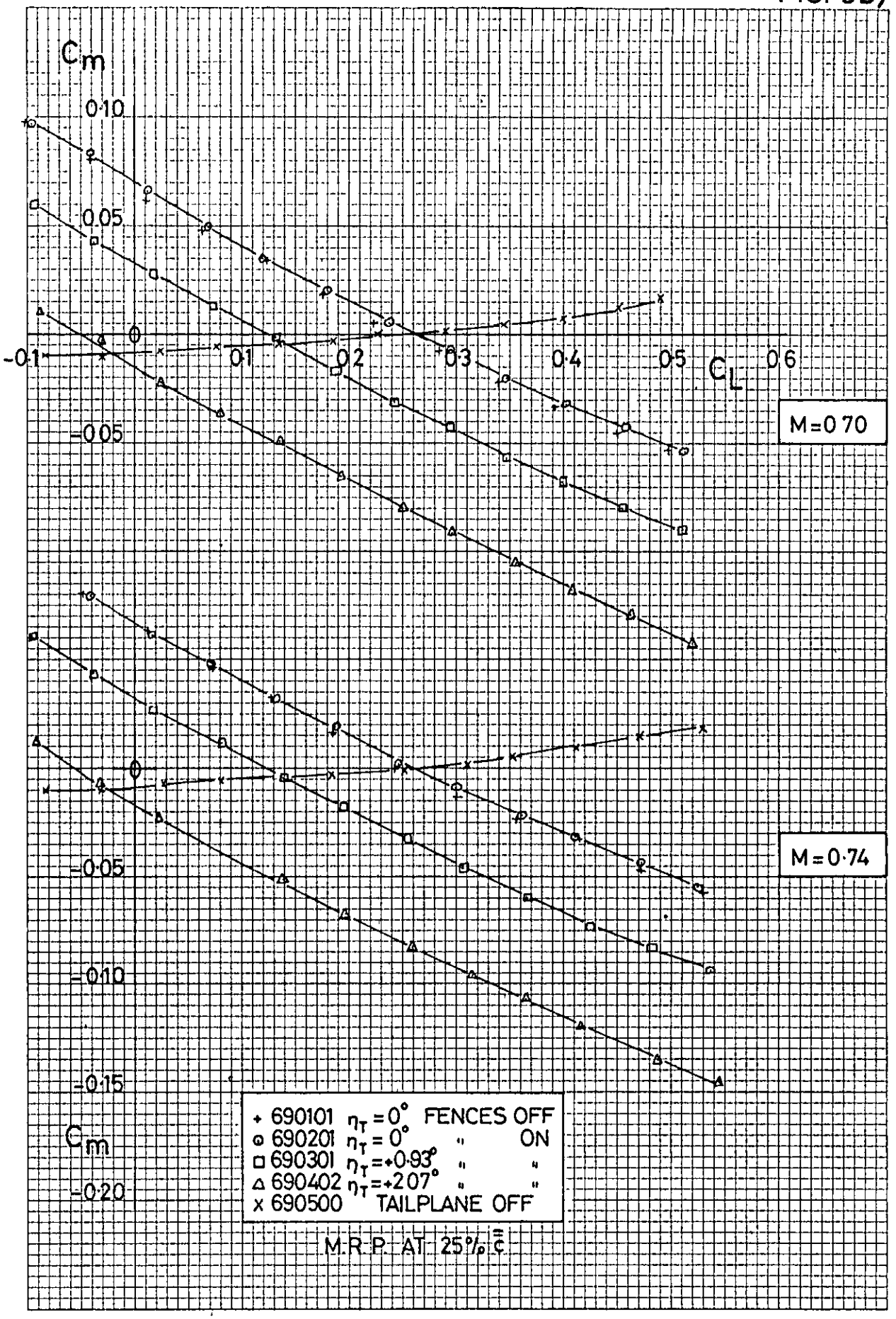

FIG. 5b) $C_m \sim C_L$

FIG. 5c)

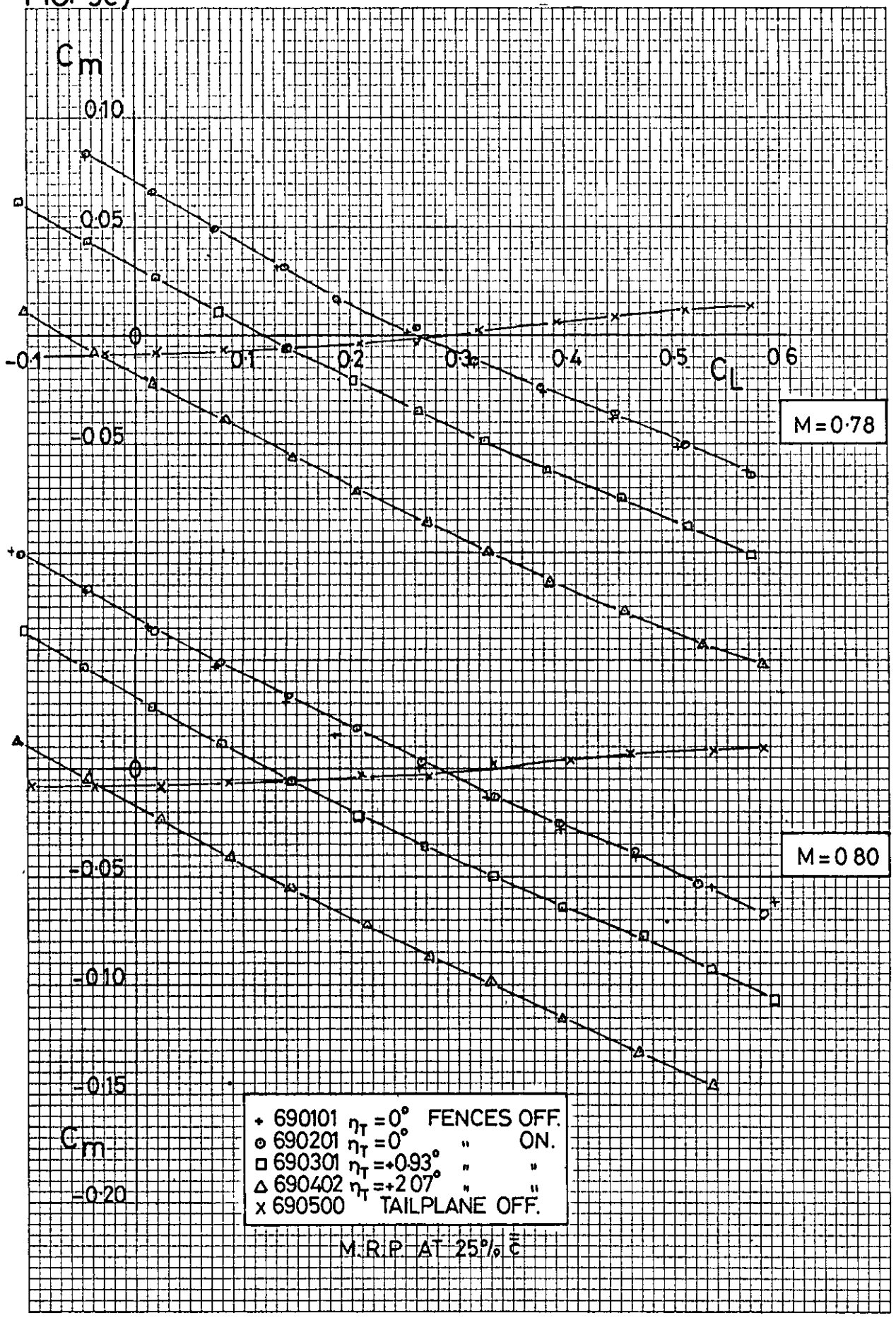

FIG. 5c) $C_m \sim C_L$.

FIG. 5d)

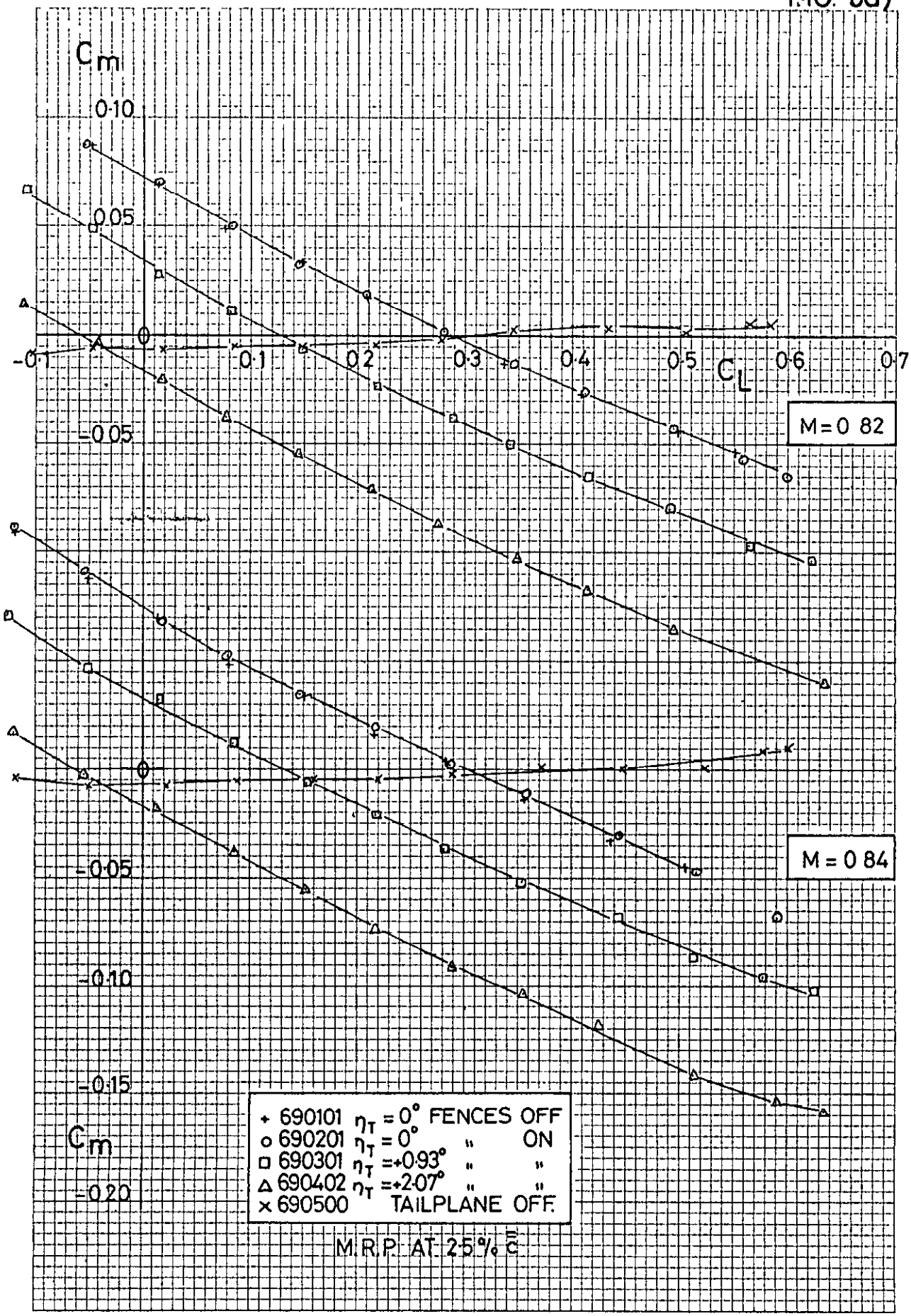

FIG. 5d) $C_m \sim C_L$.

FIG. 5e)

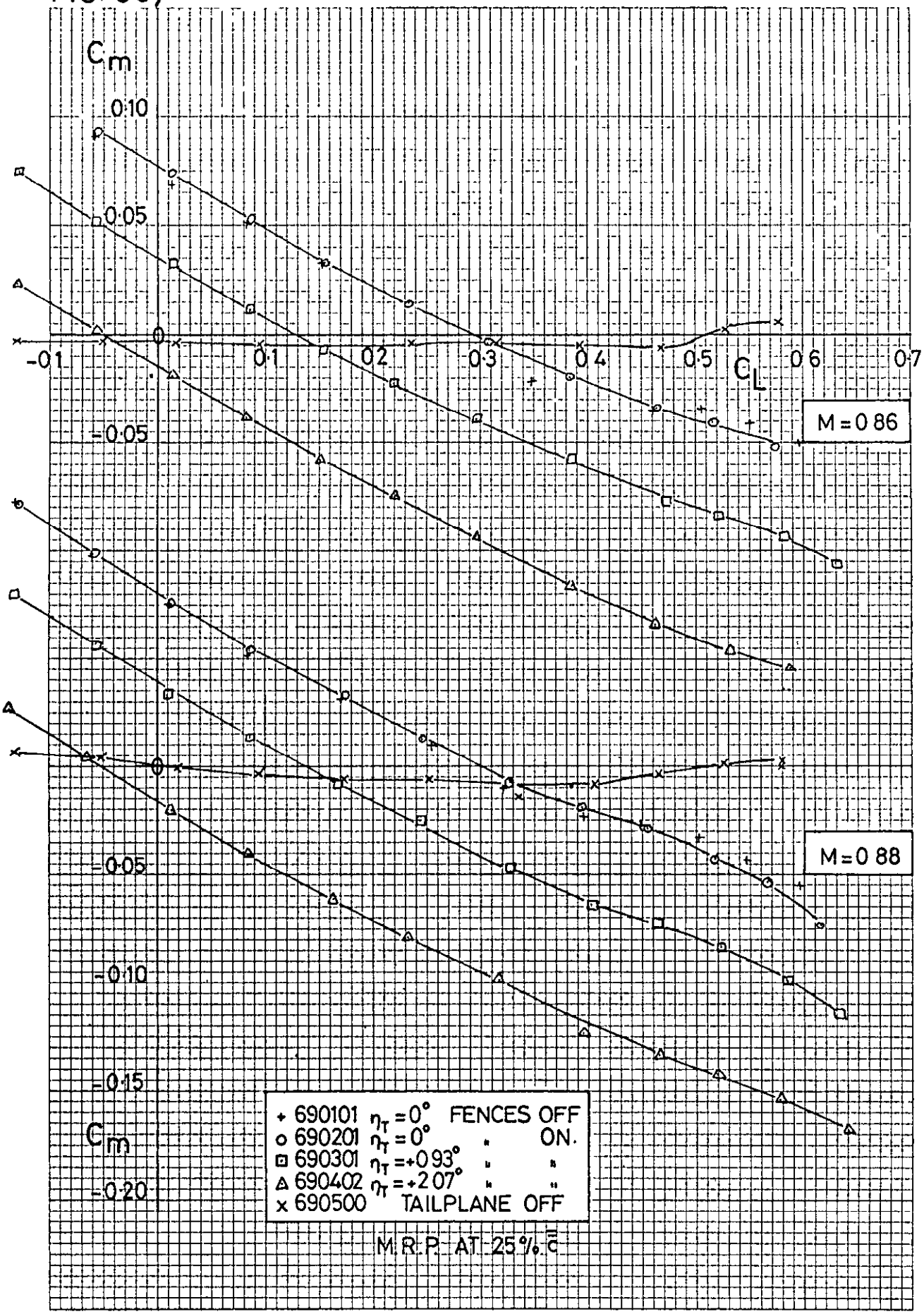

FIG. 5e) $C_m \sim C_L$.

FIG. 5f)

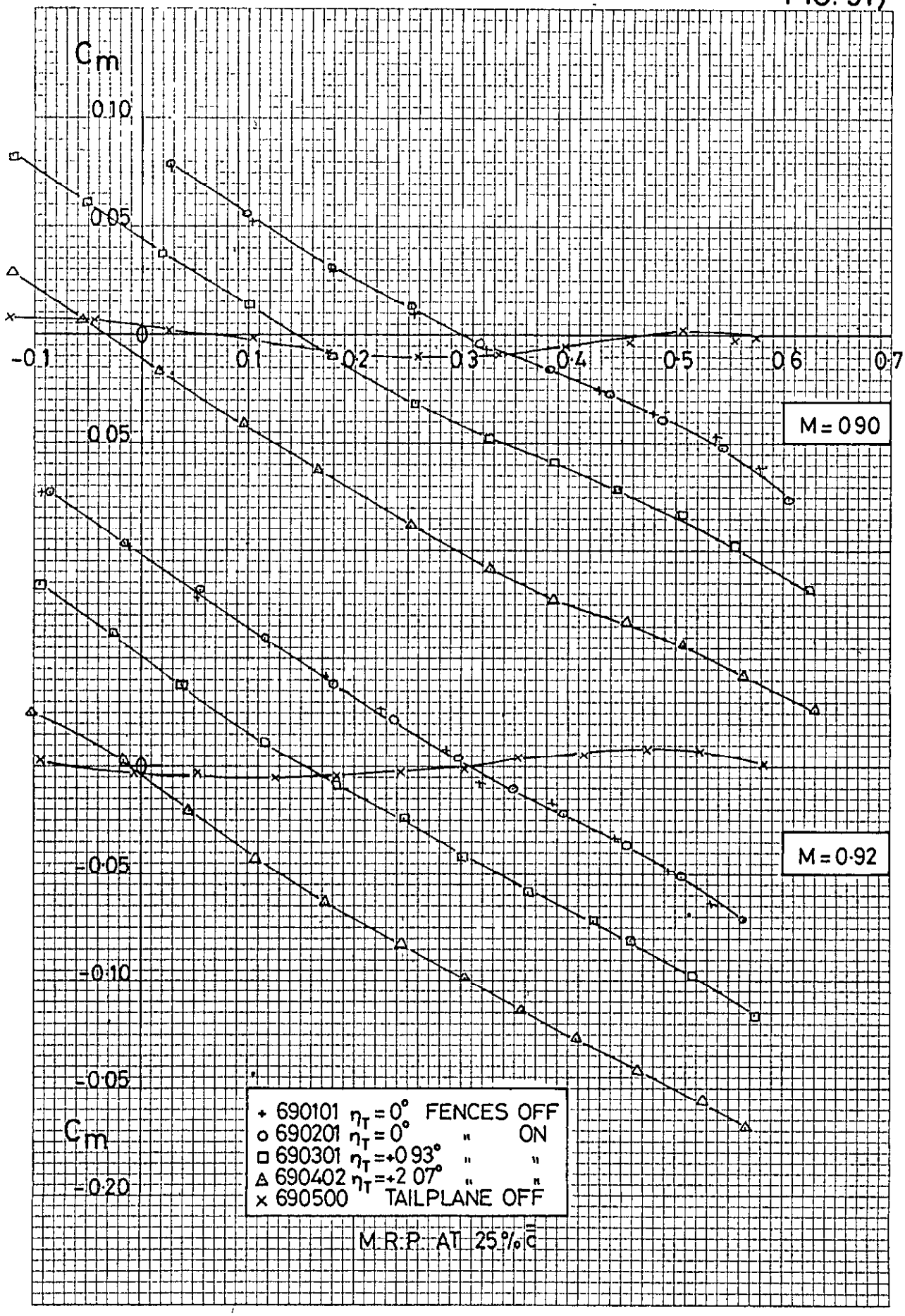

FIG. 5f) $C_m \sim C_L$

FIG. 6a)

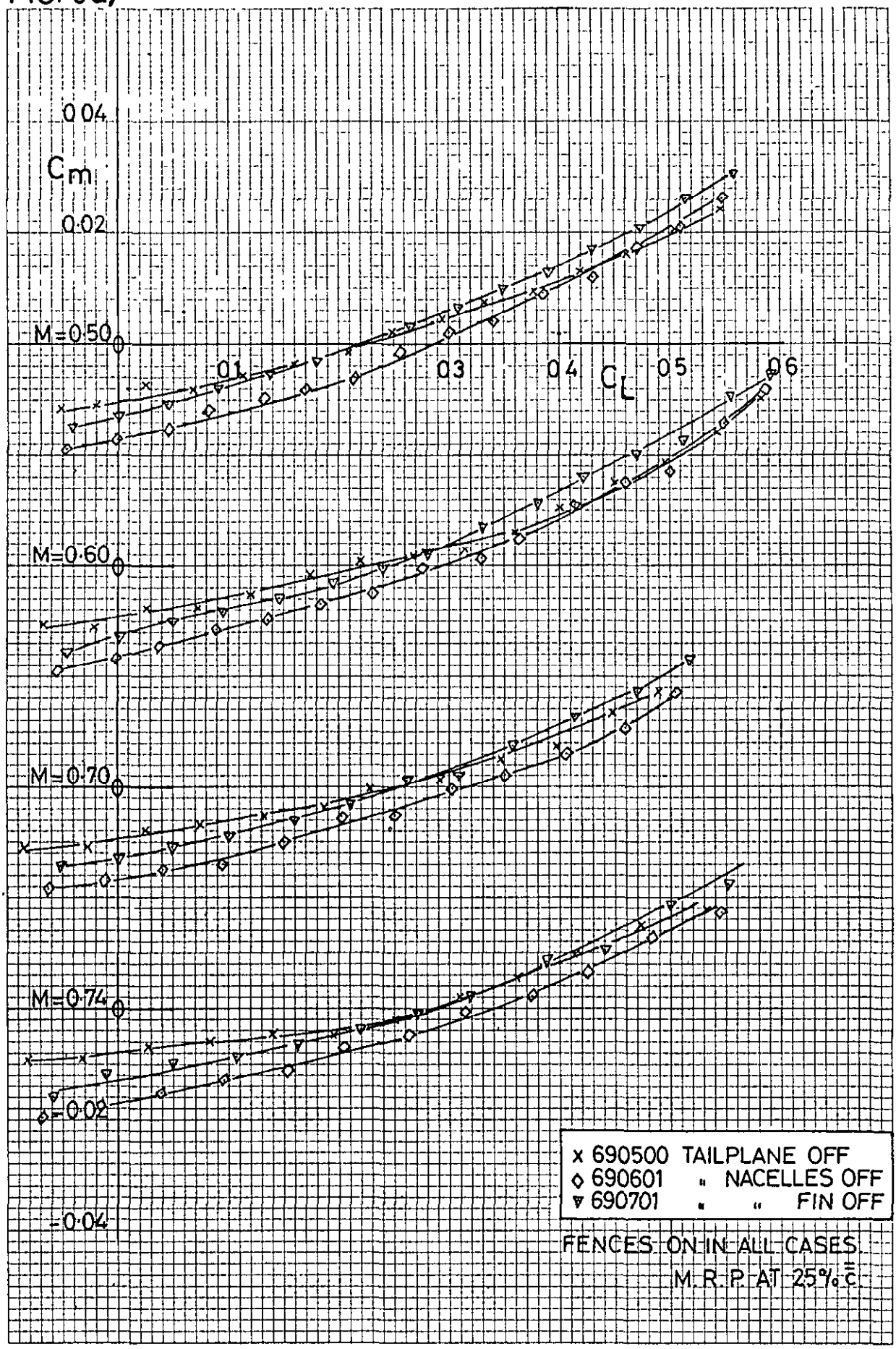

FIG. 6a) $C_m \sim C_L$

FIG. 6b)

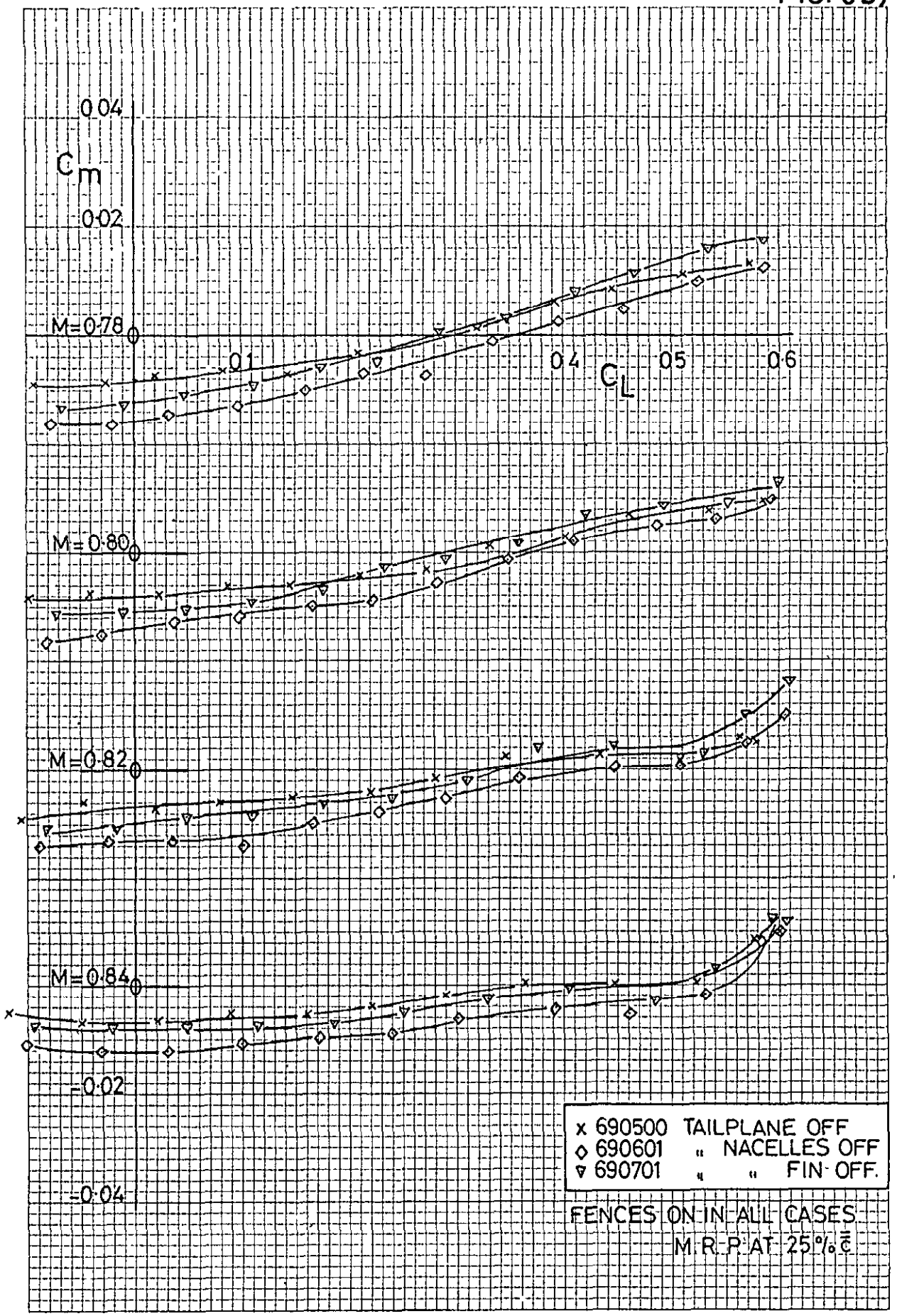

FIG. 6b) $C_m \sim C_L$.

FIG. 6c)

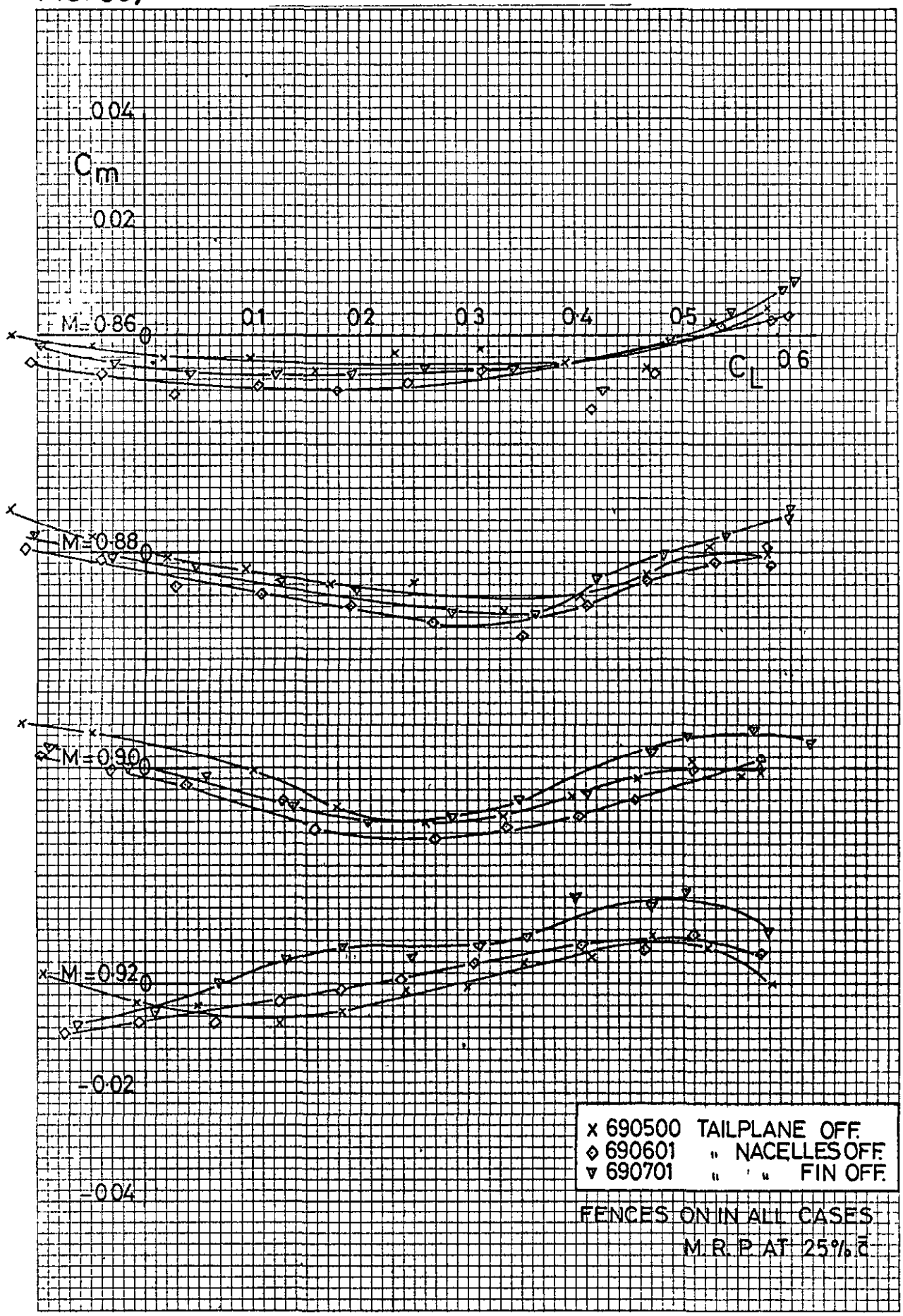

FIG. 6c) $C_m \sim C_L$.

FIG. 7a)

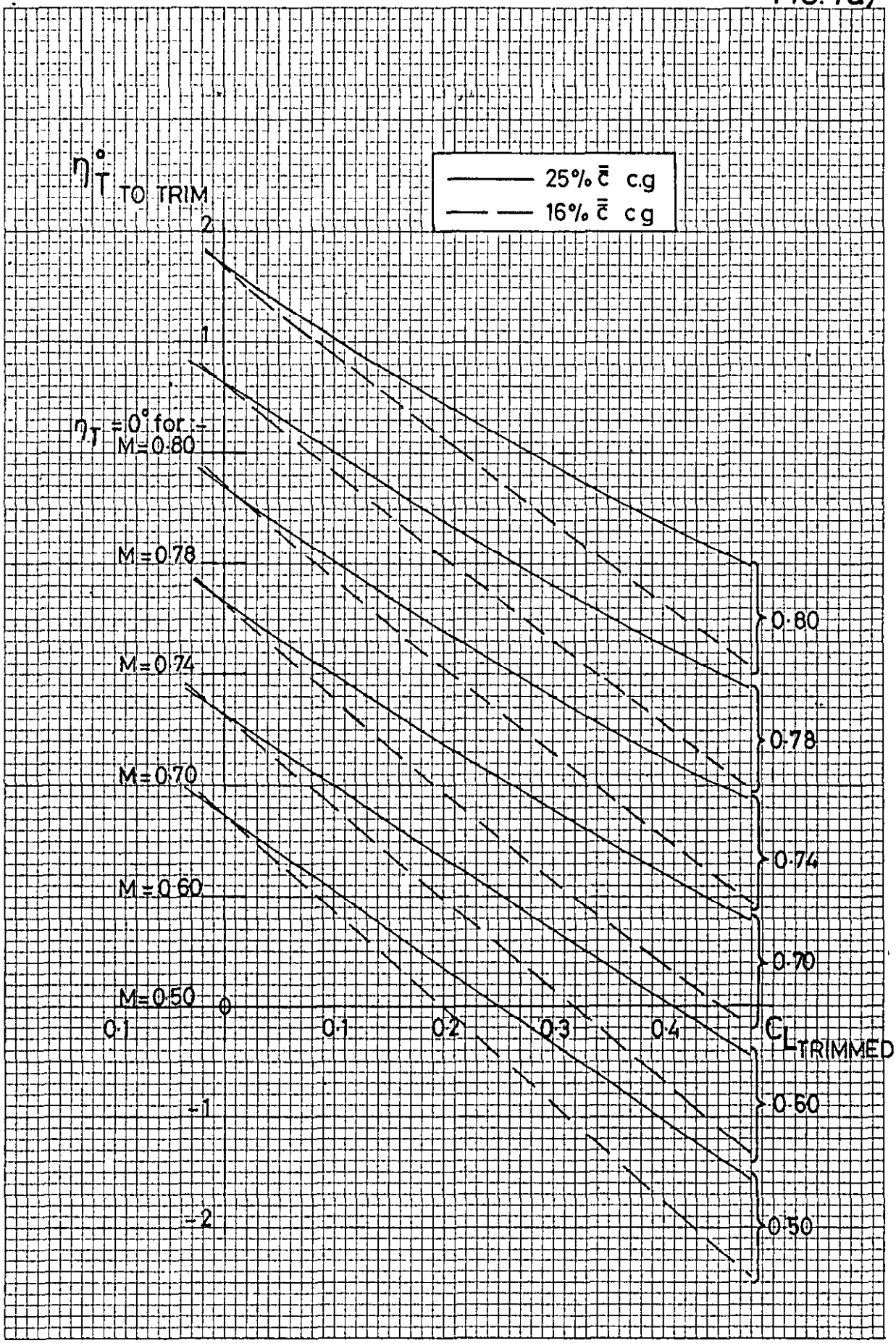

FIG. 7a) TAILPLANE ANGLE TO TRIM.

FIG. 7b)

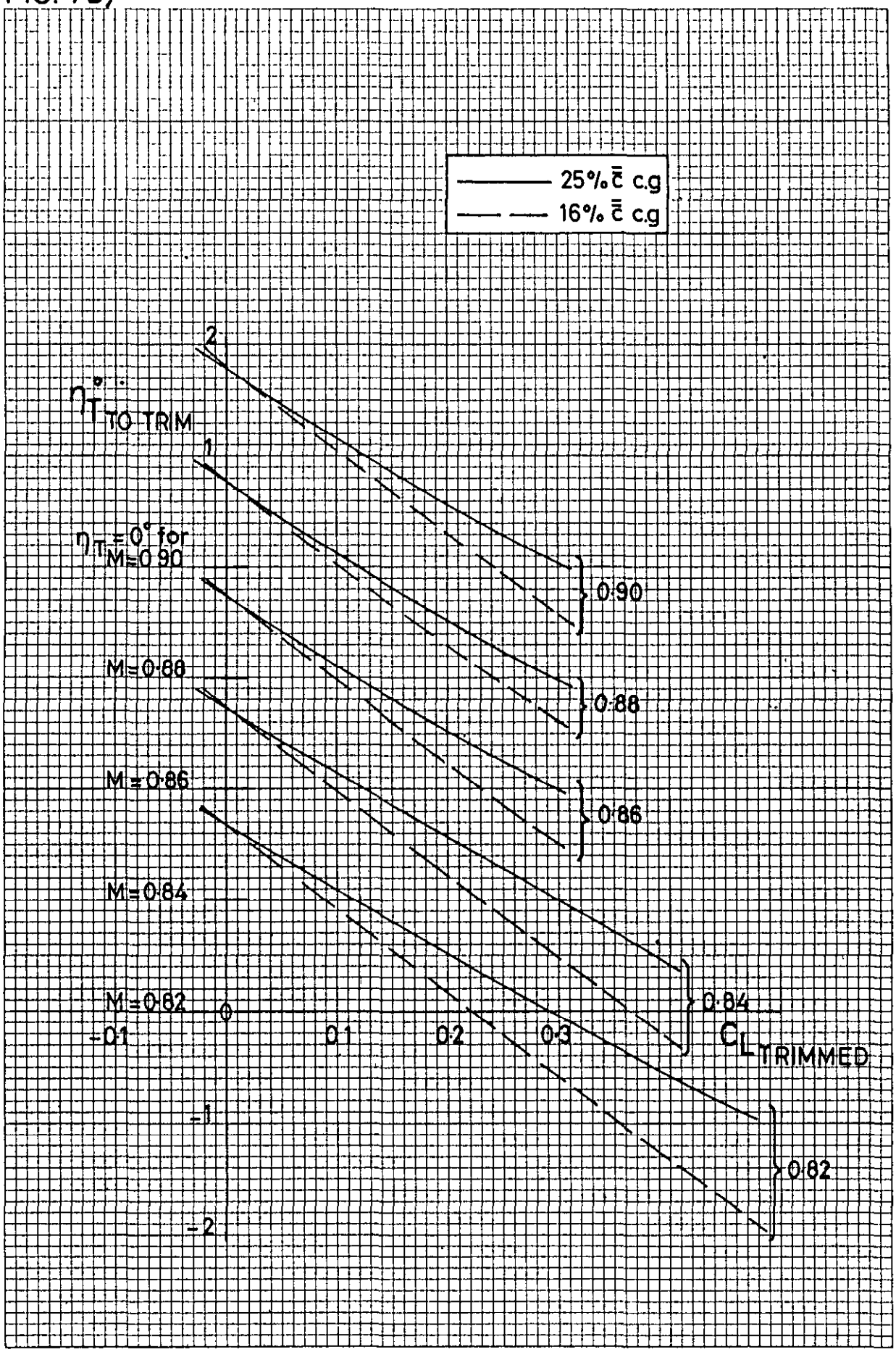

FIG. 7b) TAILPLANE ANGLE TO TRIM.

FIG. 8a)

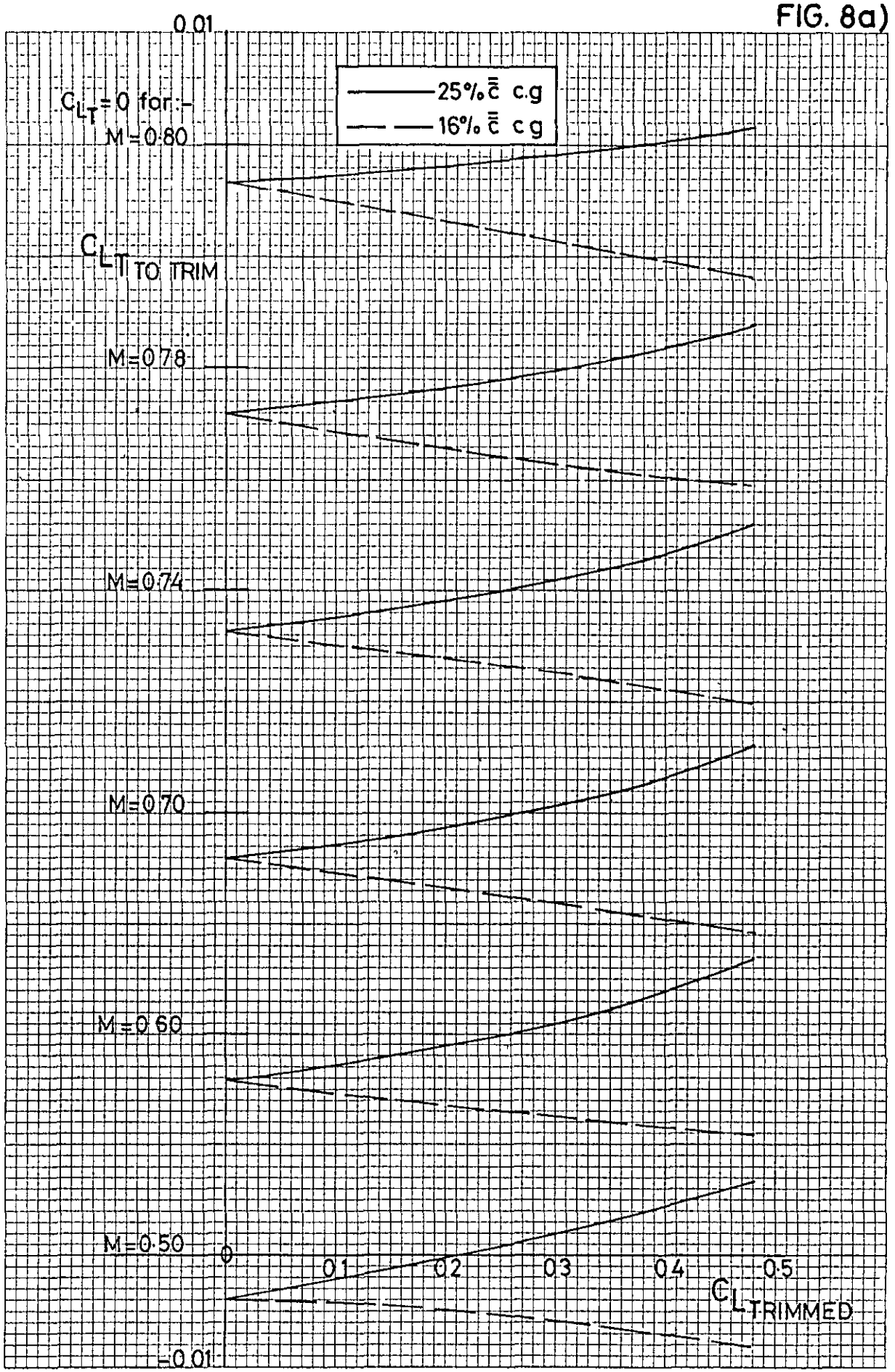

FIG. 8a) TAILPLANE LIFT TO TRIM

FIG. 8b)

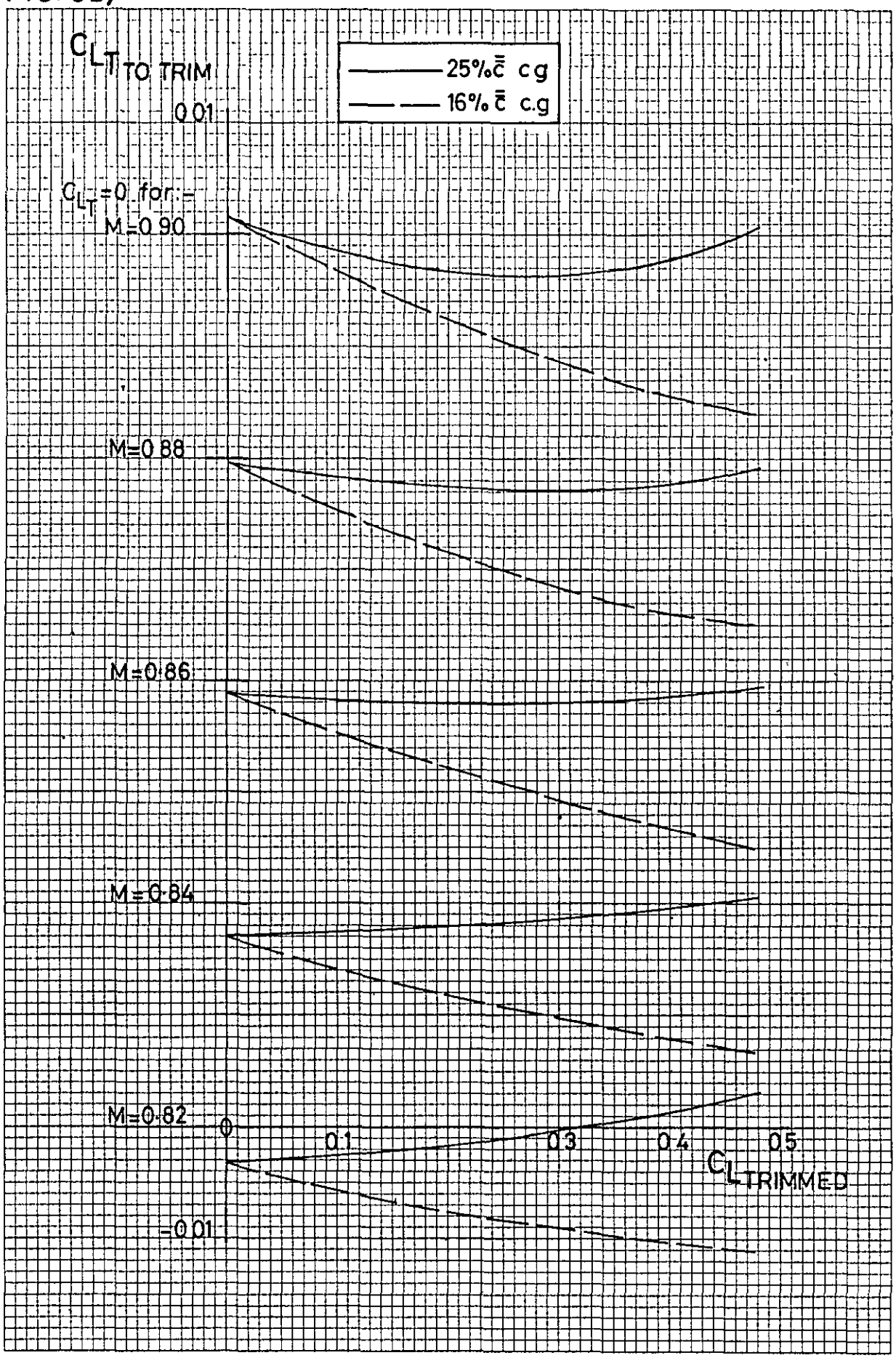

FIG. 8b) TAILPLANE LIFT TO TRIM.

FIG. 9a)

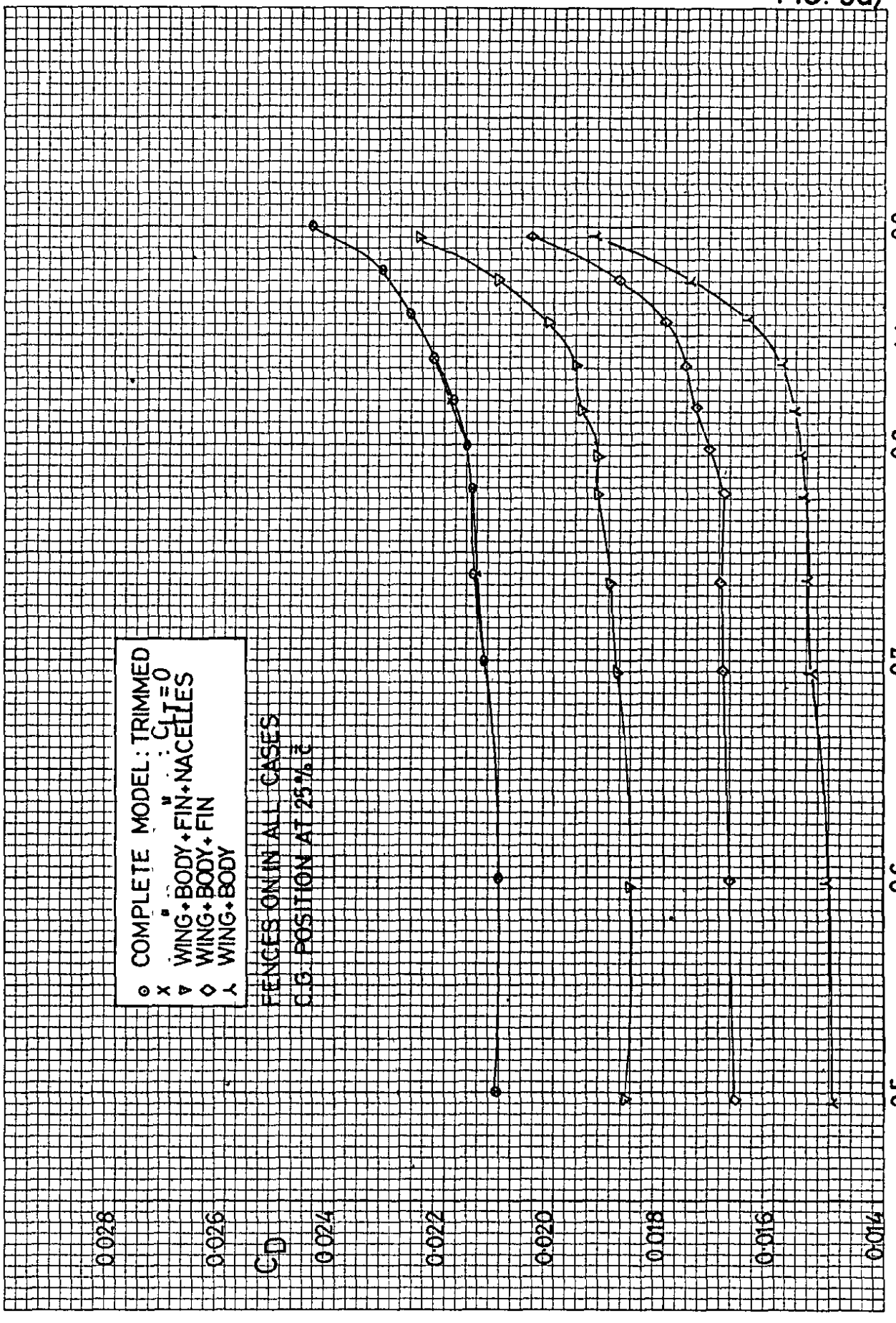

FIG. 9a) $C_D \sim M$; $C_L = 0$

FIG. 9b)

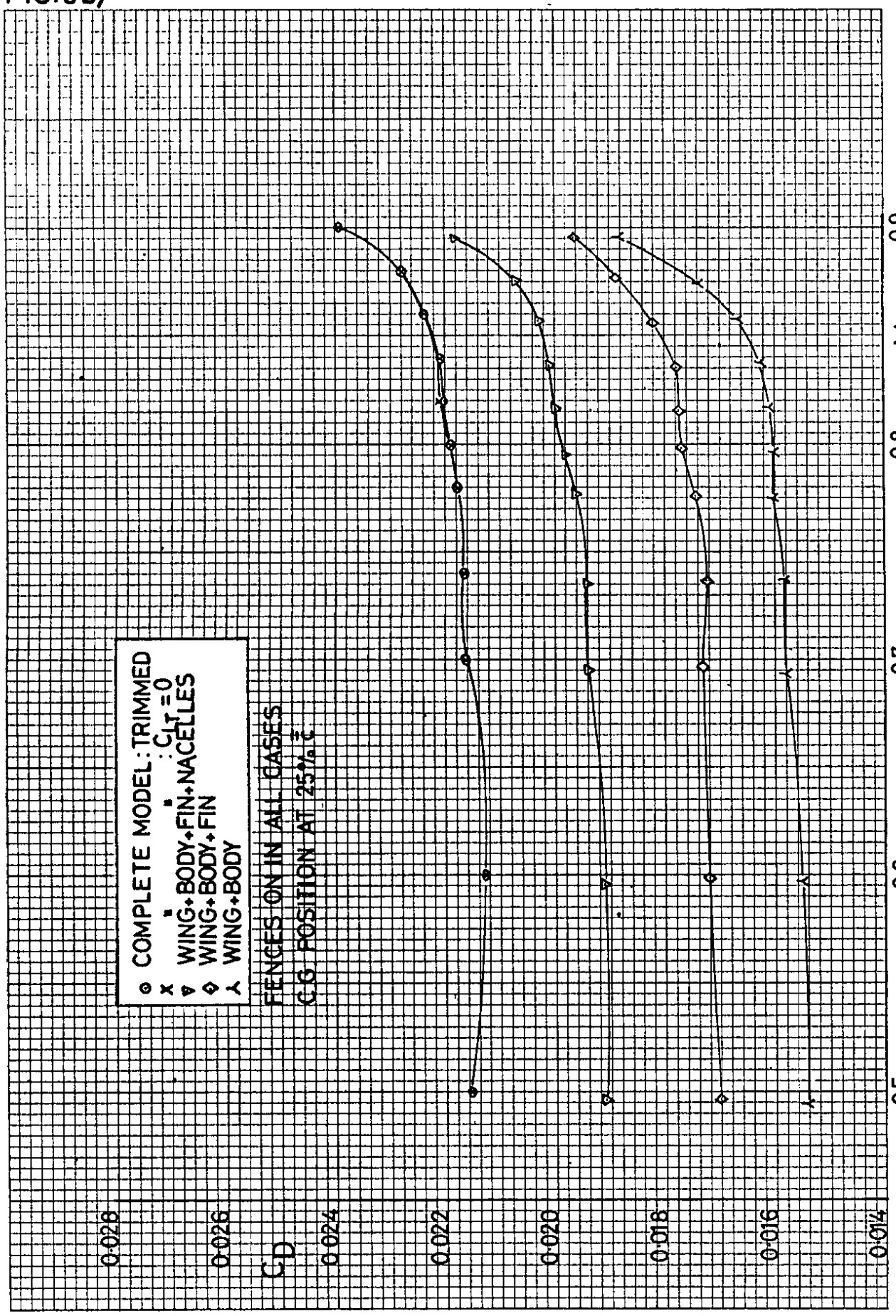

FIG. 9b) $C_L = 0{\cdot}10$

FIG. 9c)

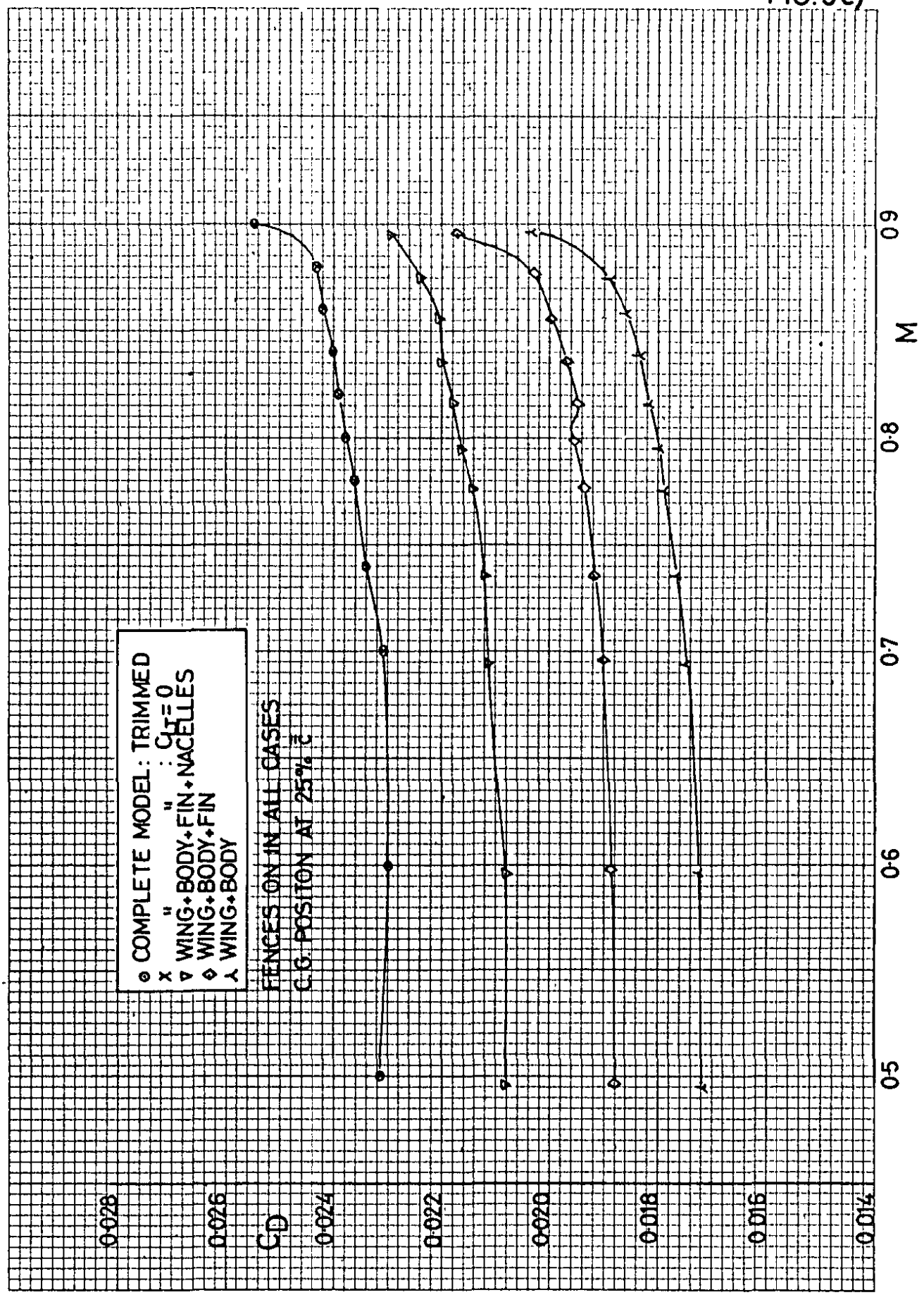

FIG. 9c) $C_L = 0{\cdot}20$.

FIG. 9d)

$C_L = 0·25$

FIG. 9d)

FIG. 9e)

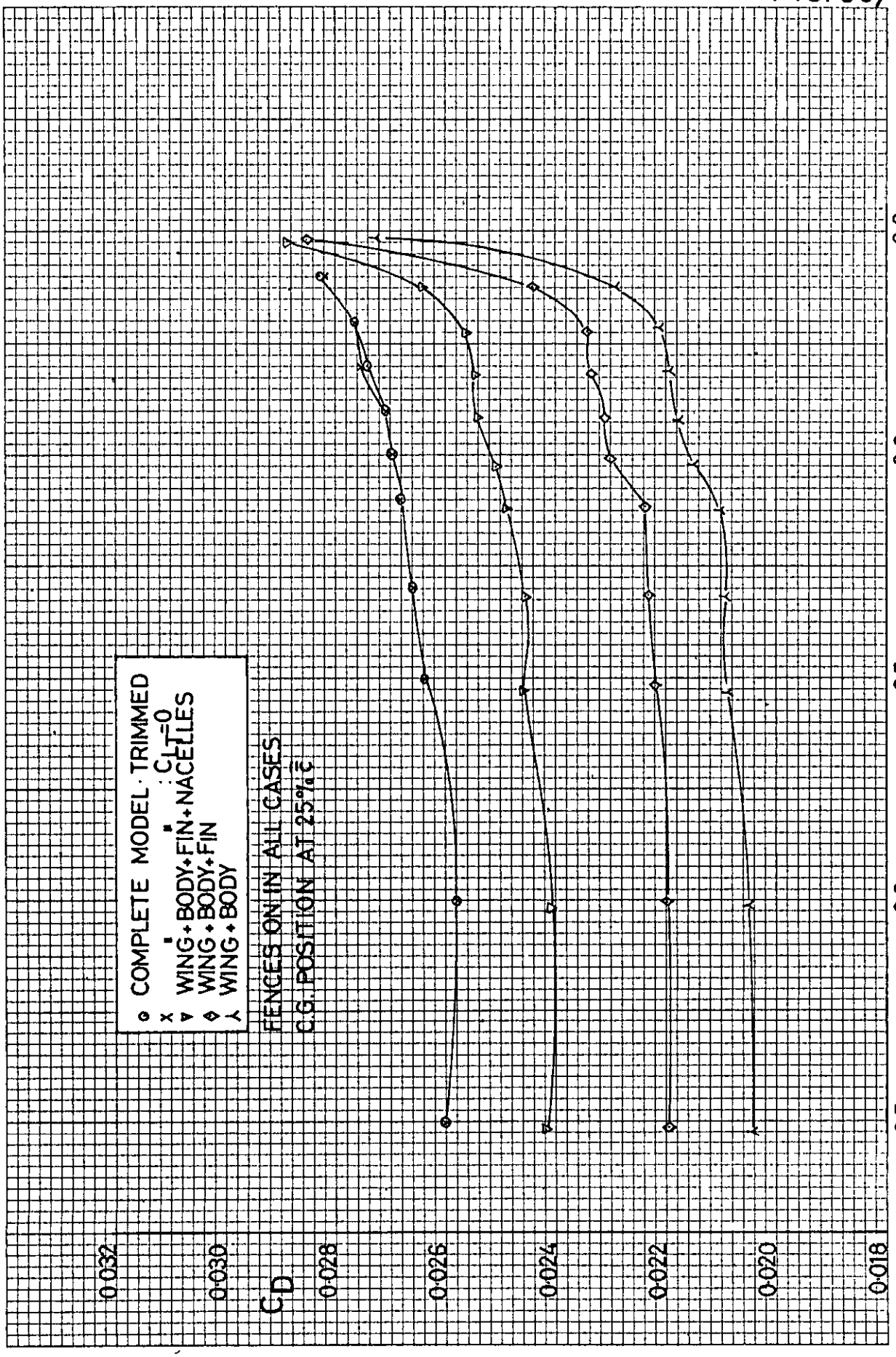

FIG. 9e) $C_L = 0{\cdot}30.$

FIG.9f)

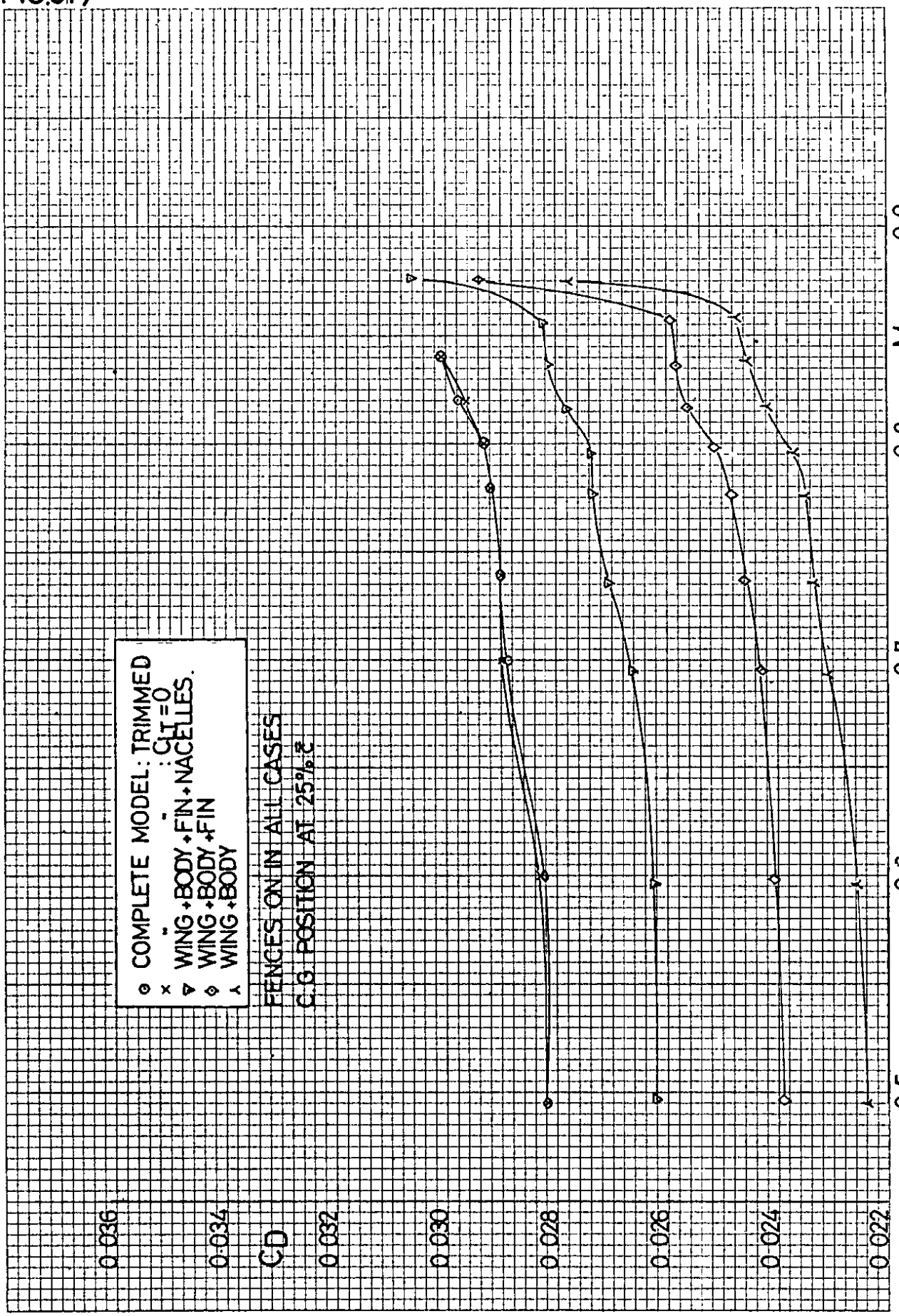

FIG.9f) $C_L = 0{\cdot}35$.

FIG. 9g)

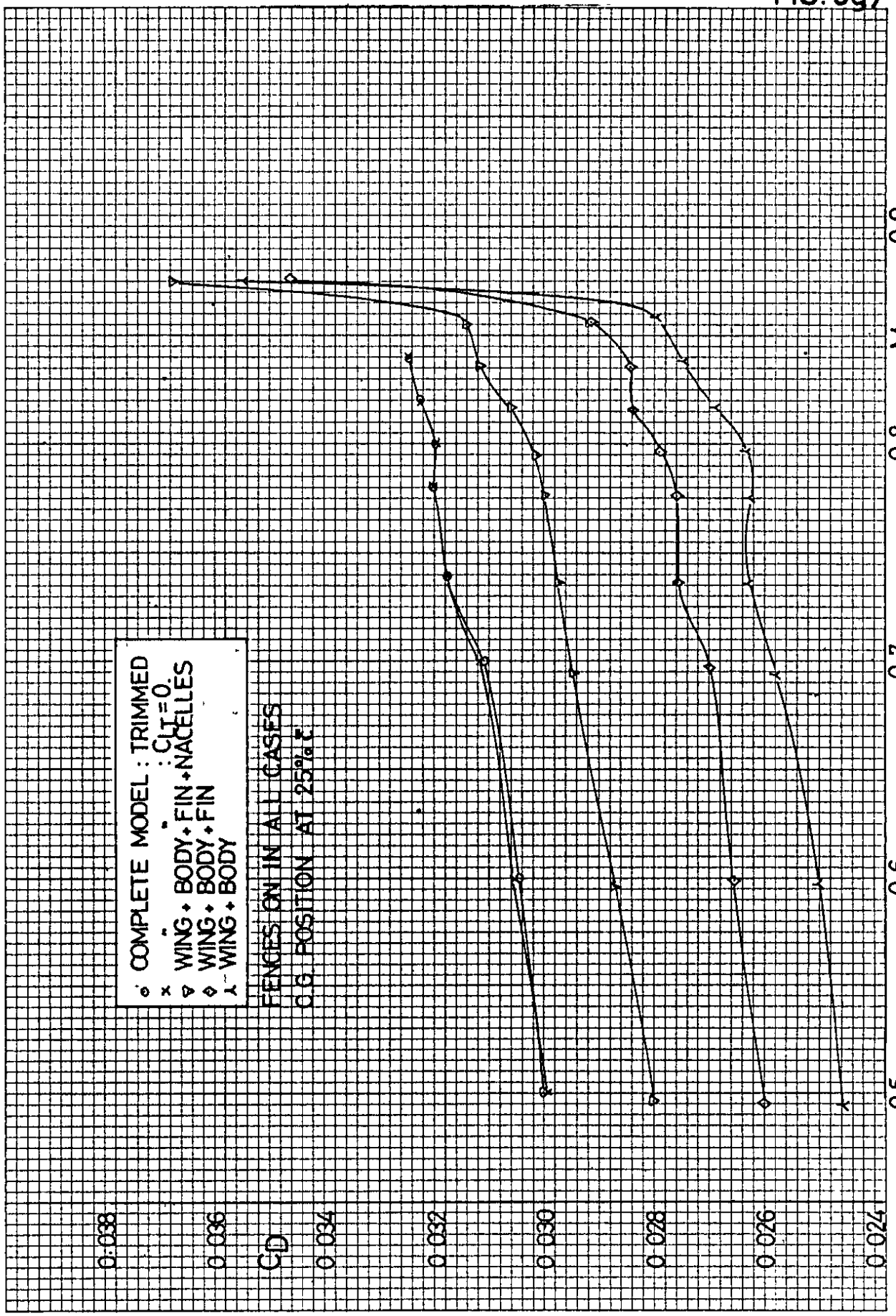

FIG. 9g) $C_L = 0{\cdot}40$.

FIG.9h)

FIG.9h)

$C_L = 0{\cdot}45$

FIG. 10.

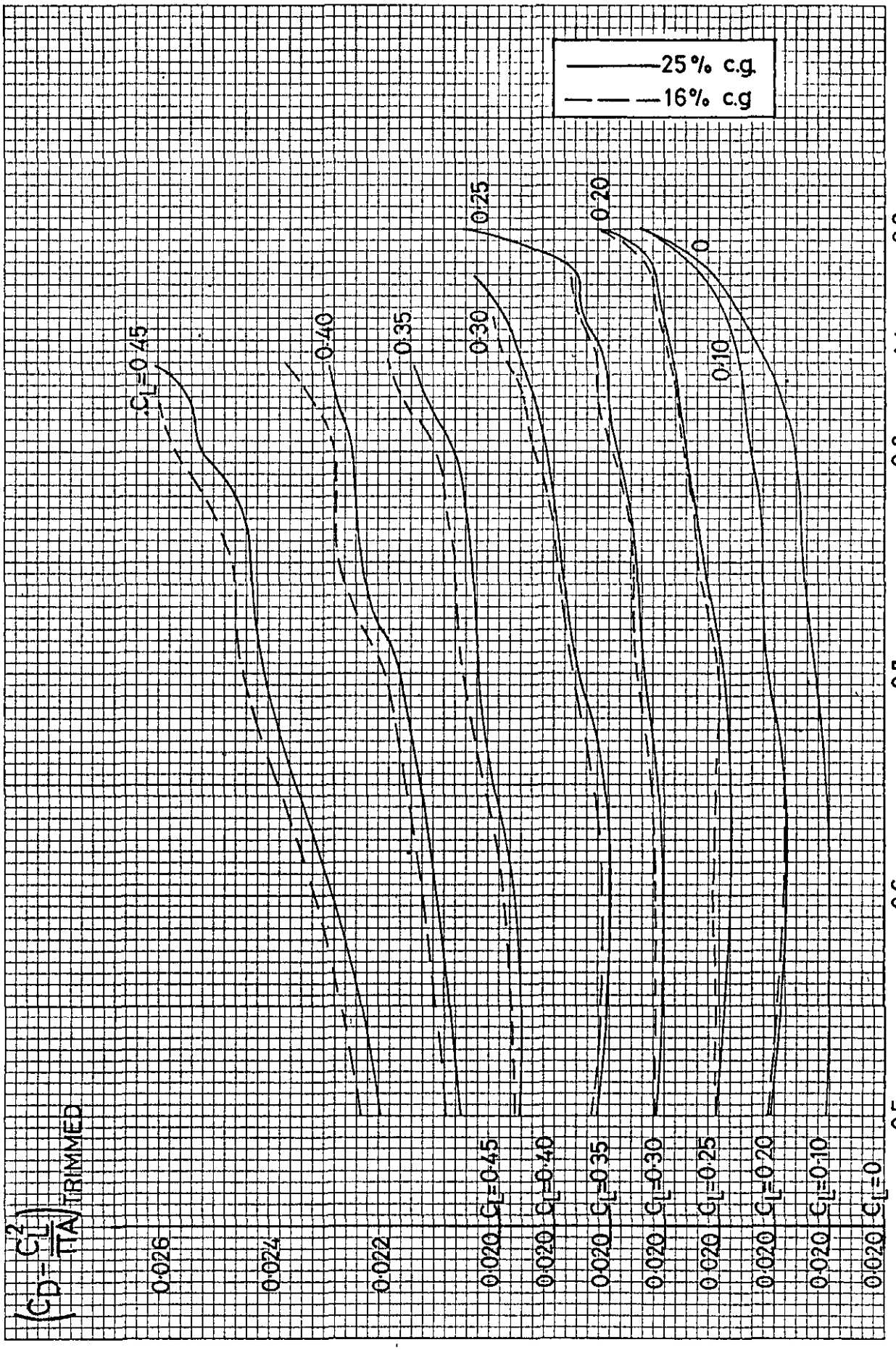

FIG. 10. $\left(C_D - \frac{C_L^2}{\pi A}\right)_{TRIMMED} \sim M$ COMPARISON FOR 25% $\bar{c}$ AND 16% $\bar{c}$ cg POSITION.

FIG. 11.

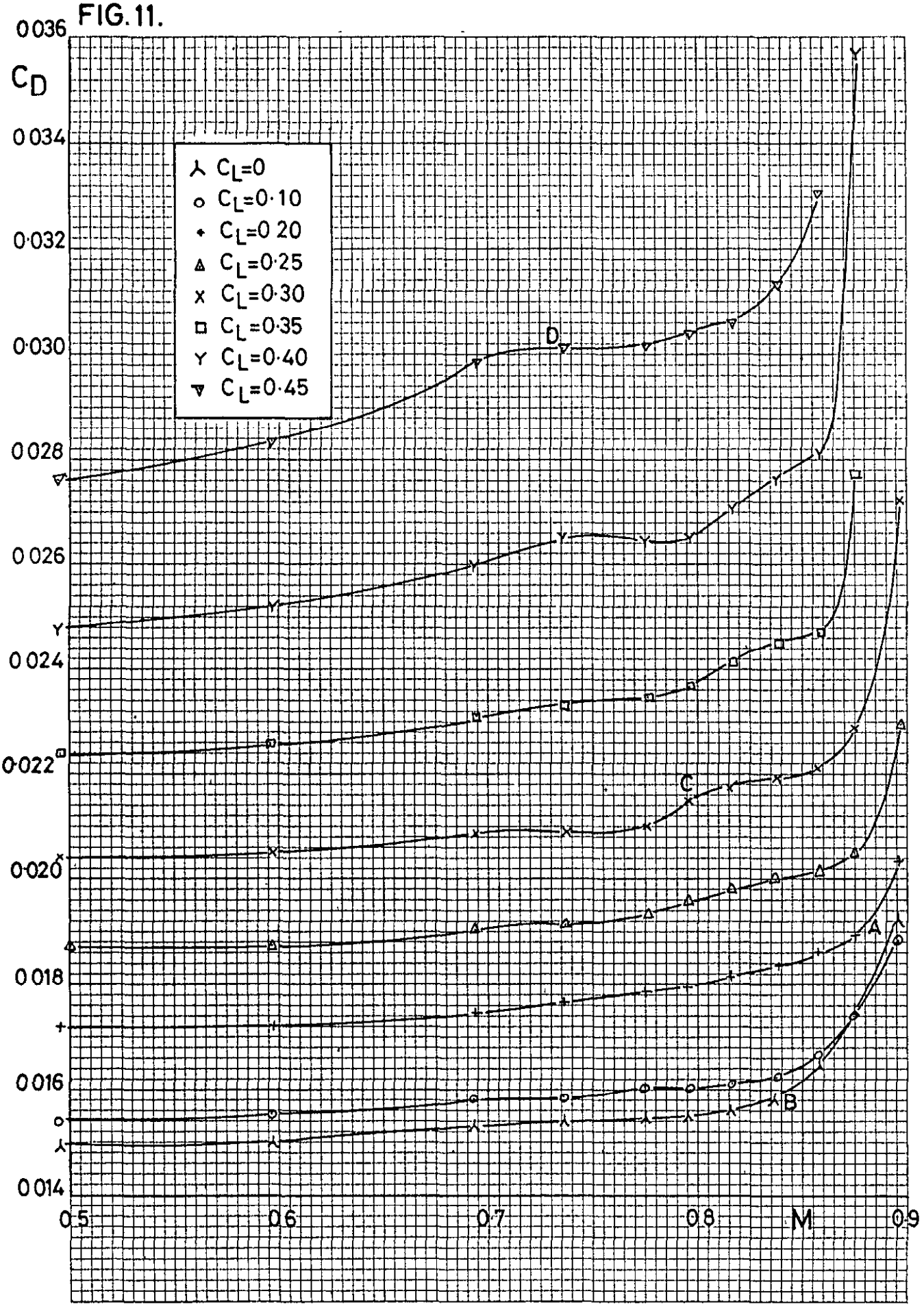

FIG. 11. $C_D \sim M$ FOR WING + BODY. $C_L = 0 \sim 0{\cdot}45$.

FIG. 12

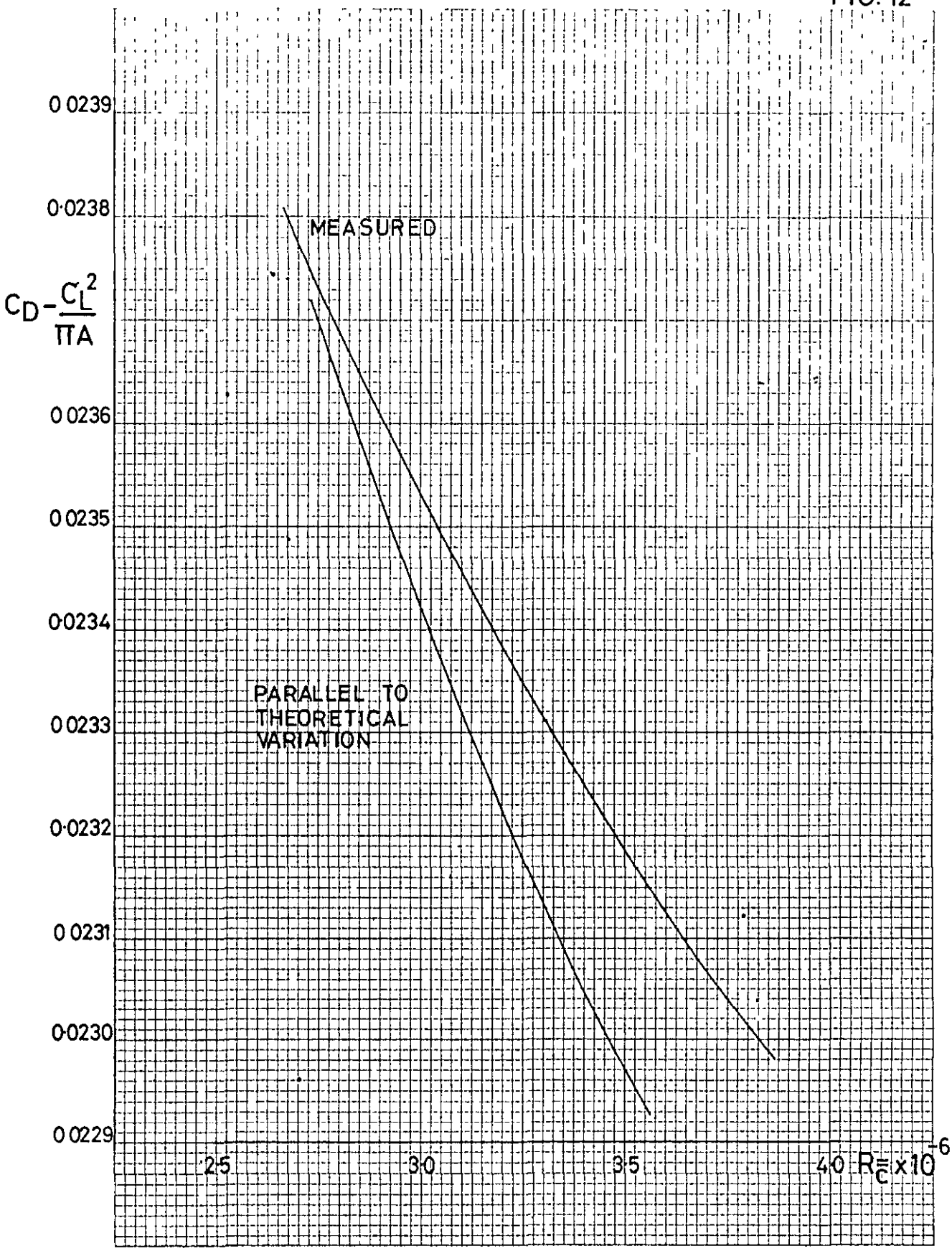

FIG. 12 $C_D - \frac{C_L^2}{\pi A} \sim R_{\bar{c}}$. COMPLETE MODEL. $\eta_T = -2°$, $M = 0.80$, $C_L = 0.30$ COMPARED WITH THEORETICAL VARIATION.

FIG. 13a)

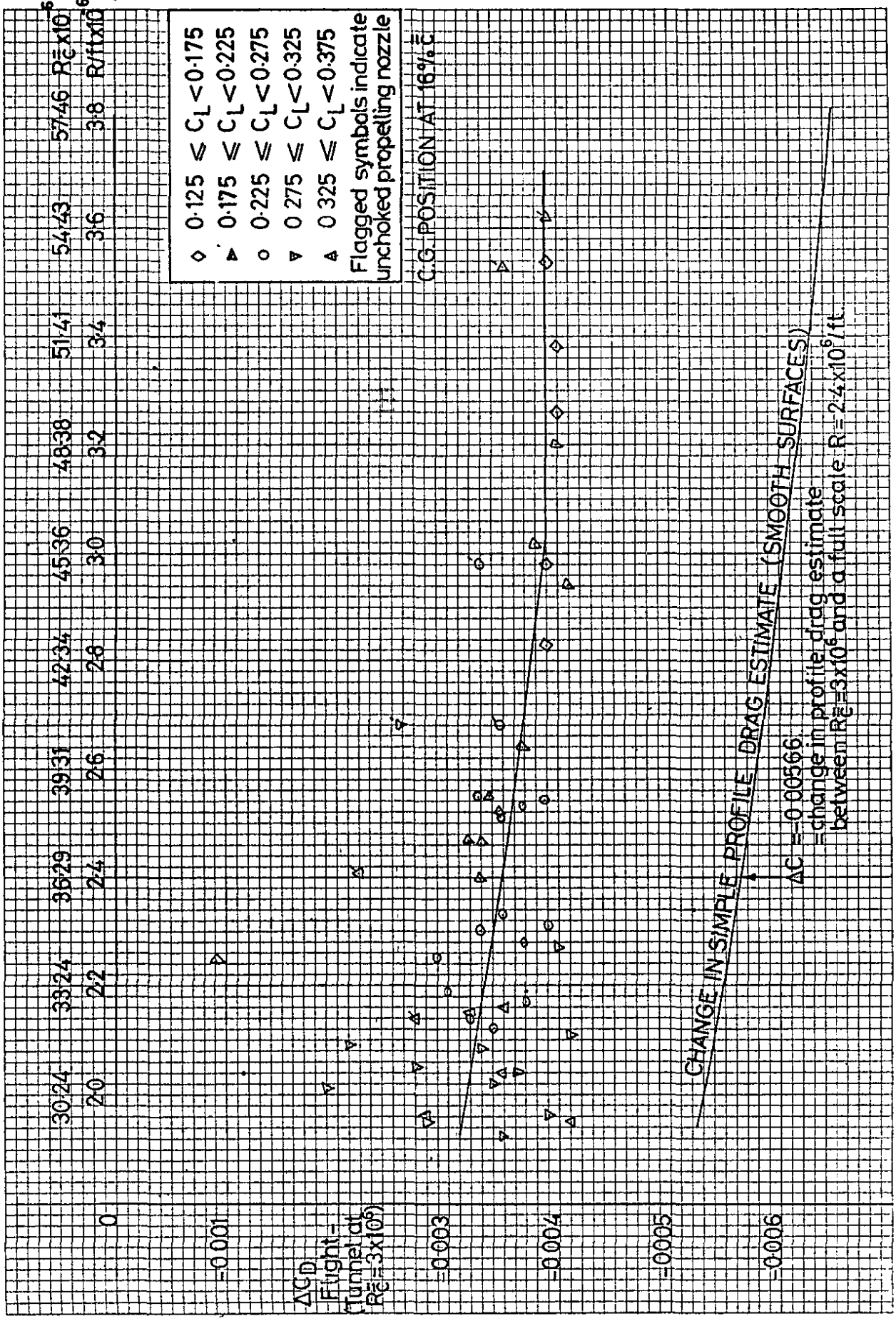

FIG.13a) ΔC_D(FLIGHT−TUNNEL) ~ R/ft FOR 16% $\bar{c}$ c.g.

(VARIATION WITH C_L)

FIG.13b)

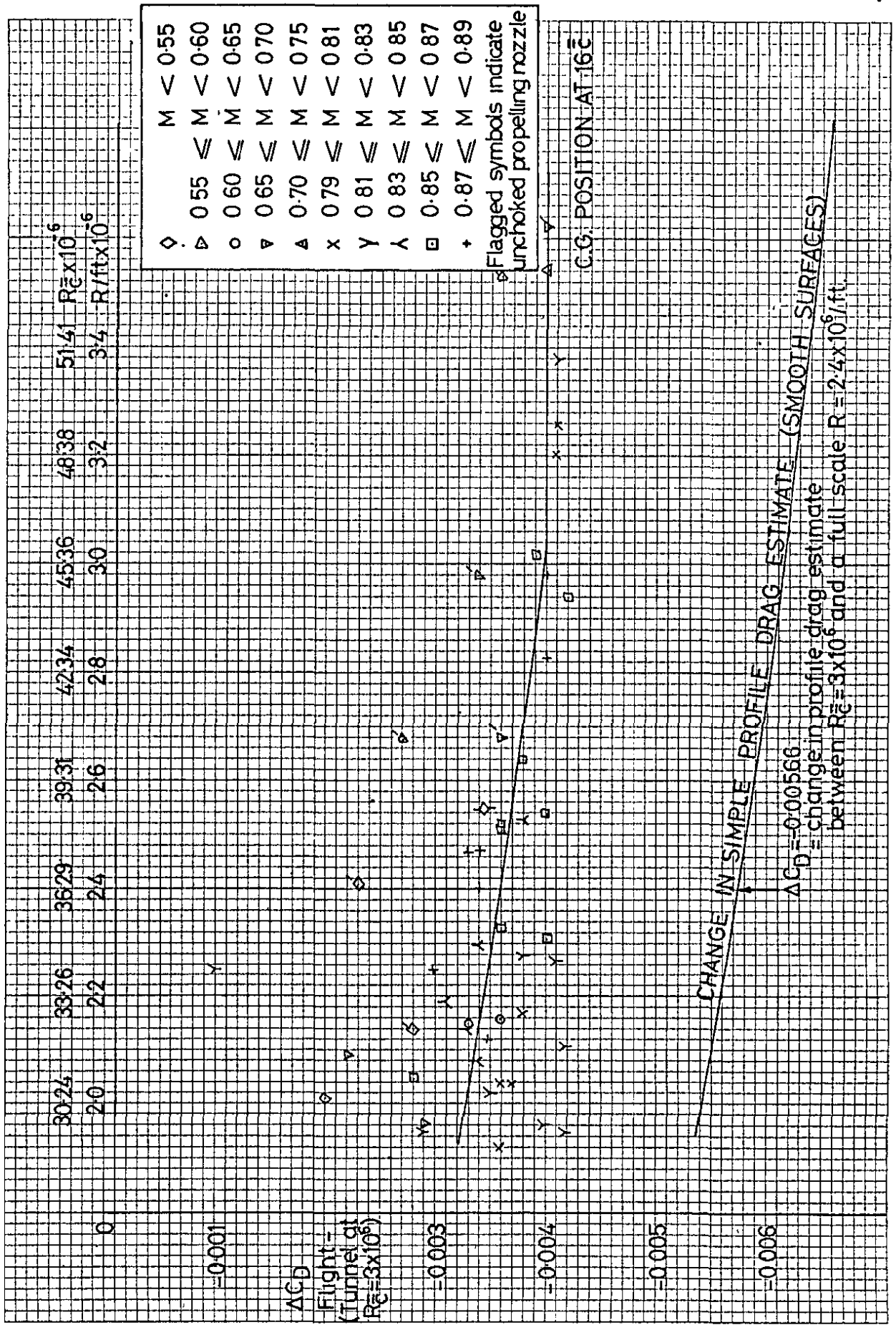

FIG. 13b) ΔC_D(FLIGHT–TUNNEL) ~ R/ft FOR 16% $\bar{c}$ c.g.

(VARIATION WITH M)

FIG.14a)

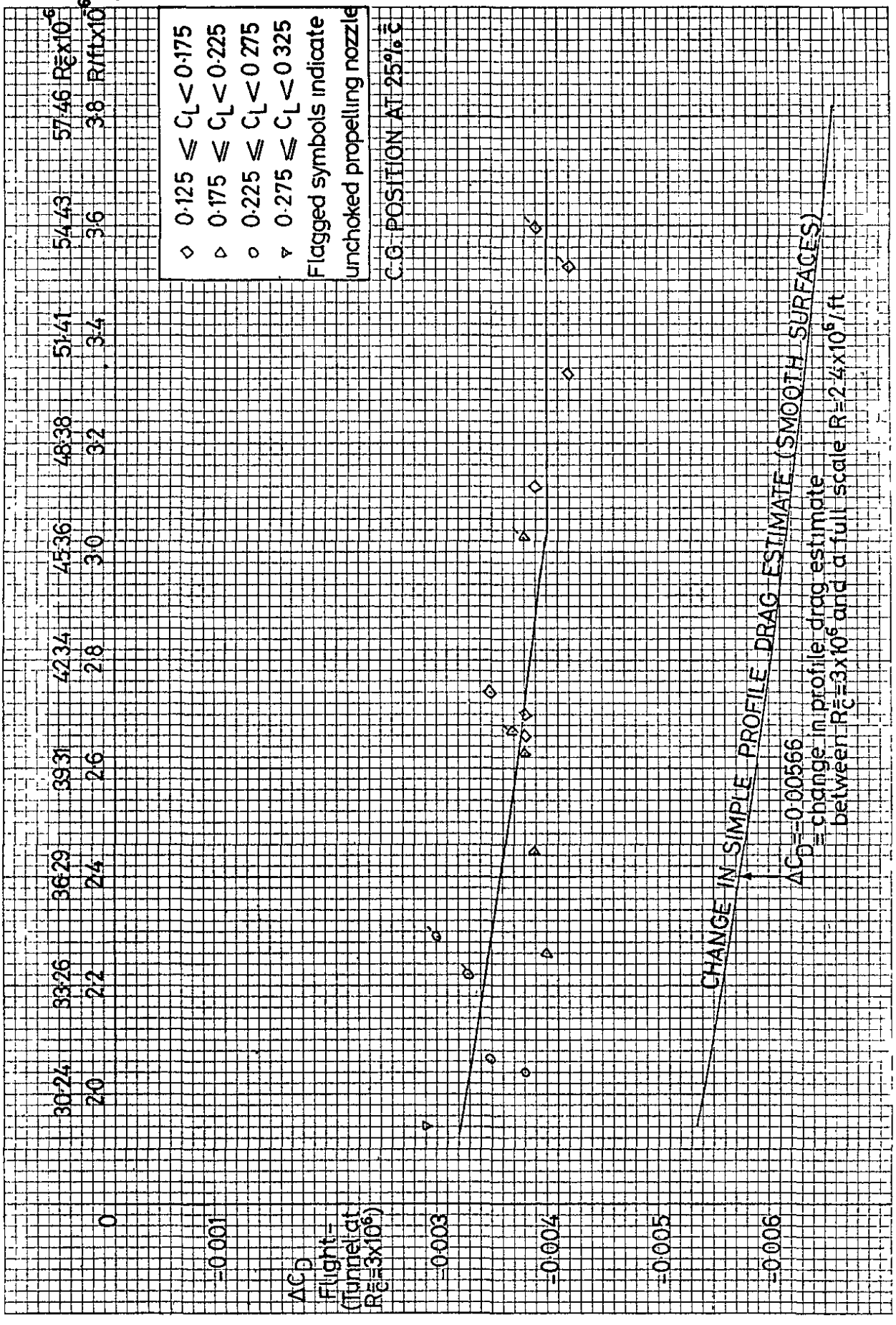

FIG.14a) ΔC_D (FLIGHT-TUNNEL) ~ R/ft FOR 25% $\bar{c}$ c.g.
(VARIATION WITH C_L)

FIG. 14b)

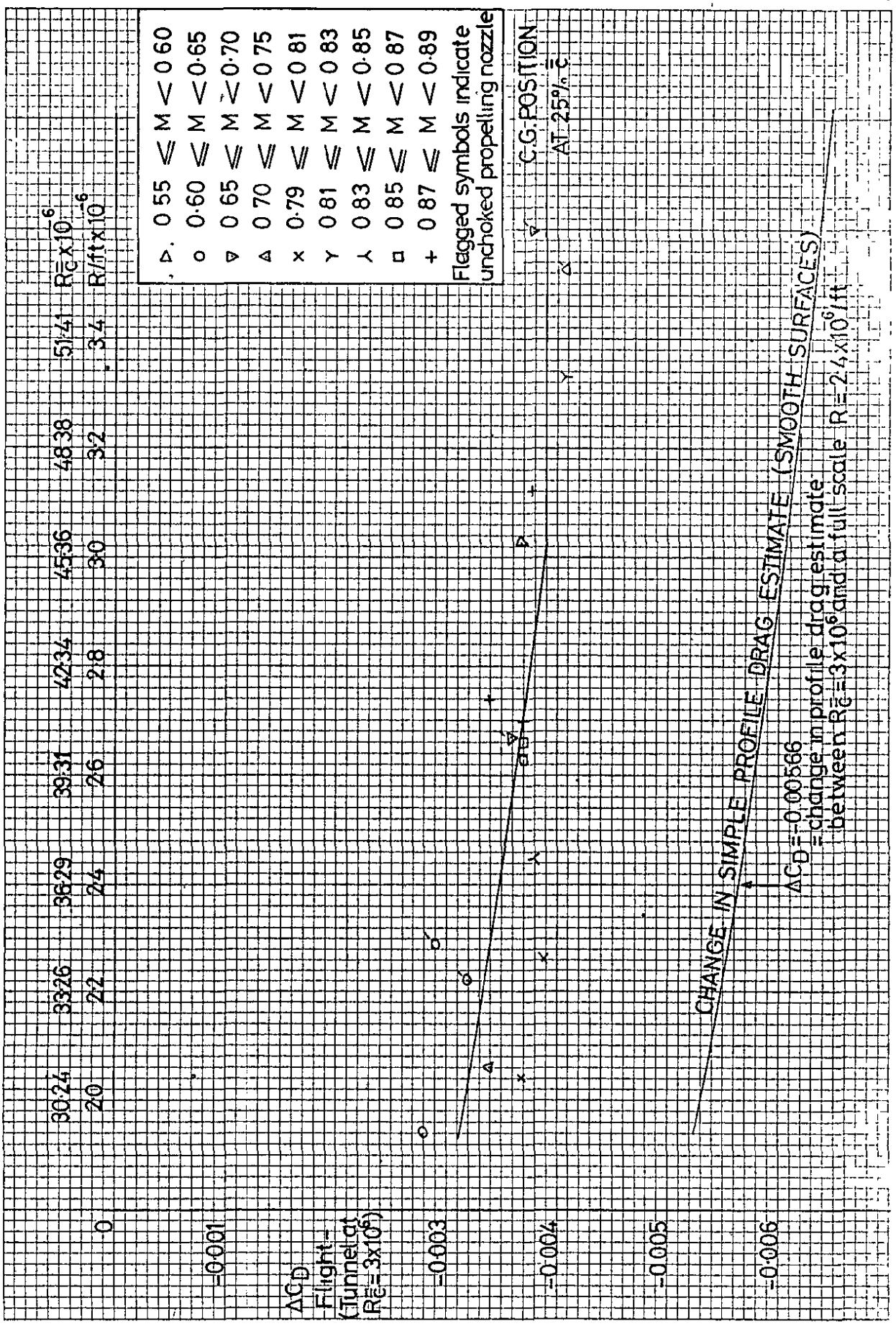

FIG. 14b) ΔC_D (FLIGHT–TUNNEL) ~ R/ft FOR 25% $\bar{c}$ c.g.

(VARIATION WITH M)

FIG. 15a)

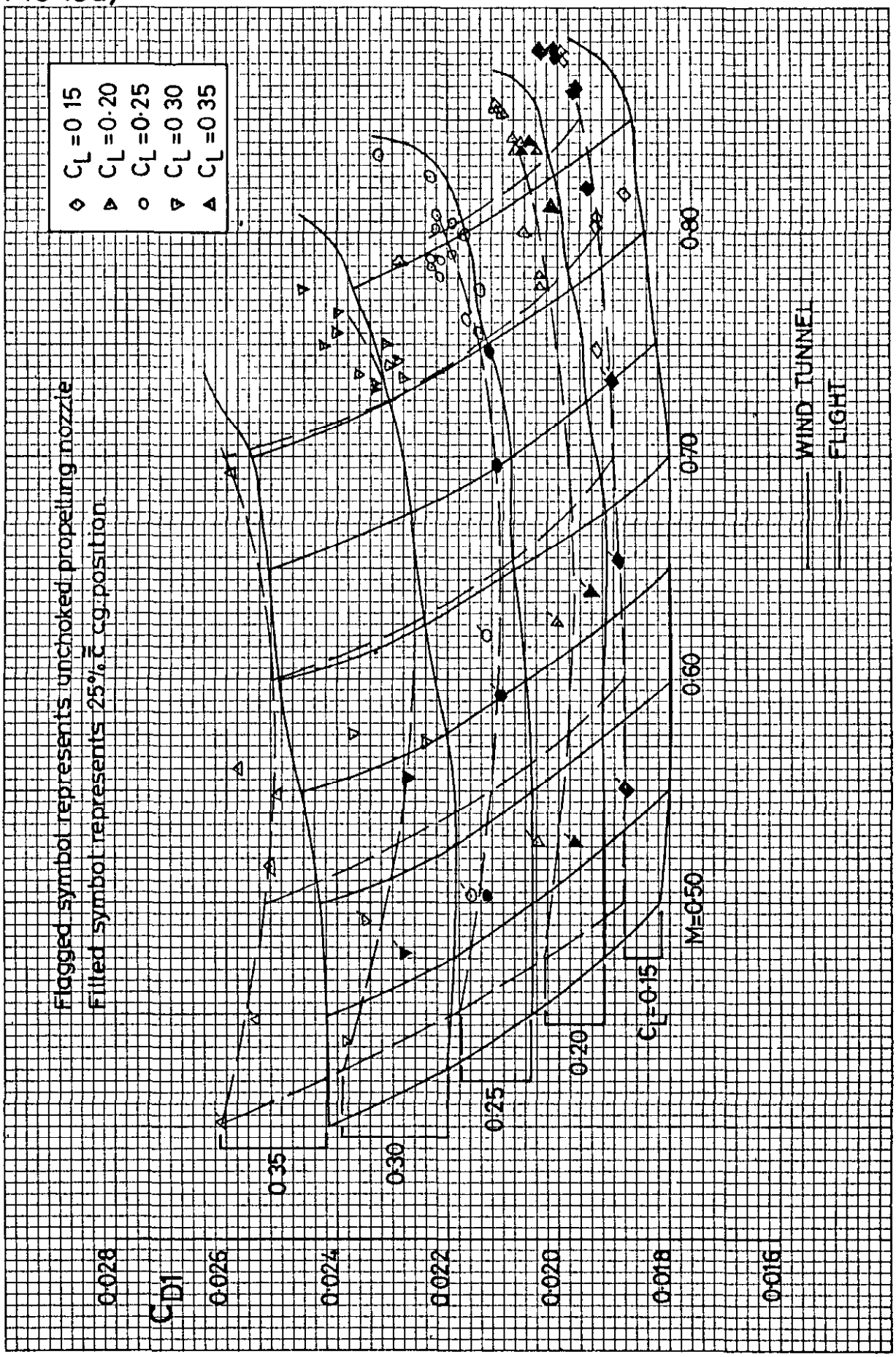

FIG. 15a) DRAG COMPARISON BETWEEN TUNNEL (CORRECTED) AND FLIGHT ("FLIGHT REYNOLDS NUMBER EFFECTS AS FOR SMOOTH SURFACE") (See Page 15)

FIG. 15b)

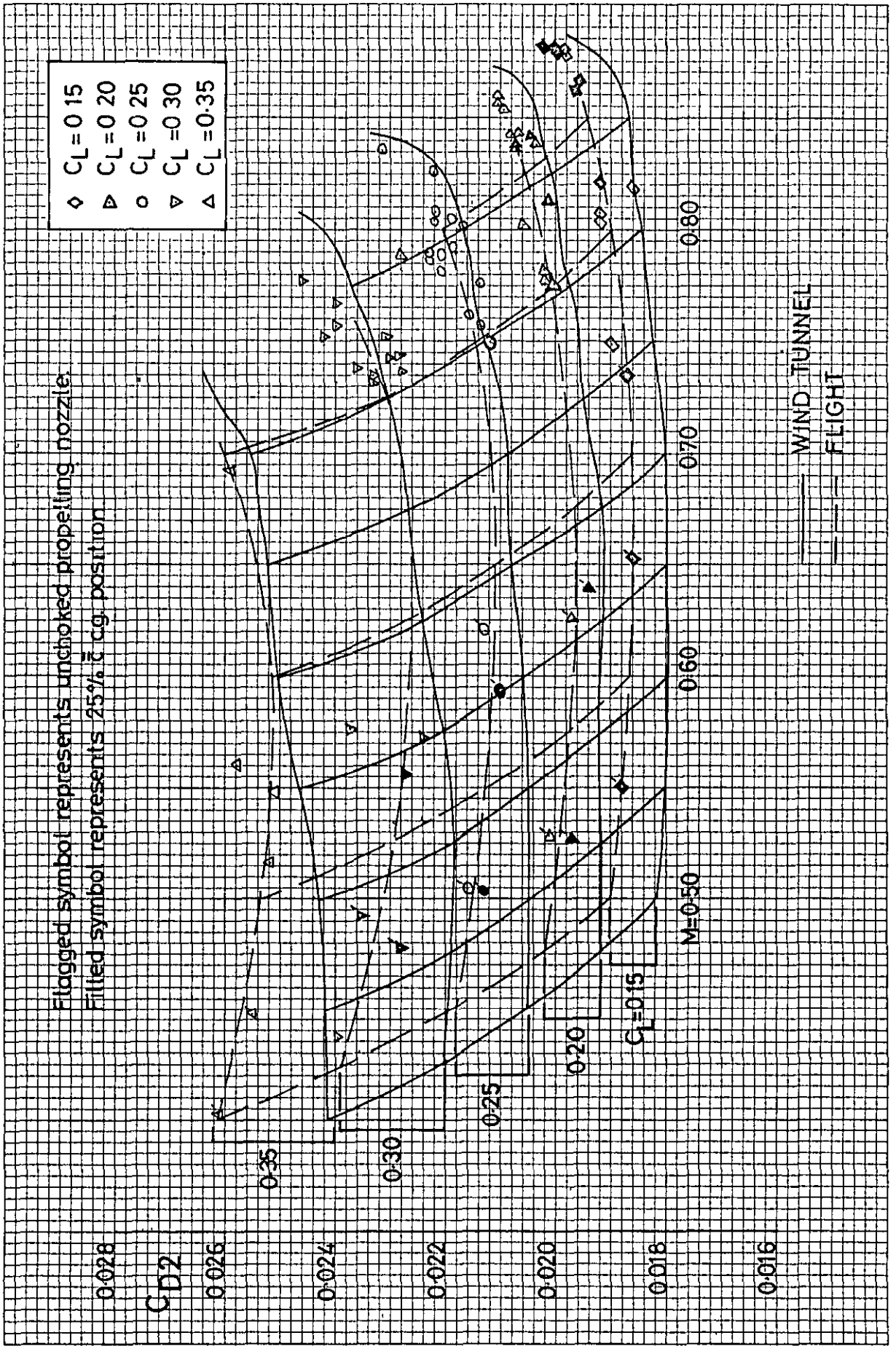

FIG. 15b) DRAG COMPARISON BETWEEN TUNNEL (CORRECTED) AND FLIGHT ("FLIGHT REYNOLDS NUMBER EFFECTS AS FOR RECOMMENDED MEAN LINE IN FIG. 13") (See Page 15)

FIG. 15c)

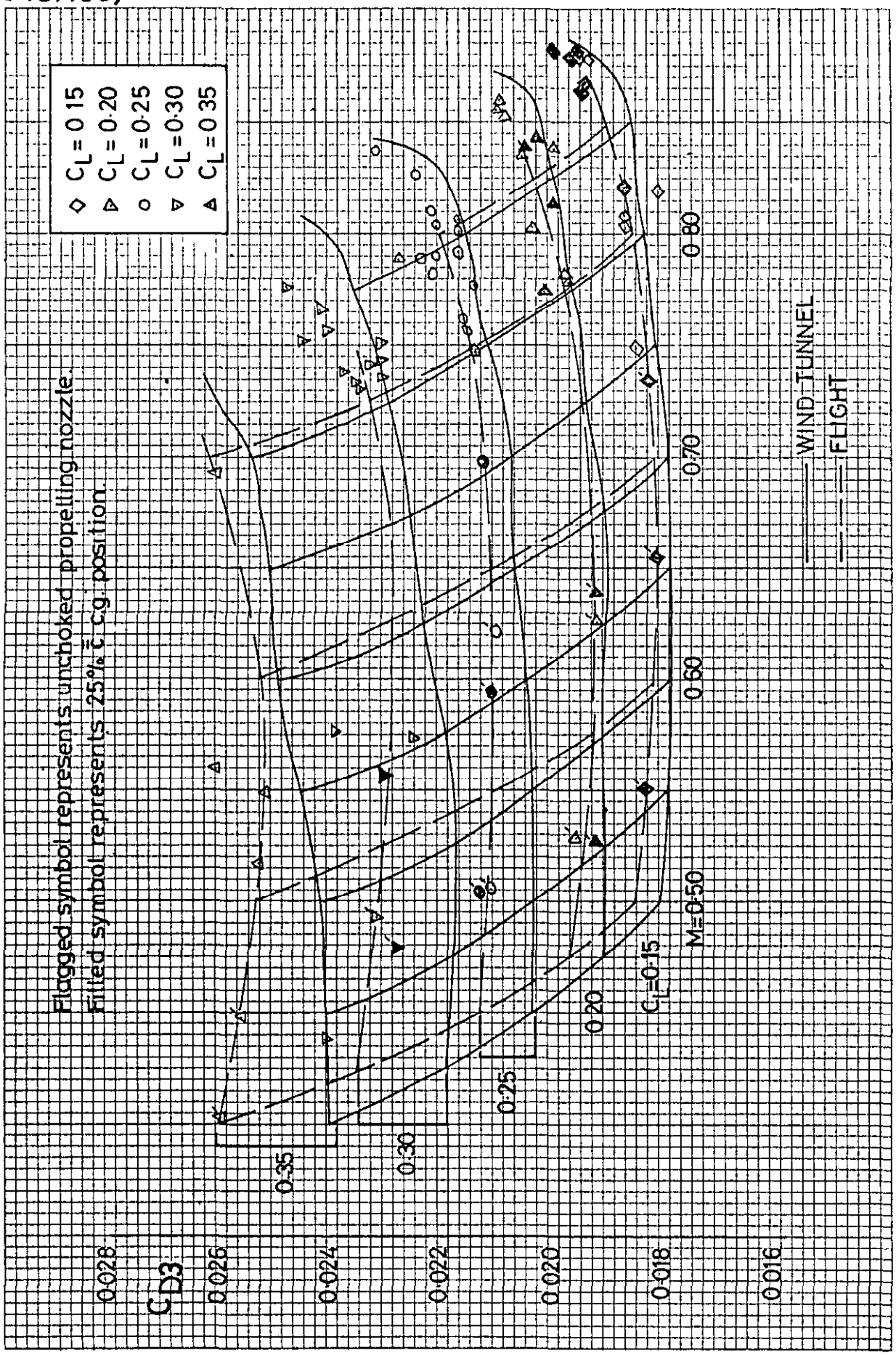

FIG. 15c) DRAG COMPARISON BETWEEN TUNNEL (CORRECTED) AND FLIGHT ("NO REYNOLDS NUMBER EFFECTS IN FLIGHT")

(See Page 15)

FIG.16

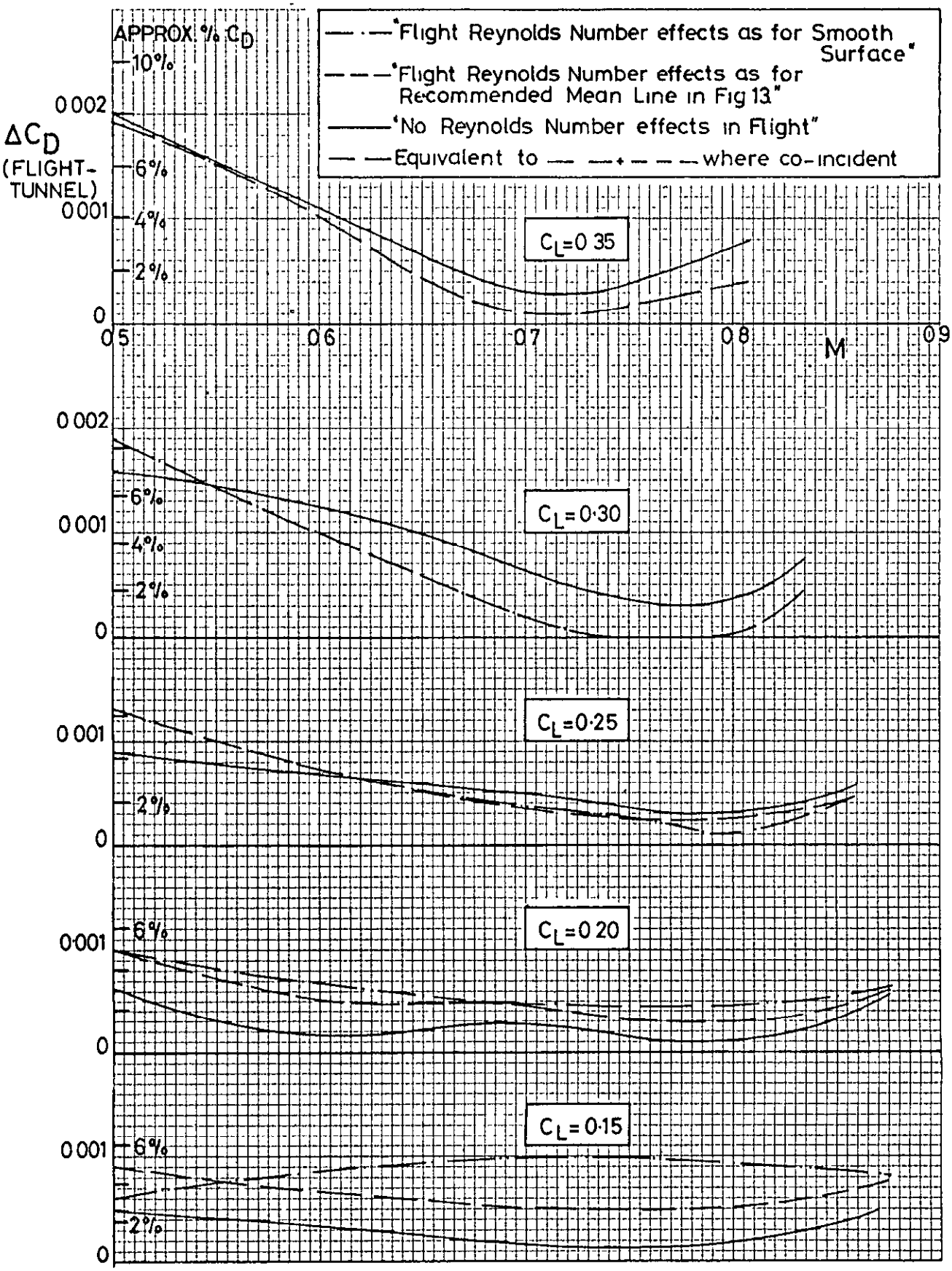

FIG. 16. ΔC_D (FLIGHT-TUNNEL) ~ M. C_L = 0·15~0·35.

C.P. No. 1170
March, 1970

Simper, J. I. and Hutton, P. G.

RESULTS OF A SERIES OF WIND TUNNEL MODEL BREAKDOWN TESTS ON THE TRIDENT 1 AIRCRAFT AND A COMPARISON WITH DRAG ESTIMATES AND FULL SCALE FLIGHT DATA

Wind tunnel measurements have been made and compared with estimates of flight data for 1:18.86 scale model of Trident 1.

Measured and estimated drags in general agree well except measured side nacelle drag increment. The general level of agreement between flight and wind tunnel results is within ±3% but is as much as 6% for low Mach numbers, probably because the propelling nozzles were unchoked. When/

C.P. No. 1170
March, 1970

Simper, J. I. and Hutton, P. G.

RESULTS OF A SERIES OF WIND TUNNEL MODEL BREAKDOWN TESTS ON THE TRIDENT 1 AIRCRAFT AND A COMPARISON WITH DRAG ESTIMATES AND FULL SCALE FLIGHT DATA

Wind tunnel measurements have been made and compared with estimates of flight data for 1:18.86 scale model of Trident 1.

Measured and estimated drags in general agree well except measured side nacelle drag increment. The general level of agreement between flight and wind tunnel results is within ±3% but is as much as 6% for low Mach numbers, probably because the propelling nozzles were unchoked. When/

C.P. No. 1170
March, 1970

Simper, J. I. and Hutton, P. G.

RESULTS OF A SERIES OF WIND TUNNEL MODEL BREAKDOWN TESTS ON THE TRIDENT 1 AIRCRAFT AND A COMPARISON WITH DRAG ESTIMATES AND FULL SCALE FLIGHT DATA

Wind tunnel measurements have been made and compared with estimates of flight data for 1:18.86 scale model of Trident 1.

Measured and estimated drags in general agree well except measured side nacelle drag increment. The general level of agreement between flight and wind tunnel results is within ±3% but is as much as 6% for low Mach numbers, probably because the propelling nozzles were unchoked. When/

When using Prandtl-Schlichting relationship to correct to flight Reynolds numbers wind tunnel results are 0 to 5% below flight data.

Appendices give details of corrections applied to wind tunnel data and tables showing the method of drag estimation.

When using Prandtl-Schlichting relationship to correct to flight Reynolds numbers wind tunnel results are 0 to 5% below flight data.

Appendices give details of corrections applied to wind tunnel data and tables showing the method of drag estimation.

When using Prandtl-Schlichting relationship to correct to flight Reynolds numbers wind tunnel results are 0 to 5% below flight data.

Appendices give details of corrections applied to wind tunnel data and tables showing the method of drag estimation.

DETACHABLE ABSTRACT CARDS

Produced and published by
HER MAJESTY'S STATIONERY OFFICE

To be purchased from
49 High Holborn, London WC1V 6HB
13a Castle Street, Edinburgh EH2 3AR
109 St Mary Street, Cardiff CF1 1JW
Brazennose Street, Manchester M60 8AS
50 Fairfax Street, Bristol BS1 3DE
258 Broad Street, Birmingham B1 2HE
80 Chichester Street, Belfast BT1 4JY
or through booksellers

Printed in England

C.P. No. 1170

SBN 11 470438 4